AD-A233 956

THE INFLUENCE OF ANISOTROPY OF THE MICROSTRUCTURE ON THE OVERALL ELASTIC-PLASTIC RESPONSE OF FIBROUS METAL-MATRIX COMPOSITES

A. Agah-Tehrani[*] and S. Wu[**]

November, 1989

[*] Assistant Professor

[**] Teaching Assistant

ABSTRACT

By means of a consistent homogenization method for obtaining the overall properties of an idealized class of metal-matrix composites with a periodic structure, the influence of anisotropy of the individual constituents on the overall response of the material has been investigated. Two classes of fibers are considered: boron (isotropic) and graphite (transversely isotropic). The plastic induced anisotropy in the matrix is modeled by a combined isotropic-kinematic hardening constitutive relation. In addition to a detailed discussion of the effect of the various components of anisotropy on the predicted response of the composite, this paper comprises comments on the computational method for determining the overall instantaneous moduli.

A-1

INTRODUCTION

An important issue pertaining to the theoretical investigation of the constitutive response of fibrous composites is to determine the nature of the influence of the properties of the individual phases on the overall response of the material. This requires a consistent averaging method for obtaining the macroscopic behavior of the composite from a knowledge of its microstructure. Such an averaging technique must take account of the inhomogeneous deformation which occurs in the scale of fiber spacing (microscale). This attribute of the averaging technique becomes particularly important when the moduli of the constituents are dependent on deformation gradient. In such cases, there will both be a variation of the deformation gradient and also a variation of the moduli on the microscale. Neglect of both fluctuations leads to serious errors in satisfying equilibrium in the microscale.

The basic assumption in the averaging process is the existence of a representative volume element (RVE) within the composite such that under conditions of an imposed overall homogeneous stress or strain, the average of field variables over any RVE (away from the boundaries of the medium) and the corresponding composite averages will be the same. In this article attention is focused on an idealized class of composites which possesses periodic microstructure. For such a class of composites, the RVE can be readily identified as the unit cell which when repeated in a specific pattern, continuously covers the interior of the composite. Overall properties can then be evaluated by analyzing the response of a unit cell to the imposed boundary conditions which simulate homogeneous stressing or straining of the composite. Currently there are two methods for utilizing the solution of the boundary value problem over the unit cell for determining the instantaneous overall properties.

In one method, the solution of the unit cell problem is used for correlating the local strain rate or stress rate field to their corresponding composite averages (Dvorak and Teply (1985) and Teply and Dvorak (1988)). This is accomplished by minimizing the total energy changes in the unit cell with respect to the difference between the local nodal velocities and the composite velocity field (fluctuating component of the local velocity field). Upper bounds to the overall instantaneous moduli can be evaluated from the displacement finite element formulation and the minimum principle for plastic strain rate, while lower bounds can be obtained from the equilibrium model and the quasi-static minimum principle in plasticity (Martin (1975)). For each minimum principle the corresponding bounds to the overall moduli are obtained by equating the energy changes in the composite to those in the unit cell. While the theoretical foundation of this method is influenced by the choice of the velocity distribution inside the unit cell and the geometry of the microstructure, it has the capability of obtaining bounds to the overall instantaneous moduli.

The second method for obtaining the overall instantaneous moduli of the composite from the results of the unit cell problem uses a singular perturbation analysis based on the multiple scales which exist in the composite: a global length scale which is associated with the loading condition and the size of the medium, and a local length scale typical of the dimensions of the unit cell (Bensoussan et al.(1978) and Sanchez-Palencia(1980)). In the limit as the ratio of the local to the global length scales tends to zero, the overall (homogenized) moduli of the periodic medium are obtained such that to the order $O(1)$ the average of the equilibrium equations for the composite over the unit cell will be identical to those for a material with the homogenized moduli. For a composite in which the constitutive behavior

of either phase is non-linear, determination of the instantaneous homogenized moduli involves utilizing the solution of the unit cell problem for obtaining the unknown functions which relate the first order perturbed velocity field to the overall rate of deformation.

For linear elastic composites with both circular unit cells and fibers, because of the axial symmetry of the problem, one can obtain explicit expressions for the homogenized constants (Murakami and Hegemier (1986)). For non-linear elastic porous materials, Abeyaratne and Triantafyllidis (1984), by using a large deformation homogenization method for obtaining the overall instantaneous nominal moduli of the medium, have analyzed the onset of localization. The most desirable feature of the homogenization method is that by being dependent on various length scales which exist in the composite, it provides a rational basis for determining the non-local terms which arise globally as a result of the macroscopic variations in the velocity gradient of the composite. However in contrast to the energy method, there is yet no available technique for bounding the homogenized moduli.

In fibrous metal matrix composites, there can be two types of anisotropy in the micro-structure; one is due to the elastic anisotropy of individual phases and the other due to the induced anisotropy as result of the plastic deformation in the matrix. The first type of anisotropy can exist if one utilizes graphite or carbon fibers as reinforcement. The plastic induced anisotropy can be associated with three different attributes of the plastic deformation in the polycrystalline matrix: the kinematic shift of the yield surface, the distortion of the yield surface, and the texture formation. The kinematic shift of the yield surface is representative of the influence of the long range self-equilibrating internal stresses, which are associated with the dislocation entanglements at junctions, grain-boundaries, or any other obstacle to dislocation motion (for example strong interface in the B/Al system), together with the internal

stresses generated as a result of the strain mismatch between the single crystals and/or the different constituents. The evolution law for the second-order internal variable (the back stress) which represent the kinematic shift of the yield surface must comprise the influence of the plastic strain rate, the dynamic recovery (Mroz et Al. (1976)), and the spin of the internal variable (Lee et al. (1983), Agah-Tehrani et al. (1987)). The latter term will only influence the growth of the back stress if the state of deformation is non-proportional. Although the significance of incorporating the induced-spin due to the anisotropy in the evolution law of the back stress has only been demonstrated for finite simple shearing of a rectangular block (Lee et al. (1983)), such terms may also influence other non-proportional deformations if the degree of non-proportionality is large enough.

The second component of the plastic induced anisotropy, which is the distortion of the yield surface, arises as the result of the differential hardening of the slip systems due to the anisotropic interaction between dislocations (Taylor and Elam (1923,1925), Kocks and Brown (1966), and Franciosi et al.(1980)). The third component of the plastic induced anisotropy, namely the texture formation, is due to the rotation of the single crystals toward a common axis. Such rotation restricts the choice of the available slip systems on which the plastic deformation can take place. Although texture formation has been only observed in the polycrystalline metals at finite strain, in certain fibrous metal-matrix composites (for example in B/Al) it is possible that the almost rigid inclusions can also limit the choice of the slip systems. Preliminary experimental observations by Dvorak et al. (1989) point to such possibility.

In the work presented here, the small displacement gradient version of the homogenization method is utilized for analyzing the influence of the elastic anisotropy of the fiber

and the plastic induced anisotropy in the matrix on the overall instantaneous moduli of the composite. The latter form of induced anisotropy is modeled through a combined isotropic-kinematic hardening. It is important to mention that the only reason for using a small displacement gradient theory is to systematically analyze the influence of various aspects of the deformation field in the microstructure on the overall moduli, and not because the failure strain of the composite is small. In metal-matrix composites with almost rigid reinforcements, like Boron-Aluminium, there can be large material rotations in the matrix adjacent to the inclusion. We defer to later work investigation of the influence of such rotations on the overall moduli of these material systems.

2. DEVELOPMENT OF AVERAGING TECHNIQUE

2.1 Homogenization Theory

The composite is modeled as a continuum composed of an elastic-plastic matrix with periodic distribution of long circular cylindrical elastic inclusions in a hexagonal array geometry—see Fig. 1. The assumed packing of the inclusions leads to transverse isotropy of the composite during elastic deformation. Two different composite systems will be considered: B/Al, Gr/Al. The matrix of both systems is assumed to be elastically isotropic while their fibers will respectively be isotropic and transversely isotropic.

The planar periodicity of the continuum enables one to express the rate dependent field variables as functions of the macroscopic independent variables (x_i, $i = 1, 2, 3$) which reflect the influence of the overall boundary conditions and/or the dimensions of the composite, and the microscopic variables (y_i, $i = 1, 2$) which represent the planar periodicity of the overall medium (dimensions of the unit cell). The two coordinate systems can be related to each other in the following manner:

$$y_i = \frac{x_i}{\varepsilon} \qquad i = 1, 2, \tag{2.1}$$

with ε as the ratio of the dimensions of the unit cell to the macroscopic dimensions of the composite. By considering the coordinate system y to representative of the fast scale and the coordinate system x to be representative of the slow scale (i.e. $\varepsilon \leq 1$), multiple asymptotic expansions can be applied to obtain a series of boundary value problems over the unit cell. This provides a convenient means of separating the local variations within the unit cell from the global variations within the composite. Neglecting the influence of the finite dimensions

of the medium permits one to utilize a regular multi-scale expansion, and to discard the singularity of the asymptotic expansions which arise as a result of the lack of planar periodicity close to the boundaries of the composite.

Since the aim of this investigation is to only analyze the effect of the anisotropy in the microstructure on the overall moduli of the composite, the gradient of displacement inside the unit cell is considered to be small. Thus, the rate equilibrium equations are represented in terms of the material derivative of the Cauchy stress, $\dot{\sigma}^{(\epsilon)}$. These equations must then be complemented by the constitutive relations which relate $\dot{\sigma}^{(\epsilon)}$ to its conjugate kinematic variable, $D^{(\epsilon)}$, the rate of deformation (strain rate). Thus in this study, the constitutive relations and the rate equilibrium equations are, respectively, as follows:

$$\dot{\sigma}_{ij}^{(\epsilon)} = C_{ijkl}(\frac{x}{\epsilon})D_{kl}^{(\epsilon)} \quad , \tag{2.2}$$

$$\frac{\partial \dot{\sigma}_{ij}^{(\epsilon)}}{\partial x_i} = 0 \quad , \tag{2.3}$$

with $D_{kl}^{(\epsilon)}$ as the symmetric part of the velocity gradient $(\partial v_k^{(\epsilon)}/\partial x_l)$ and $C_{ijkl}^{(\epsilon)}$ as the instantaneous moduli assumed to be functions only of y_i. Note that we are only concerned with problems in which the macroscopic field is homogeneous. Only constitutive relations that will lead to the symmetry of $C_{ijkl}^{(\epsilon)}$ with respect to $ij \leftrightarrow kl$, and hence to the deduction of the instantaneous moduli from a potential $U^{(\epsilon)}$ defined by

$$U^{(\epsilon)} = \frac{1}{2}\dot{\sigma}_{ij}^{(\epsilon)}D_{ij}^{(\epsilon)} \tag{2.4}$$

will be considered. By expressing the $v_i^{(\varepsilon)}$ and $\dot{\sigma}_{ij}^{(\varepsilon)}$ as asymptotic expansions in terms of ε, one

obtains

$$v_i^{(\varepsilon)} = v_i^{(0)}(x, y) + \varepsilon v_i^{(1)}(x, y) + \varepsilon^2 v_i^{(2)}(x, y) + \ldots \ldots \quad , \tag{2.5}$$

$$\dot{\sigma}_{ij}^{(\varepsilon)} = \dot{\sigma}_{ij}^{(0)}(x, y) + \varepsilon \dot{\sigma}_{ij}^{(1)}(x, y) + \varepsilon^2 \dot{\sigma}_{ij}^{(2)}(x, y) + \ldots \ldots \quad . \tag{2.6}$$

Substitution of (2.5,2.6) into (2.2,2.3) and comparison of equal powers of ε lead to the following

general conclusions-see Sanchez-Palencia(1980):

a) $v_i^{(0)}$ is independent of the microscopic variables, so that in the limit as $\varepsilon \to 0, D_{ij}^{(0)}$,

which is the symmetric part of $\partial v_i^{(0)}/\partial x_j$, can be considered to be the strain rate of the composite.
In determining the overall moduli of the composite, $\partial v_i^{(0)}/\partial x_j$ is assumed to be uniform.

b) Constitutive relations for $\dot{\sigma}_{ij}^{(0)}$ are

$$\dot{\sigma}_{ij}^{(0)} = C_{ijkl}(\frac{x}{\varepsilon})(D_{kl}^{(0)} + D_{kl(y)}^{(1)}) \quad , \tag{2.7}$$

with $D_{kl(y)}^{(1)}$ as the symmetric part of $(\partial v_k^{(1)}/\partial y_l)$

c) Micro-equilibrium equations for $\dot{\sigma}^{(0)}$ and $\dot{\sigma}^{(1)}$ are

$$\frac{\partial \dot{\sigma}_{ij}^{(0)}}{\partial y_i} = 0 \quad , \tag{2.8}$$

$$\frac{\partial \dot{\sigma}_{ij}^{(1)}}{\partial y_i} = -\frac{\partial \dot{\sigma}_{ij}^{(0)}}{\partial x_i} \quad . \tag{2.9}$$

Since the overall strain rate $(D_{ij}^{(0)})$ is independent of the local scale, (2.8) can be used to obtain

$v^{(1)}$ in terms of the strain rate $D^{(0)}$ such that

$$v_i^{(1)} = \psi_i^{kl} D_{kl}^{(0)}(x) + c_i(x) \quad , \tag{2.10}$$

with $c_i(x)$ as additive constants, and $\psi_i^{kl}(y)$ as functions which are the solution of the following

equations:

$$\frac{\partial}{\partial y_i}\left[C_{ijkl}\left(\frac{\partial \psi_l^{rs}}{\partial y_k}\right)_{sym}\right] = -\frac{\partial C_{ijrs}}{\partial y_i} \quad . \tag{2.11}$$

Since $v^{(0)}$ is to be considered as the velocity of the homogenized medium, the boundary

values for $v^{(1)}$ are such that

$$v^{(1)} = 0 \quad \text{on} \quad \partial\overline{V} \quad , \tag{2.12}$$

where $\partial\overline{V}$ is the overall boundary of the medium.

To satisfy the above boundary condition, one needs to have

$$c_i(x) = -\psi_i^{kl} D_{kl}^{(0)}(x) \quad \text{on} \quad \partial\overline{V} \quad . \tag{2.13}$$

However, this results in the dependence of $c_i(x)$ on ε, which necessitates the introduction of

boundary layers (Lions (1978)). Since determination of $c_i(x)$ is only necessary in calculating

stress terms on the order of ε, resolving the difficulties associated with these boundary layers

will not inter into an analysis based on $O(1)$.

In order to complete the formulation of the boundary value problem for determining the

functions ψ_i^{rs}, it is necessary to prescribe their value on the boundary of the unit cell. The

'classical' homogenization method only requires that these boundary conditions to be periodic, and hence leaves a degree of arbitrariness in the values of ψ_i^{rs} on the boundary of the unit cell. In the present study, this deficiency is removed by requiring that

$$\psi_i^{rs} v_i = 0 \quad \text{on} \quad \partial A \quad , \tag{2.14}$$

where ∂A is the boundary of the unit cell, and v_i is the normal to this boundary. As a result of this boundary condition, the functions ψ_i^{rs} belong to a limited range of the periodic functions. Thus the above formulation still falls within the theoretical frame work of the classical homogenization method. The attractiveness of the proposed formulation is that it leads to specific boundary conditions for determining the functions ψ_i^{rs}.

Finally, it may be of some interest to note that since in the problem under consideration the macroscopic strain rate $(D_{ij}^{(0)})$ is independent of the macroscale, the right hand side of (2.9) will be zero. This together with the boundary condition (2.14), leads to the vanishing of $v_{i,j(x)}^{(1)}$. Now by requiring that $v_i^{(2)}$ to be zero on the boundary of the unit cell, one can deduce that this term and all the higher order terms in the expansion of the velocity field are zero everywhere inside the unit cell.

2.2 Effective Moduli

Following Hill (1963), Willis (1982), and Nemat-Nasser et al. (1982), it is assumed that the periodic continuum on the average over a representative volume element (RVE) behaves similar to a homogeneous material with some moduli which are yet to be determined. These moduli can be obtained by subjecting the boundaries of the RVE to the uniform strain rate $D^{(0)}$. That is

$$v_i = D_{ij}^{(0)} x_j, \quad x \in \partial V \quad . \tag{2.15}$$

By utilizing Gauss's theorem, one can show that the mean value of the strain rate over the RVE will then be

$$\frac{1}{V}\int_{V}D_{ij}dV = \frac{1}{2V}\int_{\partial V}(v_{i}n_{j}+v_{j}n_{i})dS = D_{ij}^{(0)} .$$ (2.16)

The overall instantaneous moduli are now defined by the relation

$$<\dot{\sigma}_{ij}> = \overline{C}_{ijkl}D_{kl}^{(0)} ,$$ (2.17)

with $<\dot{\sigma}_{ij}>$ denoting the average of $\dot{\sigma}_{ij}$ over the RVE. Now by defining $<U>$ as the average of $U = \frac{1}{2}\dot{\sigma}_{ij}D_{ij}$ over the RVE, one obtains

$$<U> = \frac{1}{2V}\int_{V}\dot{\sigma}_{ij}D_{ij}dV .$$ (2.18)

Application of Gauss's theorem and the boundary condition (2.12), together with the recognition that $\dot{\sigma}_{ij}$ must satisfy the equilibrium equations in the RVE, enables one to utilize (2.18) to obtain

$$<U> = \frac{1}{2V}D_{ij}^{(0)}\int_{V}\dot{\sigma}_{ij}dV .$$ (2.19)

For the particular problem considered here, the representative volume element is a two-dimensional unit cell; thus, instead of the volume integral in (2.19), one must consider an integral over the area of the unit cell. Consequently, for the planar periodic medium under consideration, the equivalent expression to (2.19) will be

$$\overline{U}^{(\varepsilon)} = \frac{1}{2A} D_{ij}^{(0)} \int_A \dot{\sigma}_{ij}^{(\varepsilon)} dA, \qquad (2.20)$$

with $\overline{U}^{(\varepsilon)}$ as the average of $U^{(\varepsilon)}$ over the area of the unit cell. By substituting (2.6) in (2.20), one obtains an asymptotic representation for $\overline{U}^{(\varepsilon)}$. Since ε has been assumed to be very small, only the zero-order term in the representation will be considered. Recall that in problems involving macroscopic homogeneous straining, stress terms on the order of $O(\varepsilon)$ will be automatically zero. In other circumstances, neglecting terms on the order of ε is equivalent to assuming that as $\varepsilon \to 0$ the contribution of such terms to the average of the rate equilibrium equations over the unit cell can be neglected. By utilizing this assumption and (2.17), one obtains the following relation expressing $\overline{U}^{(\varepsilon)}$ in terms of the overall moduli:

$$\overline{U}^{(\varepsilon)} = \frac{1}{2} D_{ij}^{(0)} \overline{C}_{ijkl} D_{kl}^{(0)} \quad . \qquad (2.21)$$

An alternative expression for $\overline{U}^{(\varepsilon)}$ can be obtained by substituting (2.5, 2.6) in (2.18), utilizing (2.10), and following the previous argument for considering only the $O(1)$ terms. This enables one to obtain an expression for the overall moduli in the form of

$$\overline{C}_{ijkl} = \frac{1}{A} \int_A (I_{rsij} + S_{rsij}) C_{rstu}(y)(I_{tukl} + S_{tukl}) dA \quad , \qquad (2.22)$$

with

$$S_{ijkl} = \left(\frac{\partial \psi_i^{kl}}{\partial y_j} \right)_{sym} \quad , \qquad (2.23)$$

and I_{ijkl} as the fourth order identity tensor.

Thus, in order to determine the overall moduli, one needs to obtain both the variation of C_{ijkl} and ψ_i^{kl} in the microstructure, which can be accomplished by solving the unit cell problem.

Comparison of (2.17) and (2.22) with (2.2) reveals that although the O(1) homogenized moduli is non-local (because it involves integrals over a region in the composite), it has the same form as the constitutive relation in the microscale. This invariance of the form in going from the microscale to the macroscale will disappear if the macroscopic strain rate is non-homogeneous. As it is shown in Appendix A, in such cases the macroscopic constitutive relation involves dependence on both the overall strain rate and the gradient of the overall strain rate.

3. FORMULATION OF THE BOUNDARY-VALUE PROBLEM

The rate equilibrium equations of the unit cell, (2.3), are formulated through the following principle of virtual work:

$$\int_A \dot{\sigma}_{ij}^{(e)} \delta D_{ij} dA = \int_{\partial A} t_i \delta v_i d\Gamma \quad , \tag{3.1}$$

where A, ∂A, and $d\Gamma$ are respectively the area, the surface, and the differential line element on the boundary of the unit cell. For the problem under consideration, since the moduli of the matrix are dependent on the state of deformation, the solution of the equilibrium equations are needed in order to determine the variation of the C_{ijkl} inside the unit cell.

Once the variation of the moduli of the individual phases inside the unit cell is determined, one can obtain the functions ψ_i^{kl} from the variational form of (2.11), which is

$$\int_A C_{ijkl}(y) \left(\frac{\partial \psi_i^{rs}}{\partial y_k} \right)_{sym} \delta \left(\frac{\partial \phi_i}{\partial y_j} \right)_{sym} dA = - \int_A C_{ijrs}(y) \delta \left(\frac{\partial \phi_i}{\partial y_j} \right)_{sym} dA \quad , \tag{3.2}$$

with ϕ_i as any kinematically admissible velocity field. For the current problem, this implies that $\phi_i v_i = 0$ on the boundary of the unit cell.

The smallest repeating cell of the hexagonal array is shown in Fig. 1. For the problem under consideration, the composite is undergoing tensile deformation in the x_1 direction while preventing any strain in the fiber direction (x_3) and keeping the lateral surface free of traction. Due to the line symmetries within the unit cell, only analysis of a 1/4 cell is needed provided that the boundary conditions on the reduced geometry reflect the existing symmetries. In light of these symmetries, the boundary conditions for the rectangular region EFGH shown in Fig. 1 are:

$$v_1^{(e)} = -\frac{\dot{U}}{2} \quad , \quad \dot{t}_2 = 0 \quad \text{at} \quad x_1 = 0 \quad , \tag{3.3a}$$

$$v_1^{(e)} = \frac{\dot{U}}{2} \quad , \quad \dot{t}_2 = 0 \quad \text{at} \quad x_1 = \frac{3a}{2} \quad , \tag{3.3b}$$

$$v_2^{(e)}(x_1, 0) = -v_2^{(e)}(x_1, \frac{\sqrt{3}a}{2}) = \frac{W}{2} \quad , \tag{3.3c}$$

$$\dot{t}_1 = 0 \quad \text{at} \quad x_2 = 0 \,, x_2 = \frac{\sqrt{3}a}{2} \quad , \tag{3.3d}$$

$$D_{33}^{(e)} = 0 \quad , \quad \dot{t}_1 = \dot{t}_2 = 0 \quad \text{at} \quad x_3 = \text{const} \quad , \tag{3.3e}$$

where $\dot{U}$ is the prescribed displacement rate in the x_1 direction, and W is the unknown displacement rate in the x_2 direction which is determined by the zero average traction rate in the x_2 direction along the lateral surfaces. That is

$$\int_{x_1=0}^{x_1=1.5a} \dot{t}_2 d\Gamma = 0 \quad \text{at} \quad x_2 = 0 \quad , \tag{3.4a}$$

$$\int_{x_1=0}^{x_1=\frac{a}{2}} \dot{t}_2 d\Gamma = 0 \quad \text{at} \quad x_2 = \frac{\sqrt{3}a}{2} \quad . \tag{3.4b}$$

Further reductions of the 1/4 unit cell can be achieved by observing that if the rectangular region EFGH in Fig. 1 is divided into two halves by a line through the central point O, a 180° rotation about the point O can cover the region EFGH with the region EFIK leaving the stresses and strains unchanged. When ξ is a length which measures coordinate on the dividing line IK, with ξ = 0 at point O, the additional boundary conditions to be prescribed along this line

are

$$u_i(\xi) = -u_i(-\xi) \, , \, i = 1,2 \tag{3.5a}$$

$$t_i(\xi) = t_i(-\xi) \, , \, i = 1,2 \tag{3.5b}$$

For the two dimensional problem under consideration, due to the prescribed deformation state of the composite, the only periodic functions which can be determined are : ψ^{11}, ψ^{22}, ψ^{12}, and ψ^{33}. In light of the displacement boundary conditions of the unit cell problem, the boundary conditions for these functions are

$$\begin{Bmatrix} \psi_1^{rs} = 0 & \text{at } x_1 = 0, x_1 = \dfrac{3a}{2} \\ \psi_2^{rs} = 0 & \text{at } x_2 = 0, x_2 = \dfrac{\sqrt{3}a}{2} \end{Bmatrix} \quad \text{for } rs = 11,22,12,33. \tag{3.6}$$

The boundary condition associated with the inversion symmetry will be

$$\begin{Bmatrix} \psi_i^{rs}(\xi) = -\psi_i^{rs}(-\xi) \, , \, i = 1,2 \\ t_i^{rs}(\xi) = t_i^{rs}(-\xi), i = 1,2 \end{Bmatrix} \quad \text{for } rs = 11,22,12,33, \tag{3.7}$$

with t^{rs} as the tractions along the side IK corresponding to the problem of determining the ψ_i^{rs}'s.

In order to complete the formulation of the boundary value problem, one needs to specify the constitutive relations for the individual phases. Since the objective of this study is to analyze the influence of the anisotropy of the microstructure on the overall response of the composite, two types of fiber reinforcements will be considered, Boron and Graphite. Boron is characterized by a linear isotropic elastic constitutive relation with two independent elastic

constants, while Graphite is characterized by a transversely linear isotropic constitutive relation with five independent elastic constants. The elastic properties of both types of fiber along with those of matrix are shown in Table 1.

The constitutive relation for the aluminium matrix is developed by assuming that $\dot{\sigma}$ can be expressed as

$$\dot{\sigma} = C^{e(m)}:(D - D^P) \quad , \tag{3.8}$$

with $C^{e(m)}$ as the elastic moduli of the matrix, and D^P the rate of plastic deformation in the matrix. The symbol : in (3.8) represents the trace operator.

For the combined isotropic-kinematic hardening model, the von Mises yield condition takes the form

$$(\sigma' - \alpha):(\sigma' - \alpha) = \frac{2}{3}\bar{\sigma}^2 \quad , \tag{3.9}$$

where σ' is the deviatoric part of the Cauchy stress, $\bar{\sigma}$ the scalar representing the isotropic component of the current tensile yield stress, and α the second order tensor representing the kinematic shift of the yield surface.

By assuming the coincidence of the yield function and the plastic potential, D^P can be expressed as

$$D^P = \sqrt{\frac{3}{2}} \, \dot{\bar{\varepsilon}}^P \, m \quad , \tag{3.10}$$

where $\dot{\bar{\varepsilon}}^P$ is the generalized plastic strain rate ($\dot{\bar{\varepsilon}}^P = \sqrt{\frac{2}{3}D^P:D^P}$), and m is the unit normal to the yield surface expressed in (3.9)

$$m = \sqrt{\frac{3}{2}} \frac{\sigma' - \alpha}{\overline{\overline{\sigma}}} \quad , \tag{3.11}$$

The constitutive relation for the evolution of α which takes account of both the direct influence of the plastic strain rate and the embedded induced anisotropy is considered to be

$$\dot{\alpha} = cD^P + \overline{W}\alpha - \alpha\overline{W} \quad , \tag{3.12}$$

with

$$\overline{W} = \frac{\chi}{\sqrt{\alpha:\alpha}}(\alpha D^P - D^P \alpha) \quad , \tag{3.13}$$

where c is the classical Prager-Ziegler hardening modulus, and χ is a non-dimensional material parameter which controls the contribution of the spin to the evolution of induced anisotropy (Lee et al.(1988)). The latter component will be non-zero only if the principal axis of strain tensor rotates in the body, i.e. if the state of deformation is non-proportional. For the case of simple shearing, which is an example of non-proportional deformation, in order to ensure that the spin of the eigentriad of the embedded anisotropy is not larger than the average spin of the material particle, only negative values of χ must be considered. Thus, for the structure of the above evolution law to be physically appropriate for deformation modes, we are assuming that the value of χ is in general negative.

Utilization of (3.9-3.13) together with the consistency condition leads to the following expression for D^P :

$$D^P = \frac{1}{H}(m:\dot{\sigma})\, m \quad , \tag{3.14}$$

with

$$H = \frac{2}{3}h + c + \chi\left[m:\frac{1}{\sqrt{\alpha:\alpha}}(\alpha^2 m + m\alpha^2 - 2\alpha m\alpha)\right] \quad , \tag{3.15}$$

and h as the isotropic hardening modulus. The parameters h and c are obtained from the uniaxial true stress-natural strain curve. This curve is represented by a piecewise power law

$$\frac{\varepsilon}{\varepsilon_y} = \begin{cases} \dfrac{\sigma}{\sigma_y} & \text{for} \quad \sigma \leq \sigma_y \\ \left(\dfrac{\sigma}{\sigma_y}\right)^n & \text{for} \quad \sigma \geq \sigma_y \end{cases} \quad , \tag{3.16}$$

with ε as the natural strain, σ as the true stress, σ_y as the uniaxial yield stress, ε_y as the uniaxial yield strain, and n as the hardening exponent.

Substitution of (3.14) into (3.8) and inversion of the resulting equation lead to the following constitutive relation:

$$\dot{\sigma} = C:D \quad , \tag{3.17}$$

with

$$C_{ijkl} = 2\mu\left[\frac{1}{2}(\delta_{ik}\delta_{jl} + \delta_{il}\delta_{jk}) + \frac{\nu}{1-2\nu}\delta_{ij}\delta_{kl} - \frac{2\theta\mu}{H+2\mu}m_{ij}m_{kl}\right] \quad , \tag{3.18}$$

$$\theta = \begin{cases} 1 & \text{if} \quad \overline{\sigma} = \overline{\sigma}_{max} \quad \text{and} \quad \dot{\overline{\sigma}} > 0 \\ 0 & \text{if} \quad \overline{\sigma} < \overline{\sigma}_{max} \quad \text{or} \quad \dot{\overline{\sigma}} < 0 \end{cases} \quad , \tag{3.19}$$

μ and ν are respectively the shear modulus and the Poisson's ratio of the matrix.

In the following, the parameter β will be referred to as the ratio of the isotropic to kinematic hardening. During the actual computation, this parameter is considered to be equal to

$$h = \beta H_{axial} \quad , \tag{3.20}$$

$$c = \frac{2}{3}(1-\beta)H_{axial} \quad , \tag{3.21}$$

with H_{axial} as the uniaxial hardening modulus.

Thus, in a strict sense, β is not equal to h/c. However, within the range $(0,1)$, the two parameters are directly proportional to each other. So that β can be considered as the ratio of the isotropic to kinematic hardening.

4. FINITE ELEMENT FORMULATION

Due to the material non-linearities in the matrix and the geometry of the unit cell, finite element analysis was used to solve the elasto-plastic boundary value problems formulated in the previous section. Three different fiber volume fractions were considered: $c_f = 20\%$, $c_f = 45\%$, and $c_f = 60\%$. The finite element mesh for the 20% fiber volume fraction consisted of 455 element, while that for the 45% and 60% fiber volume fraction consisted of 485 elements —see Fig. 2. Eight-node isoparametric elements were utilized as velocity interpolation shape functions. This type of element is particularly suited for capturing the large variations in the stress and displacement gradient which take place across the interface between the fiber and the matrix. A total of 18 steps were utilized for the analysis with the magnitude of the prescribed transverse displacement increment (ΔU) at $x_1 = 0$ during each step being 0.001 a where a is the size of the unit cell—see Fig. 1.

The mixed boundary conditions of the unit cell problem, which are stated in (3.3,3.5), are prescribed in a manner similar to that proposed by Needleman(1970). This involves the following steps:

a) Because of the velocity boundary condition (3.3c), the nodal values of the velocity component v_2 on the boundary $x_2 = 0$ are set equal to each other. Utilizing this equality and the fact that the average of t_2 along this edge is zero (see 3.4a), the unknown nodal values corresponding to this velocity component can be then eliminated by adding the rows of the stiffness matrix corresponding to these nodes and setting the sum of the nodal forces equal to zero. The same procedure can used for the nodes on the edge $x_2 = \sqrt{3}\,a/2$. As a result of this procedure, the nodal values of the velocity component v_2 on the lateral surfaces can be rep-

resented by only two unknowns. Since the value of these two unknowns are opposite to each other, further reduction in the number of unknowns can be achieved by subtracting the columns of the stiffness matrix associated to these two nodes.

b) Because of the traction boundary condition (3.5b), subtraction of the rows of the stiffness matrix corresponding to the nodal values of the velocity components of the nodes on the edge IK, see Fig. 1, leads to zero effective nodal force. By utilizing the boundary condition (3.5a), one can then reduce by half the number of unknowns corresponding to the edge IK.

It must be mentioned that although the above steps lead to substantial reductions in the number of unknowns in the problem, they will cause an increase in the bandwidth of the overall stiffness matrix. The boundary conditions of the problems for determining the ψ^r's are similar to those associated with the unit cell, except that the lateral surfaces of the mesh are considered to be fixed in the problems of finding the ψ^r's—see (3.6). This boundary condition has the desired characteristic that the finite element mesh used to solve the unit cell problem is identical to the mesh that was used to obtain ψ^r's. The new boundary conditions are needed if the prescribed velocity field is to be identified with the zero-order term of the asymptotic expansion of the $v^{(\epsilon)}$. Because of the difference between the boundary conditions of the unit cell problem and those of the problems for determining the ψ^r's, the stiffness matrices which will be used to solve for the unknown nodal values in the two problems will not be identical.

Due to the rate-independence of the constitutive relations, the finite element rate equations can be considered to be incremental equations. These equations were solved through

elasto-plastic constitutive relation in the matrix-see Mallett (1985), Suh et al.(1989).

5. NUMERICAL RESULTS

5.1 Elastic Properties

Figures 3 through 7 present the variation of the predicted homogenized elastic properties of both B/Al and Gr/Al with fiber volume fraction. Also shown in these figures are the results of the Voigt and Kelvin models. These figures, in general, indicate that the relation of the homogenized moduli to those predicted by the Kelvin and Voigt models is dependent on the type of the material system considered. While all the components of the homogenized elastic moduli of Gr/Al fall in between the results predicted by the Kelvin and Voigt models, the same does not hold for those of B/Al. In order to explain this observation, we will next examine the relation of each component of the homogenized moduli to the values predicted by the Kelvin and Voigt models. Figure 3 indicates that the homogenized transverse modulus $\overline{C}^{*}_{1111}$ of both Gr/Al and B/Al lies in between the values predicted by the Kelvin and Voigt models, with the transverse homogenized modulus of B/Al being very close to the Kelvin model. The relation of $\overline{C}^{*}_{1122}$ to those predicted by the Kelvin and Voigt models can be seen from Fig. 4. It may be of some interest to note that this component of the homogenized moduli of B/Al agrees almost identically with the Kelvin model, with the latter being higher in real numbers. Figure 5 shows the variation of the transverse shear modulus with the fiber volume fraction. The results indicate that although for small fiber volume fractions the homogenized transverse shear modulus of B/Al is lower than that predicted by the Kelvin model, these values are in general very close to the prediction of the Kelvin model. Based on the results of Figs 2-5, one can conclude that the transverse homogenized elastic properties of the composite are more closer to the predictions of the Kelvin model than to those of the Voigt model. Figure 6 shows

that for all fiber volume fractions, the homogenized modulus $\overline{C}^*_{1133}$ of B/Al is lower than that predicted by the B/Al. Finally, Fig. 7 indicates that the homogenized axial modulus of both B/Al and Gr/Al agrees well with the Voigt model.

In obtaining the overall elastic moduli, the Voigt model, by assuming the equality and uniformity of the strain components in both phases, violates the equilibrium in the microscale and the compatibility across the fiber/matrix interface. Because of the above characteristics, the Voigt model provides an upper bound to the actual strain energy of the composite. Thus, the overall moduli, which are determined based on this model, are supposed to provide an upper bound to the actual moduli of the composite. In contrast to this, the Kelvin model, by considering the equality and uniformity of stress components in both phases, violates the equilibrium in the microscale and continuity of traction across the fiber/matrix interface. Since the Kelvin model provides a lower bound to the actual strain energy of the composite, the overall moduli obtained from this model has been identified with the lower bound to the actual moduli of the composite. The current results suggest that for certain material systems there is no one to one correspondence between obtaining bounds to the overall strain energy of the composite and the individual components of the overall moduli. Moreover, they indicate that the components of the homogenized moduli are not uniformly close to those predicted by either the Kelvin or the Voigt model, and their relation to the so called upper and lower bounds vary from one component to another. This poses questions with regard to the ability of obtaining unique upper and lower bounds for all the components of the overall moduli.

5.2 Development of the Plastic Zone

In this section we will examine the influence of the type of the fiber and its volume fraction on the development of the plastic zone. This is accomplished by presenting the

contours of the effective stress $\overline{\sigma}$ during progressive stages of the deformation. Since the initial tensile yield stress in the matrix is $\sigma_y = 40000$ psi, the contours of $\overline{\sigma}$ greater than this value belong to the plastic zone. The results shown are for the matrix in which $n = 5$, $\beta = 0.5$, and $\chi = 0.0$. At small fiber volume fractions ($c_f = 20\%$), the B/Al composite initially yields at the fiber/matrix interface along the x_1 axis—see Fig. 8. By increasing the fiber volume fraction in the same material system, the location of the first yield point moves up the fiber/matrix interface such that when $c_f = 45\%$ initial yield takes place at $27°$ from the x_1 axis (Fig. 9). The magnitude of this angle increases to $32°$ when $c_f = 60\%$ (Fig. 10). This clearly indicates that in dilute B/Al composites, the interaction between the fibers does not influence the location of the material point at which plastic deformation initiates, while at large volume fractions the interaction between the fibers alters the location of such a material point so that it ultimately lies at the interface along the line that connects the fiber to its nearest neighbor. In Gr/Al composites, since the transverse modulus of the fiber is significantly lower than that of the matrix, during transverse deformation the fiber behaves similar to a void. For this reason, the location of the material point at which plastic flow commences is not dependent on the fiber volume fraction and yielding always initiates at the fiber/matrix interface along the x_2 axis (Figs. 11-13).

During the subsequent plastic deformation, the development of the plastic zone in B/Al composites is also dependent on the fiber volume fraction. This is such that in $c_f = 20\%$, there will be a second plastic zone along the x_2 axis at step 5th—see Fig. 14—followed by almost general yielding of the unit cell in step 6th—see Fig. 15. The shape of the plastic zone for this fiber volume fraction did not change following the subsequent transverse deformation. In contrast to this, the plastic zone in $c_f = 45\%, 60\%$ develops in a counter clockwise manner from the x_1 to the x_2 axis—see Figs. 16,17. The characteristic feature of the this zone is that

up to step 18 there is a persistent elastic core around the fiber/matrix interface on the x_2 axis. In Gr/Al composites the development of the plastic zone is opposite to that in the B/Al composites; that is, the plastic zone develops in a clockwise manner from the x_2 axis toward the x_1 axis—see Figs. 18-21. In contrast to B/Al composites, the extent of the plastic zone in Gr/Al composites decreases by increasing the fiber volume fraction.

Although the above observations are limited to the particular matrix considered, the results for other types of the matrices indicate the same trend. Thus, the details of the plasticity in the matrix has no significant influence on the development of the plastic zone, and it is the type of the fiber and its volume fraction that influence the development of the such zone.

5.3 Stress-Strain Response

In this section we will discuss the influence of the anisotropy of the microstructure on the variation of the transverse stress with transverse strain. Figures 22 through 24 represent variation of the macroscopic transverse stress with the prescribed transverse strain in B/Al. The parameter χ was zero in all the matrix constitutive relations that were used to obtain the results. These figures reflect the sensitivity of the macroscopic stress-strain relation to the ratio of the isotropic to kinematic hardening β. The results indicate that, irrespective of the fiber volume fraction, reducing β leads to the softening of the predicted stress-strain curve. This is not surprising since by decreasing β, the contribution of the total hardening to the increase in the radius of the yield surface decreases, which in turn leads to reduction in the magnitude of the stress increment. Comparison of Fig. 22 and Fig. 24 indicates that the influence of β becomes more pronounced by increasing the fiber volume fraction. This can be explained by noting that $\bar{\varepsilon}^p$, which is a measure of the amount of the plastic deformation taken place in the matrix, increases by increasing the fiber volume fraction. Thus, since the back stress evolves from zero initial value, at small plastic strains the magnitude of the stress increment is mostly controlled by the isotropic component of the total hardening, while at large plastic strains, due to the generated back stress, the magnitude of the stress increment is influenced by both the isotropic and the kinematic component of the total hardening. For a given β, the increase in fiber volume fraction leads to an increase in the level of the stress-strain curve, compare Fig. 22 with Fig. 24. This can be explained in light of the fact that the transverse elastic modulus of boron is larger than that of aluminum, so that an increase in the fiber volume fraction leads to an increase in the stiffness of the composite in the transverse direction and hence to the increase in the stress levels.

Figures 25 through 27 represent the variation of the macroscopic transverse stress with prescribed transverse strain in Gr/Al. The parameter χ was zero in all the matrix constitutive relations that were used to obtain the results. These figures in general indicate that increasing the fiber volume fraction leads to softening of the material. This is in accordance with the fact that the transverse elastic modulus of graphite is much smaller than that of aluminum so that increase in the fiber volume fraction leads to a decrease in the transverse stiffness of the composite and hence to a decrease of the transverse stress level. Similar to the case of B/Al, the reduction in β leads to a decrease of the macroscopic transverse stress. The influence of β on the overall response is more apparent in small fiber volume fractions. Also similar to the case of B/Al, the increased hardening in the matrix (which is represented by the decrease in the hardening exponent n) leads to an increase in the stress level. The influence of changing n is more dominant in small fiber volume fractions than in the large volume fractions.

Tables 2 through 4 represent the influence of the parameter χ on the average transverse stress at the 18th step. Prior to discussing these results, it is important to recall that in general, incorporating the influence of the spin terms in the evolution of the back stress will alter the stress analysis if and only if the state of deformation is non-proportional. The degree of this influence increases with the increase in the degree of non-proportionality. In light of this observation, we will now examine the results presented in Tables 2-4. First, note that the parameter χ has almost no influence on the results of Gr/Al. This is not surprising since, as was explained previously, the macroscopic average stress of Gr/Al shows very little sensitivity to the type of the plastic constitutive relations in the matrix. This behavior is in contrast to the influence of χ on the response of B/Al. There, incorporating χ in the matrix constitutive relation leads to a decrease of the predicted macroscopic stress. For a given hardening

exponent, the magnitude of the softening is reduced by decreasing the fiber volume fraction. This is in accordance with the fact that in large fiber volume fractions the degree of non-proportionality of the deformation field in the matrix increases, leading to a more dominant influence of the spin term. The results for $n = 10$ (not shown here) indicate that while in large fiber volume fractions ($c_f = 45\%, 60\%$) the influence of the softening due to the induced-spin decreases by decreasing the amount of the hardening in the matrix, i.e. by increasing the hardening exponent, in smaller fiber volume fractions, $c_f = 20\%$, the amount of softening was reduced with decrease in the hardening exponent.

5.4 Overall Instantaneous Moduli

In this section, the influence of the microstructure on the variation of the overall instantaneous moduli with prescribed transverse strain will be discussed. The results presented in these figures are all for the case when $\chi = 0$. Figures 28 through 33 indicate that regardless of the type of the reinforcement, there is a reduction in $\overline{C}_{1111}$ as a result of the plastic deformation in the matrix. These figures also indicate that for each type of metal-matrix composite, the reduction in this modulus will be more pronounced by decreasing β, i.e. by decreasing the isotropic component of the hardening. The numerical results for $n = 10$ show that the influence of β on the overall modulus is more apparent in matrices with small hardening exponent. In spite of the above similarity, there is a fundamental difference in the manner in which the fiber volume fraction influences the reduction of $\overline{C}_{1111}$ in B/Al and in the Gr/Al. In B/Al, increase of the fiber volume fraction increases the reduction of stiffness (Figs. 28,30, and 32). However, in Gr/Al an increase in the fiber volume fraction from 20% to 45% leads to a slight increase in the stiffness reduction, while from 45% to 60% leads to a significant decrease in the reduction of $\overline{C}_{1111}$. The fore-mentioned difference is indicative of the fact that in B/Al,

since the transverse elastic modulus of boron is large compare to that of the matrix, an increase in the fiber volume fraction intensifies the amount of the plastic deformation in the matrix and hence increases the reduction in the overall stiffness, while in Gr/Al, since the transverse modulus of the fiber is smaller than that of the fiber, an increase in the fiber volume fraction lessens the amount of the plastic deformation in the matrix. For a given fiber volume fraction, the type of the fiber has also a significant influence on the reduction of C_{1111}. In small fiber volume fractions, there is a more dramatic stiffness reduction in Gr/Al compared to in B/Al— see Figs. 28,29. However, this changes as the fiber volume fraction increases, such that in $c_f = 60\%$ there is more reduction in B/Al compare to Gr/Al— see 32,33. In view of the previous discussion, this is to be expected, since the influence of the plastic deformation in Gr/Al is more pronounced in small fiber volume fractions, while in B/Al it is more dramatic in large fiber volume fractions.

Figures 34 through 39 show the variation of $\overline{C}_{2222}$ with the prescribed transverse strain in B/Al and Gr/Al. All of the above observations on the behavior of $\overline{C}_{1111}$ also hold for $\overline{C}_{2222}$. Comparison of these figures with those corresponding to $\overline{C}_{1111}$ indicates that following the onset of the plastic deformation, the transverse isotropy of the effective moduli of the composite will be lost. This implies that utilization of the transversely isotropic plastic potentials in modeling the overall plastic deformation of the composite is not appropriate, and one has to take account of the induced anisotropy in the transverse direction due to the asymmetric development of the plastic zone.

Figures 40 through 45 represent the variation of $\overline{C}_{1122}$ with the prescribed transverse deformation in B/Al and Gr/Al. The results corresponding to B/Al indicate that the modulus

$\overline{C}_{1122}$ increases by increasing the prescribed transverse strain. The magnitude of this increase will be reduced by increasing β. In contrast to this, the variation of $\overline{C}_{1122}$ with prescribed deformation in Gr/Al is very much dependent on the size of the fiber volume fraction. This dependence is such that in $c_f = 20\%$, Fig. 41, and $c_f = 45\%$, Fig. 42, the $\overline{C}_{1122}$ modulus slightly decreases initially and then increases and finally drops, while in $c_f = 60\%$, Fig. 45, it continuously drops. The magnitude of the final drop in the modulus decreases by increasing the isotropic component of the total hardening.

Figures 46 through 51 show the variation of the transverse shear modulus, $\overline{C}_{1212}$ with the prescribed transverse strain. In both composite systems, this modulus drops with the monotonic increase in the prescribed deformation. The magnitude of this reduction decreases by increasing the isotropic component of the hardening. For a given fiber volume fraction, the drop of the transverse shear modulus is more pronounced in Gr/Al than in B/Al, for example compare 46,47. For fiber volume fractions up to $c_f = 45\%$, the reduction of the transverse shear modulus of B/Al decreases monotonically by increasing the fiber volume fraction; compare 46,48,50, while in Gr/Al, it increases. Further increase of the fiber volume fraction leads to small changes in the overall transverse shear modulus.

Figures 52 through 57 show the variation of $\overline{C}_{1133}$ with prescribed transverse strain in B/Al and Gr/Al. Figure 52 indicates that in B/Al this modulus initially increases and then drops. In contrast to this, $\overline{C}_{1133}$ of Gr/Al will continuously decrease with prescribed transverse strain; see Fig. 53. In B/Al the magnitude of the total change of this modulus will not exceed 7%, while it can reach as high as 26% in Gr/Al. For both material systems, the drop of $\overline{C}_{1133}$ will decrease by increasing the isotropic component of the hardening. The variation of the

axial modulus $\overline{C}_{3333}$ in both material systems was observed to be negligible.

.

CONCLUSIONS

A consistent homogenization method has been used to study the influence of the anisotropy in the microstructure on the overall response of fibrous metal-matrix composites. In formulating the numerical method for determining the effective properties of the composite, our study has shown that the prescribed boundary conditions of the periodic functions, which are needed to relate the fluctuating velocity field inside the unit cell to the overall strain rate, have a significant influence on the instantaneous overall properties. In the current study, we chose the boundary conditions that led to the coincidence of the mesh for both the unit cell problem and the micro-boundary value problem.

The results indicate that for a given fiber volume fraction, the type of the reinforcement has the strongest influence on the overall response. This is not surprising since the properties of the fiber strongly influence the concentration of the velocity gradient and stress field around the fiber/matrix interface which in turn influence the average of the field variables over the unit cell. The other parameter which can also influence the overall instantaneous moduli is the hardening exponent of the matrix. This influence is such that decreasing the isotropic component of the total hardening enhances reduction of the overall instantaneous moduli which takes place during the prescribed transverse straining of the composite. For the particular deformation state considered here, the results clearly demonstrate that while inclusion of the influence of the spin term in the evolution of the back stress softens the effective response of B/Al composite in the transverse direction, such terms have very little influence on the overall response of Gr/Al.

An immediate extension of the current study is the inclusion of the influence of the possible large material rotations which can take place at the inclusion/matrix interface of certain fibrous metal-matrix composites, particularly those in which the transverse modulus of the fiber is much higher than that of the matrix.

A more important contribution to the micromechanical analysis of fibrous metal-matrix composites is the development of averaging methods in cases where the overall stress (strain) field is nonhomogeneous. This problem poses a fundamental dilemma from the point of view that in such cases one needs a discriminating criterion for assessing the influence of the higher order terms in the asymptotic expansions that are used to obtain the effective moduli.

Acknowledgements

REFERENCES

Abeyaratne, R. and N. Triantafyllidis (1984), "An investigation of localization in a porous elastic material using homogenization theory," *J. Appl. Mech.*, **51**, 481-486.

Agah-Tehrani, A., E. H. Lee, R. L. Mallett and E. T. Onat (1987), "The theory of plastic deformation at finite strain with induced anisotropy modeled as combined isotropic-kinematic hardening," *J. Mech. Phys. Solids*, **35**, 519-539.

Benssoussan, A., J. L. Lions and G. Papanicoliou (1978), *Asymptotic analysis for periodic structures*, North-Holland Publishing Co., Amsterdam.

Dvorak, G. J. and J. Teply (1985), "Periodic hexagonal array models for plasticity analysis of composite materials," in *Plasticity Today: Modeling, Methods, and Application*, ed. A. Sawczuk, Elsevier, 623.

Dvorak, G. J., Y. A. Bahei-El-Din, Y. Macheret and C. H. Liu (1988), "An experimental study of elastic-plastic behavior of a fibrous boron-aluminium composite," *J. Mech. Phys. Solids*, **36**, 655-687.

Franciosi, P., M. Berveiller and A. Zaoui (1980), "Latent hardening in copper and aluminium single crystals," *Acta Metall.*, **28**, 273-283.

Hill, R. (1963), "Elastic properties of reinforced solids: some theoretical principles," *J. Mech. Phys. Solids*, **11**, 357-372.

Kocks, U. F. and T. J. Brown (1966), "Latent hardening in aluminium," *Acta Metall.*, **14**, 87-98.

Lee, E. H., R. L. Mallett and T. B. Wertheimer (1983), "Stress analysis for anisotropic hardening in finite deformation plasticity," *J. Appl. Mech.*, **50**, 554-560.

Lions, J. L. (1978), "Remarks on some asymptotic problems in composite and in perforated materials," in *Variational Methods in the Mechanics of Solids*, Ed. Nemat-Nasser, Pergamon Press, Oxford, 3-19.

Mallett, R.L. (1985), "Finite increment formulation of the Prandtl-Reuss constitutive equations," Trans. 2nd Army Conf. on Applied Mathematics and Computing, Rensselear Polytechnic Institute, 285-301.

Martin, J. B. (1975), *"Plasticity: Fundamentals and General Results,"* MIT press, 796-822.

Mroz, Z., H. P. Shrivastava and H. P. Dubey (1976), "A Non-Linear hardening and its application to cyclic loading," *Acta Mechanica*, 15, 51-61.

Murakami, H. and G. A. Hegemier (1986), "A mixture model for unidirectionally fiber-reinforced composites," *J. Appl. Mech.*, 53, 765-773.

Needleman, A. (1972), "Void growth in an elastic-plastic medium," *J. Appl. Mech.*, 39, 964-970.

Nemat-Nasser, S., T. Iwakuma, and M. Hejazi (1982), "On composites with periodic structure," *Mech. Materials*, 1, 239-267.

Sanchez-Palencia, E. (1980), Non-homogeneous medium and vibration theory, Lecture Notes in Physics, No. 127, Springer-Verlag Publishing Co., Berlin.

Suh, Y. S., A. Agah-Tehrani (1989), "Stress analysis of axisymmetric extrusion in the presence of strain-induced anisotropy modeled as combined isotropic-kinematic hardening," submitted to *Comp. Meth. Appl. Mech. Engng*.

Taylor, G. I. and C. F. Elam (1923), "The distortion of an aluminium crystal during a tensile test," *Proc R. Soc. London*, Series A, 102, 643-667.

Taylor, G. I. and C. F. Elam (1925), "The Plastic deformation and fracture of aluminium crystals," *Proc. R. Soc. Lond,* Series A, **108,** 28-51.

Teply, J. L. and G. J. Dvorak (1988), "Bounds on overall instantaneous properties of elastic-plastic composites," *J. Mech. Phys. Solids,* **36,** 29-58.

Willis, J. R. (1981), "Variational and related methods for overall properties of composites," *Advances in Applied Mechanics,* **21,** 1-78.

APPENDIX A

In this Appendix we present some of the implications of the variation of macroscopic velocity gradient on the development of the homogenization method. It is assumed that the nature of these variations are such that one can still identify two length scales in the medium. Thus, we are excluding problems which involve a macroscopic crack, or the emergence of regions across which large changes in the velocity gradient takes place. In order for the analysis to be valid for arbitrary deformations, the rate equilibrium equations will be expressed in terms of the material derivative of the nominal stress, $\dot{S}$. These equations will be complemented by the constitutive relations which relate $\dot{S}$ to its conjugate kinematic variable $\dot{F}$ which is the material derivative of the velocity gradient. It is assumed that these constitutive relations can be obtained from the derivatives of a potential $U^{(e)}$. By considering an updated Lagrangian formulation these constitutive relations will be

$$\dot{S}_{ij}^{(e)} = \frac{\partial U^{(e)}}{\partial L_{ji}^{(e)}} \tag{A.1}$$

or

$$\dot{S}_{ij}^{(e)} = C_{ijkl}(x,y)L_{lk}^{(e)} \tag{A.2}$$

with $C_{ijkl} = C_{klij}$ and $L_{lk}^{(e)}$ as the velocity gradient $(\partial v_l^{(e)}/\partial x_k)$.

It is important to note that because of the variations in the macroscopic velocity gradient the potential $U^{(e)}$ depends on both the macroscopic and the microscopic coordinates. The rate equilibrium equations will be

$$\frac{\partial \dot{S}_{ij}^{(e)}}{\partial x_i} = 0 . \tag{A.3}$$

By expressing the above field variables as asymptotic expansions in terms of ε and substituting these series into the expression for the velocity gradient and (A.1,2,3), one can arrive at the following conclusions:

$$\frac{\partial v_i^{(0)}}{\partial y_k} = 0 , \tag{A.4}$$

$$L_{ik}^{(\varepsilon)} = (\frac{\partial v_i^{(0)}}{\partial x_k} + \frac{\partial v_i^{(1)}}{\partial y_k}) + \varepsilon(\frac{\partial v_i^{(1)}}{\partial x_k} + \frac{\partial v_i^{(2)}}{\partial y_k}) + \cdots\cdots , \tag{A.5}$$

$$\acute{S}_{ij}^{(0)} = C_{ijkl}(\frac{\partial v_i^{(0)}}{\partial x_k} + \frac{\partial v_i^{(1)}}{\partial y_k}) , \tag{A.6}$$

$$\acute{S}_{ij}^{(1)} = C_{ijkl}(\frac{\partial v_i^{(1)}}{\partial x_k} + \frac{\partial v_i^{(2)}}{\partial y_k}) , \tag{A.7}$$

$$U^{(\varepsilon)} = \frac{1}{2}(v_{j,i(x)}^{(0)} + v_{j,i(y)}^{(1)})C_{ijkl}(v_{l,k(x)}^{(0)} + v_{l,k(y)}^{(1)}) +$$

$$\frac{\varepsilon}{2}[(v_{j,i(x)}^{(0)} + v_{j,i(y)}^{(1)})C_{ijkl}(v_{l,k(x)}^{(1)} + v_{l,k(y)}^{(2)}) +$$

$$(v_{j,i(x)}^{(1)} + v_{j,i(y)}^{(2)})C_{ijkl}(v_{l,k(x)}^{(0)} + v_{l,k(y)}^{(1)})] + \cdots\cdots . \tag{A.8}$$

$$\frac{\partial \acute{S}_{ij}^{(0)}}{\partial y_i} = 0 , \quad \frac{\partial \acute{S}_{ij}^{(1)}}{\partial y_i} = -\frac{\partial \acute{S}_{ij}^{(0)}}{\partial x_i} . \tag{A.9}$$

By assuming periodicity of the variables over the unit cell, the 1st micro equilibrium equation in (A.9) can be used to obtain

$$v_i^{(1)} = \Psi_i^{rs}(x,y) L_{rs}^{(0)} , \tag{A.10}$$

In the above representation, we have assumed that Ψ_i^{rs} are zero on the boundary of the unit cell. This assumption eliminates the need for introducing the additional terms which only depend on the macroscopic coordinates. By substituting (A.10) into (A.7) and using the result in the second micro equilibrium equation of (A.9), one obtains

$$\frac{\partial}{\partial y_i}(C_{ijkl}v^{(2)}_{l,k(y)}) = B_{jpqk}\frac{\partial L^{(0)}_{pq}}{\partial x_k} \quad , \tag{A.11}$$

where

$$B_{jpqx} = -\frac{\partial}{\partial y_i}\left\{C_{ijkl}\left[\frac{\partial \Psi_l^{rs}}{\partial L^{(0)}_{pq}}L^{(0)}_{rs} + \Psi_l^{pq}\right]\right\} - C_{kjqp} - $$

$$\frac{\partial C_{kjmn}}{\partial L^{(0)}_{pq}}[L^{(0)}_{nm} + \Psi^{rs}_{n,m(y)}L^{(0)}_{rs}]$$

$$-C_{kjmn}\Psi^{pq}_{n,m(y)} - C_{kjmn}\frac{\partial \Psi^{rs}_{n,m(y)}}{\partial L^{(0)}_{pq}}L^{(0)}_{rs} \quad . \tag{A.12}$$

If the above equation can be used to determine $v^{(2)}$ in terms of the variation of the overall velocity gradient such that

$$v^{(2)}_i = \Phi^{pqr}_i\frac{\partial L^{(0)}_{pq}}{\partial x_r} \quad , \tag{A.13}$$

then one can determine the average of $U^{(\epsilon)}$ to obtain

$$\overline{U}^{(\epsilon)} = \frac{1}{2}L^{(0)}_{rs}\overline{C}_{rstu}L^{(0)}_{tu} + \frac{\epsilon}{2}\left[L^{(0)}_{rs}\overline{T}_{rspqt}\frac{\partial L^{(0)}_{pq}}{\partial x_t} + \frac{\partial L^{(0)}_{pq}}{\partial x_t}\overline{T}_{pqtrs}L^{(0)}_{rs}\right] + O(\epsilon^2) \quad , \tag{A.14}$$

where

$$\overline{C}_{rstu} = \int_A P_{jirs}C_{ijkl}P_{lktu}dA \quad , \tag{A.15}$$

$$P_{jirs} = I_{jirs} + \Psi^{rs}_{j,i(y)} \quad , \tag{A.16}$$

$$\overline{T}_{rspqt} = \int_A P_{jirs} C_{ijkl} R_{lkpqt} \quad , \tag{A.16}$$

$$R_{lkpqt} = \left(\psi_l^{pq} + \frac{\partial \Psi_l^{mn}}{\partial L_{pq}^{(0)}} L_{mn}^{(0)} \right) \delta_{lk} + \Phi_{l,k(y)}^{pqt} \quad . \tag{A.17}$$

The above expression for the average energy yields the following macroscopic constitutive relation:

$$<\dot{S}_{ij}^{(e)}> = \overline{C}_{ijkl} L_{lk}^{(0)} + \varepsilon \overline{T}_{ijpqt} \frac{\partial L_{pq}^{(0)}}{\partial x_t} \quad . \tag{A.18}$$

The above equation reflects the fact that in materials with non-linear microstructure, the non-homogeneity of the macroscopic field leads to the emergence of the non-local terms whose structure were not present at the micro level. The macroscopic equilibrium equations can be shown to be

$$\frac{\partial <\dot{S}_{ij}^{(0)}>}{\partial x_i} + \varepsilon \frac{\partial <\dot{S}_{ik}^{(1)}>}{\partial x_i} = 0 \quad . \tag{A.19}$$

	E_A $(10^6$ psi $)$	G_A $(10^6$ psi $)$	ν_A	E_T $(10^6$ psi $)$	G_T $(10^6$ psi $)$
6061 Aluminum	10.5	3.95	0.33	10.5	3.95
Boron	58.0	24.2	0.20	58.0	24.2
T-50 Graphite	56.0	2.2	0.41	1.1	0.38

Table 1   Elastic Properties of Matrix and the Fibers

(a)

χ \ β	1.0	0.7	0.5	0.2
0.0	65544.13	63158.44	61530.82	59030.76
-4.0	65544.13	63148.67	61512.12	58991.75

(b)

χ \ β	1.0	0.7	0.5	0.2
0.0	47282.44	46274.01	45581.17	44506.77
-4.0	47282.44	46274.96	45582.92	44510.04

Table 2

The dependence of the average stress $< \sigma_{11} >$ on χ. The values are taken at step 18. $c_f = 20\%$, $n = 5$. (a) and (b), respectively, represent the results for the B/Al and Gr/Al.

(a)

χ \ β	1.0	0.7	0.5	0.2
0.0	77099.26	73430.76	70935.57	67115.71
-4.0	77099.26	73348.54	70783.46	66819.03

(b)

χ \ β	1.0	0.7	0.5	0.2
0.0	34622.04	34166.45	33851.95	33362.94
-4.0	34622.04	34166.50	33852.06	33363.19

Table 3

The dependence of the average stress $< \sigma_{11} >$ on χ. The values are taken at step 18. $c_f = 45\%$, $n = 5$. (a) and (b), respectively, represent the results for the B/Al and Gr/Al.

(a)

β χ	1.0	0.7	0.5	0.2
0.0	90871.1	85519.4	81870.24	76267.33
-4.0	90871.1	85000.03	80902.69	74361.07

(b)

β χ	1.0	0.7	0.5	0.2
0.0	27260.81	26987.13	26794.79	26491.21
-4.0	27260.81	26987.15	26794.83	26491.38

Table 4

The dependence of the average stress $< \sigma_{11} >$ on χ. The values are taken at step 18. $c_f = 60\%$, $n = 5$. (a) and (b), respectively, represent the results for the B/Al and Gr/Al.
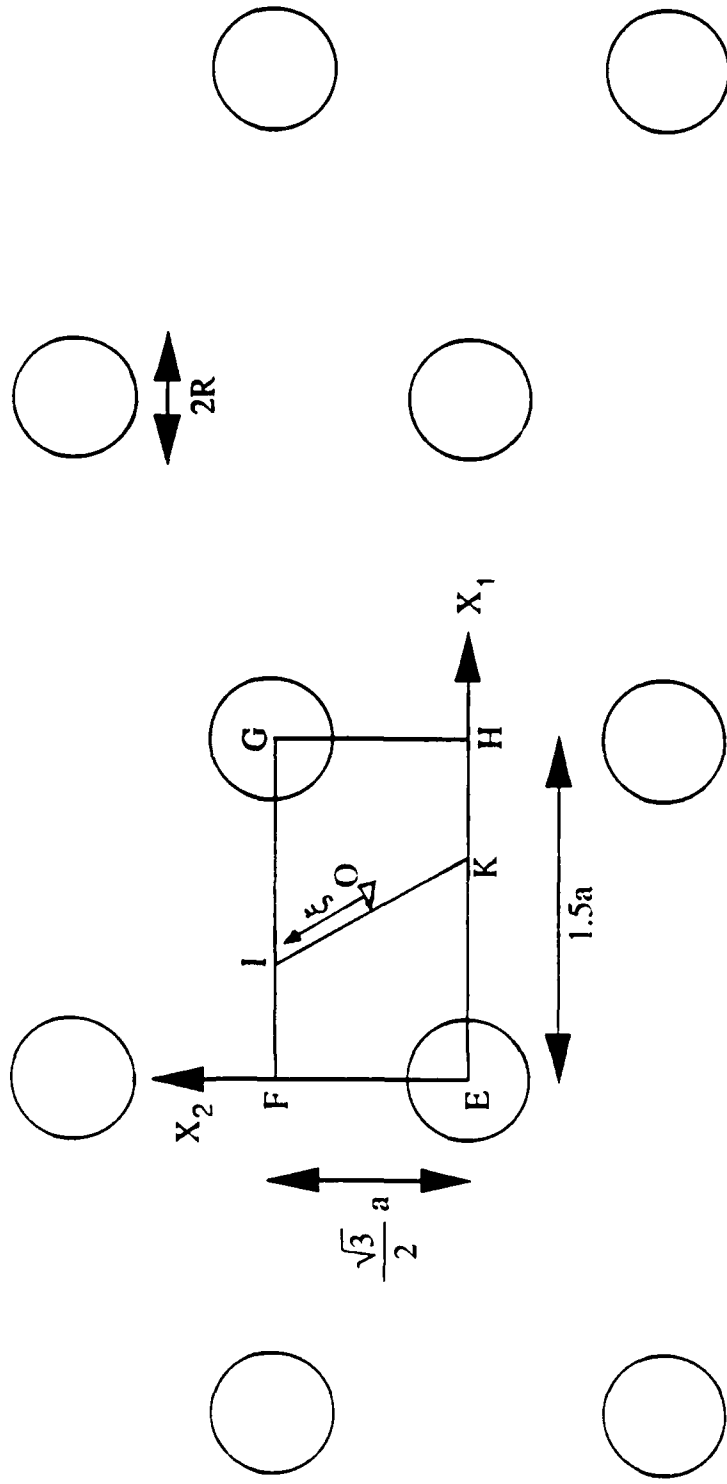
Fig. 1. Hexagonal periodic array of circular cylindrical fibers
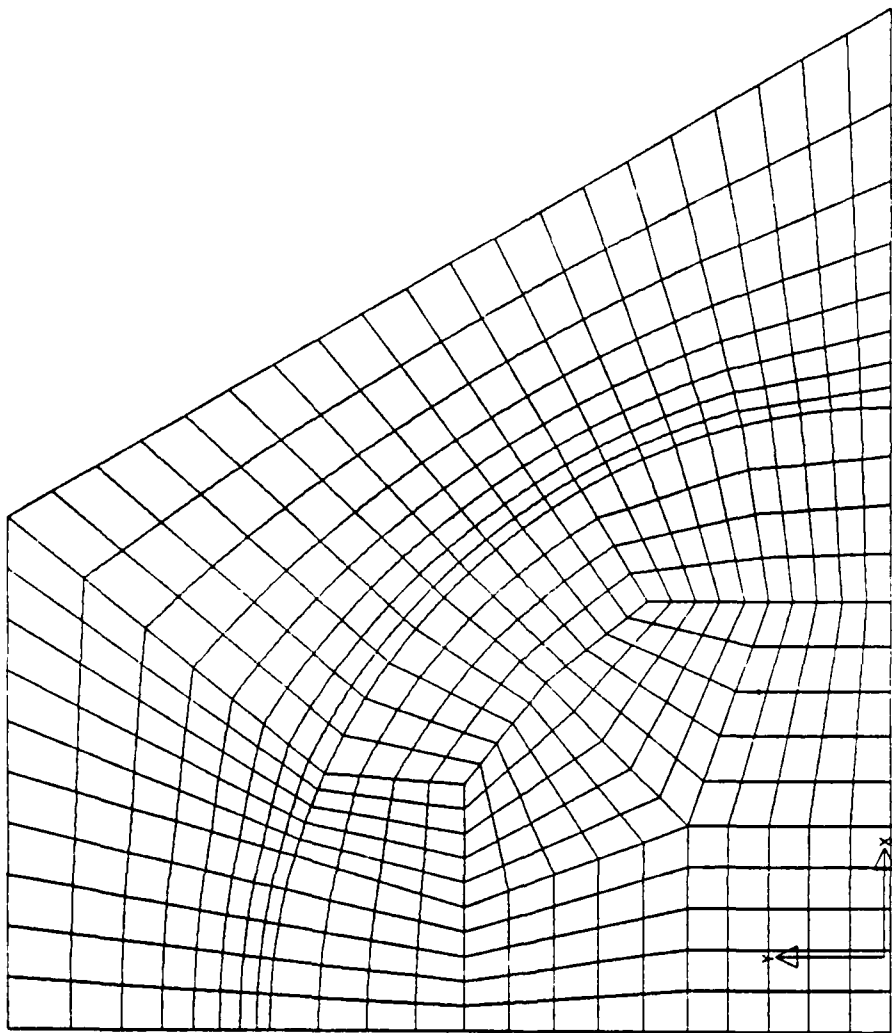
Fig. 2. The finite element mesh for $c_f = 45 \%$
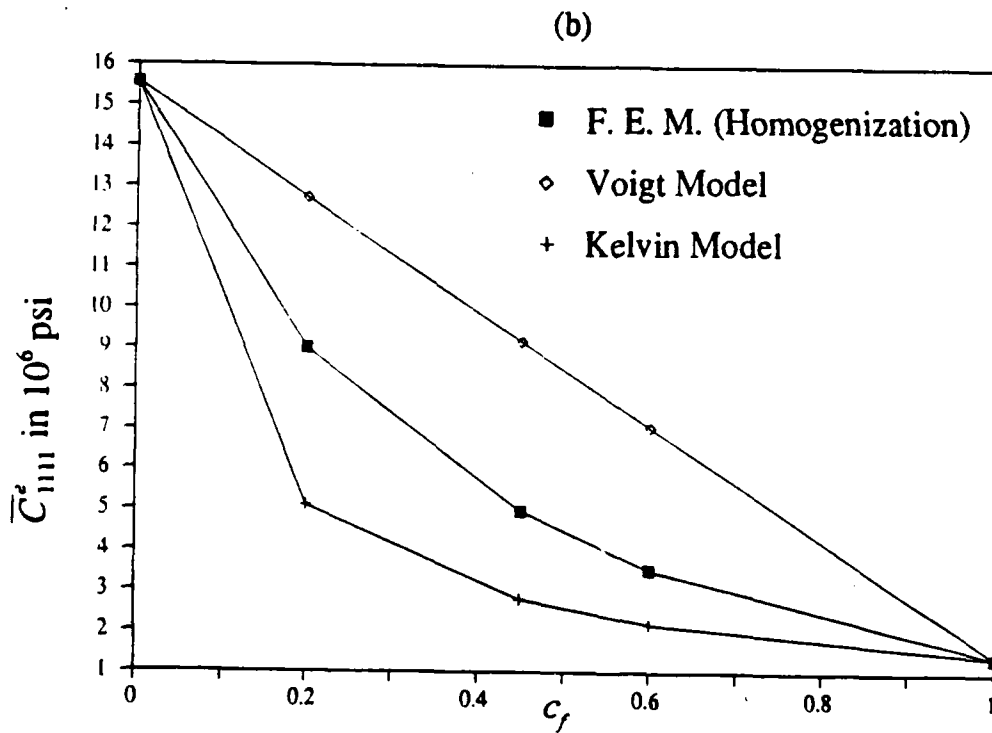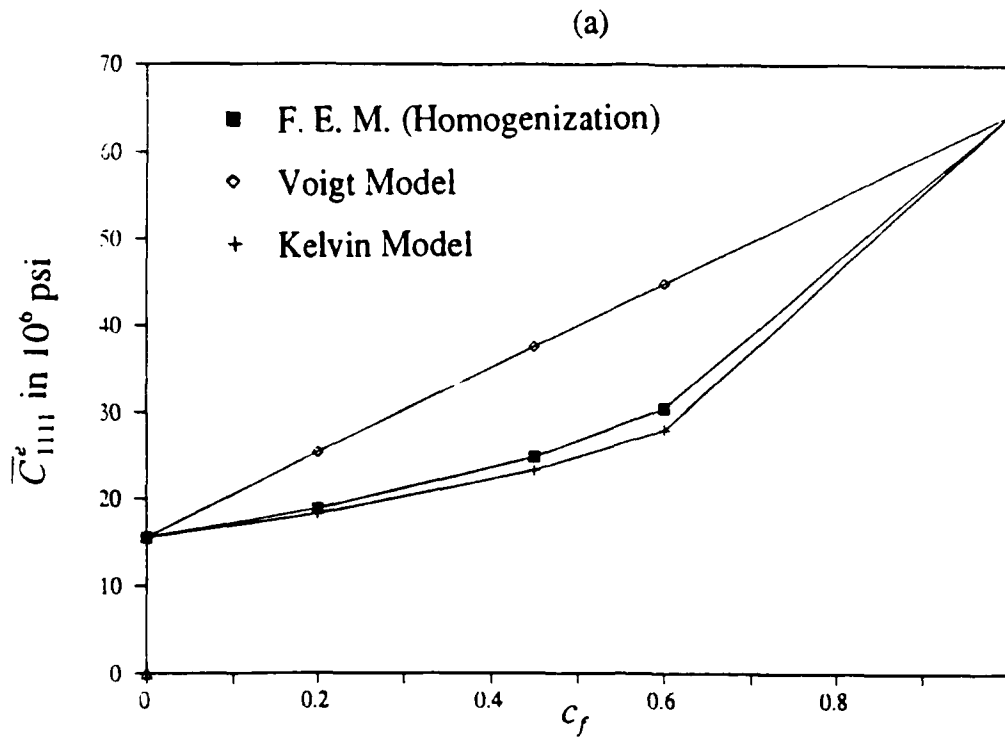
Fig. 3. Variation of the composite elastic moduli $\overline{C}^e_{1111}$ with fiber volume fraction c_f. (a) and (b), respectively, represent the results for the B/Al and Gr/Al.
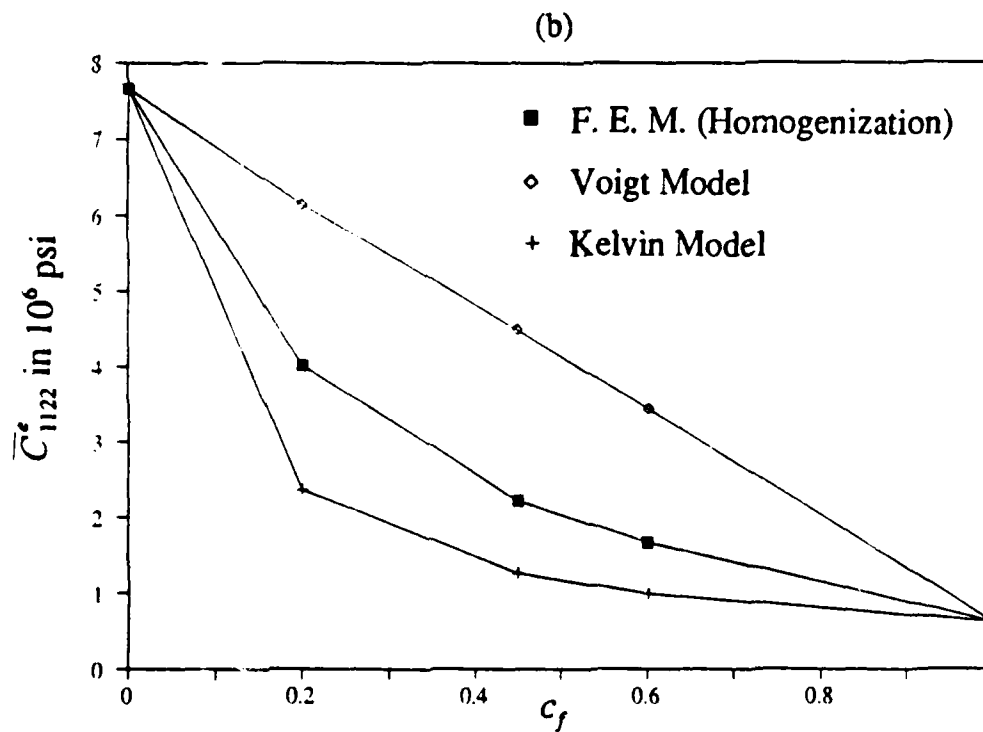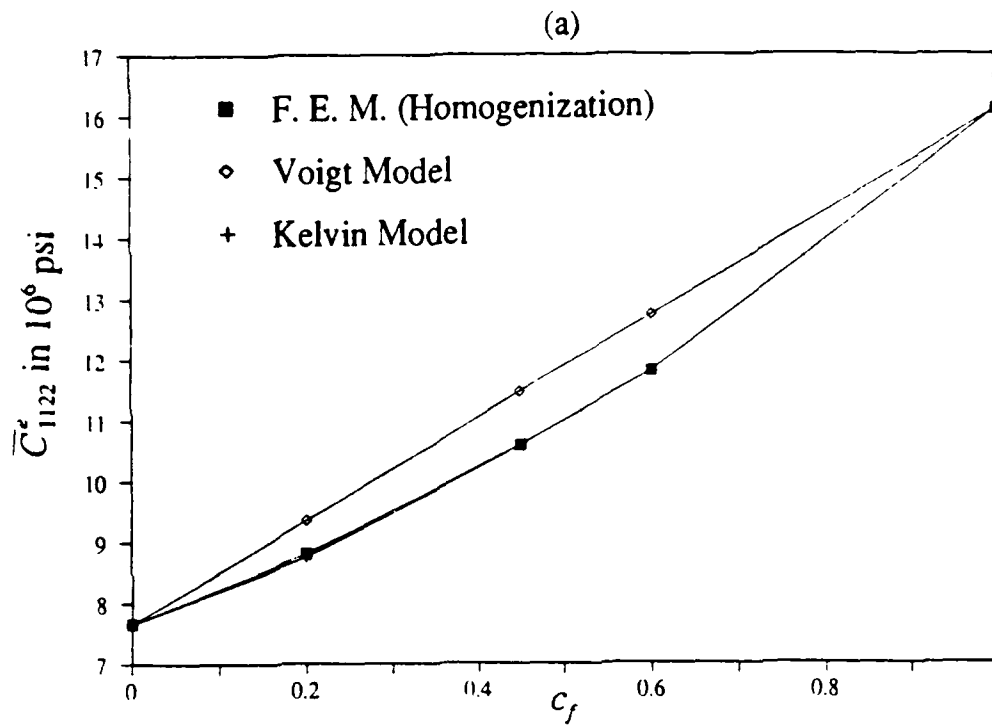
Fig. 4. Variation of the composite elastic moduli $\overline{C}^e_{1122}$ with fiber volume fraction c_f. (a) and (b), respectively, represent the results for the B/Al and Gr/Al.

(a)

$\overline{C}^e_{1212}$ in 10^6 psi

- ■ F. E. M. (Homogenization)
- ◊ Voigt Model
- + Kelvin Model

c_f

(b)

$\overline{C}^e_{1212}$ in 10^6 psi

- ■ F. E. M. (Homogenization)
- ◊ Voigt Model
- + Kelvin Model

c_f
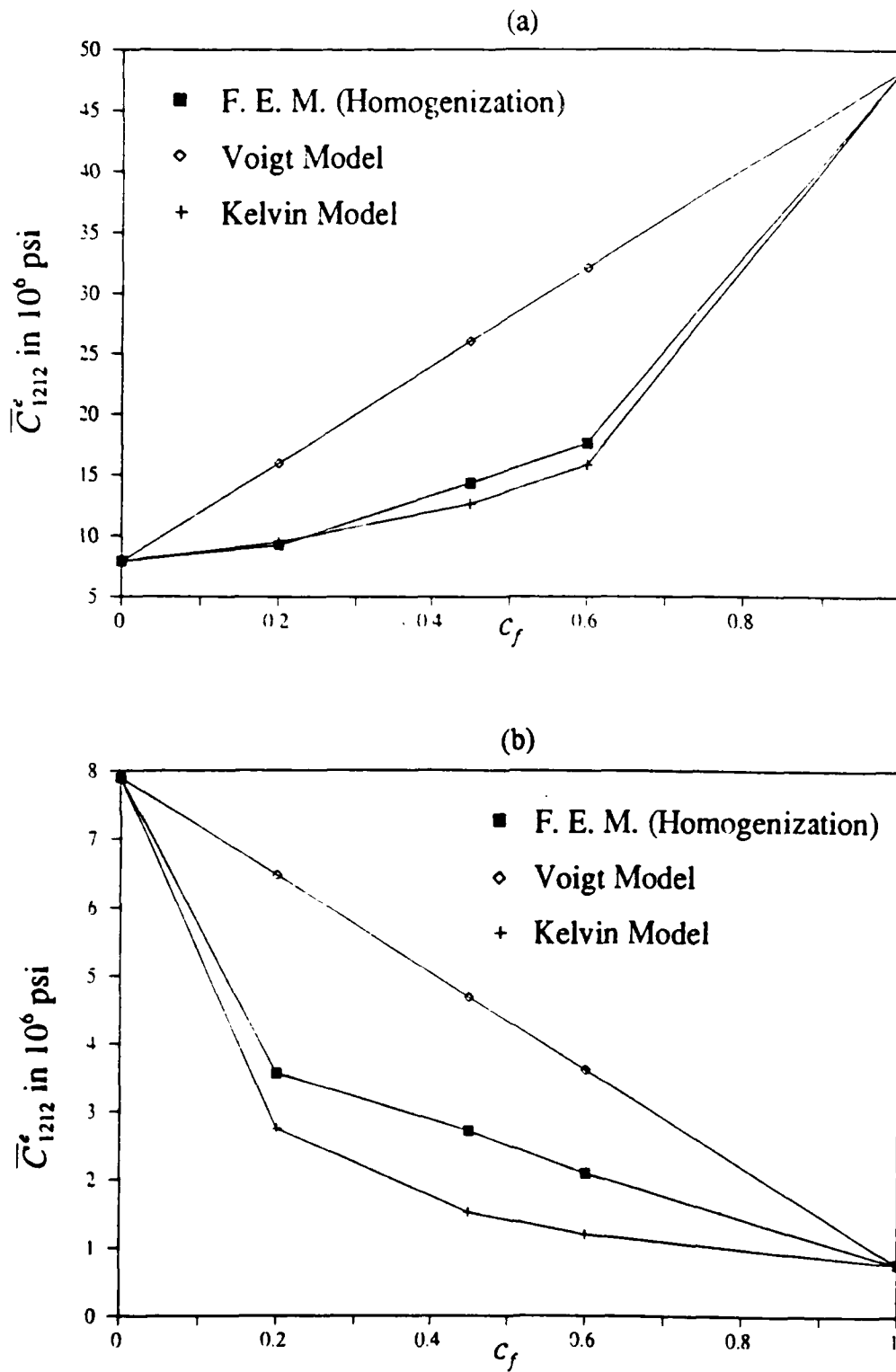
Fig. 5. Variation of the composite elastic moduli $\overline{C}^e_{1212}$ with fiber volume fraction c_f. (a) and (b), respectively, represent the results for the B/Al and Gr/Al.
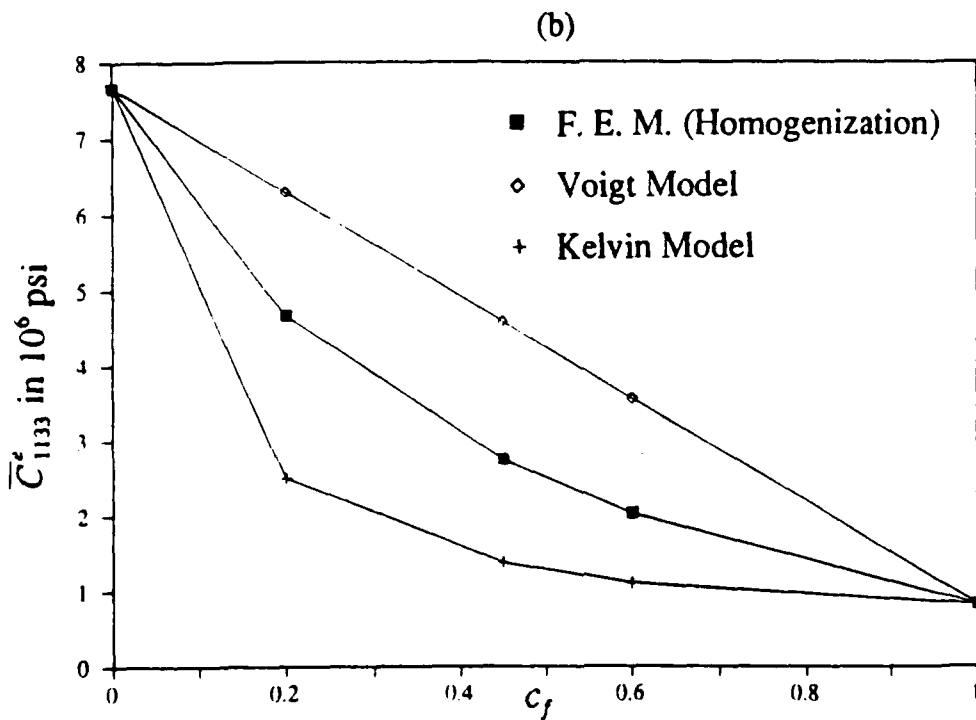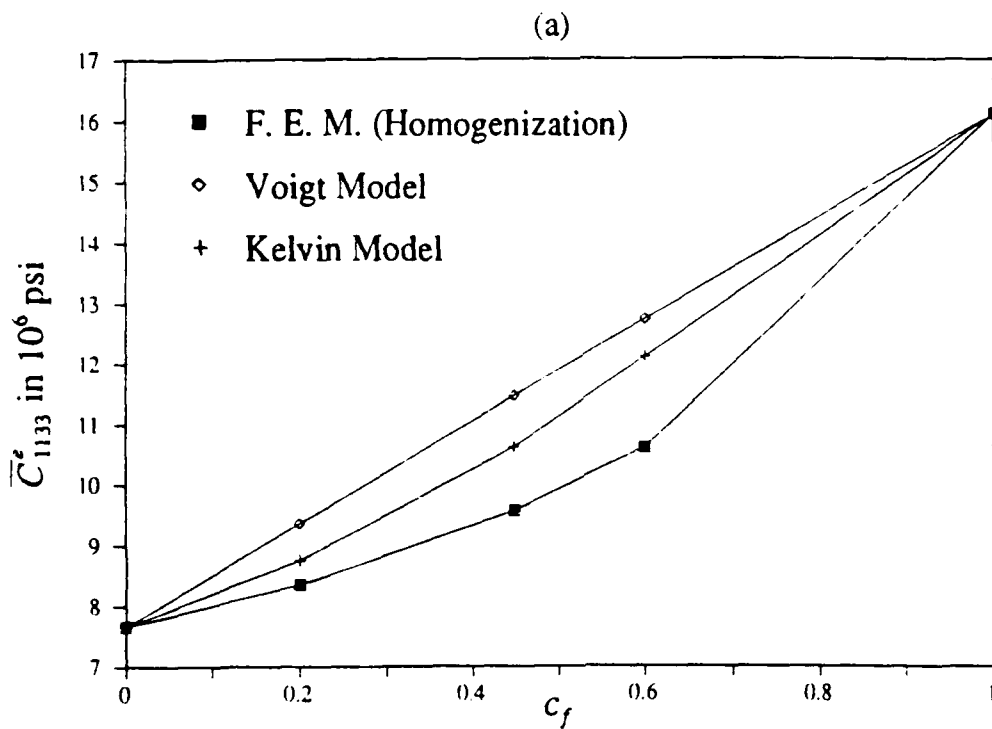
Fig. 6. Variation of the composite elastic moduli $\overline{C}^e_{1133}$ with fiber volume fraction c_f. (a) and (b), respectively, represent the results for the B/Al and Gr/Al.
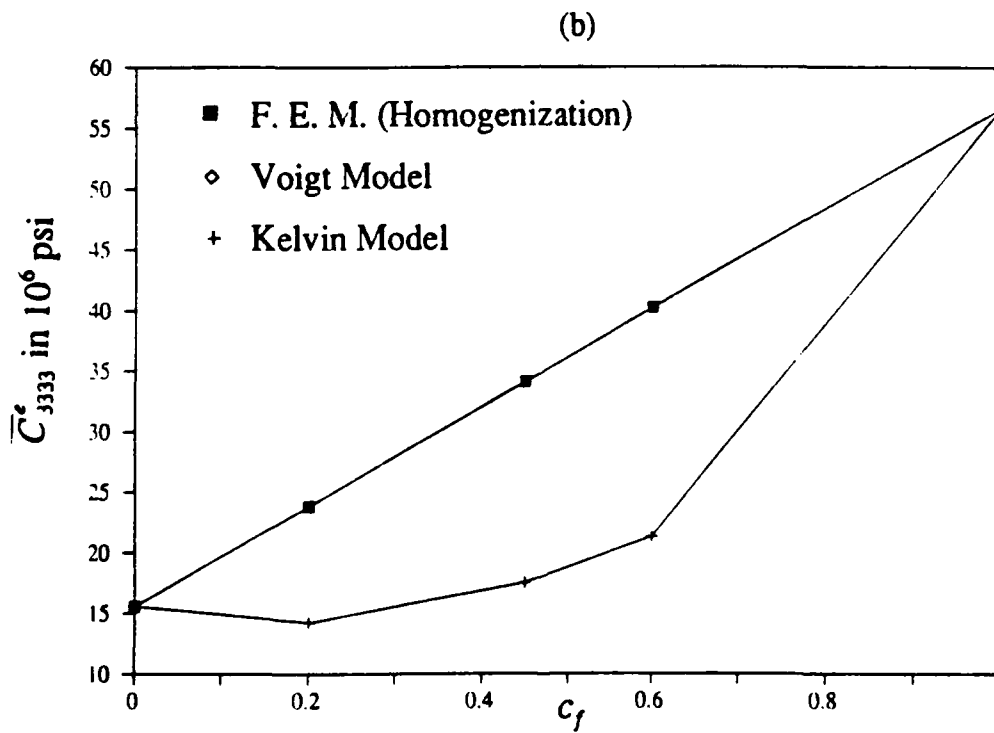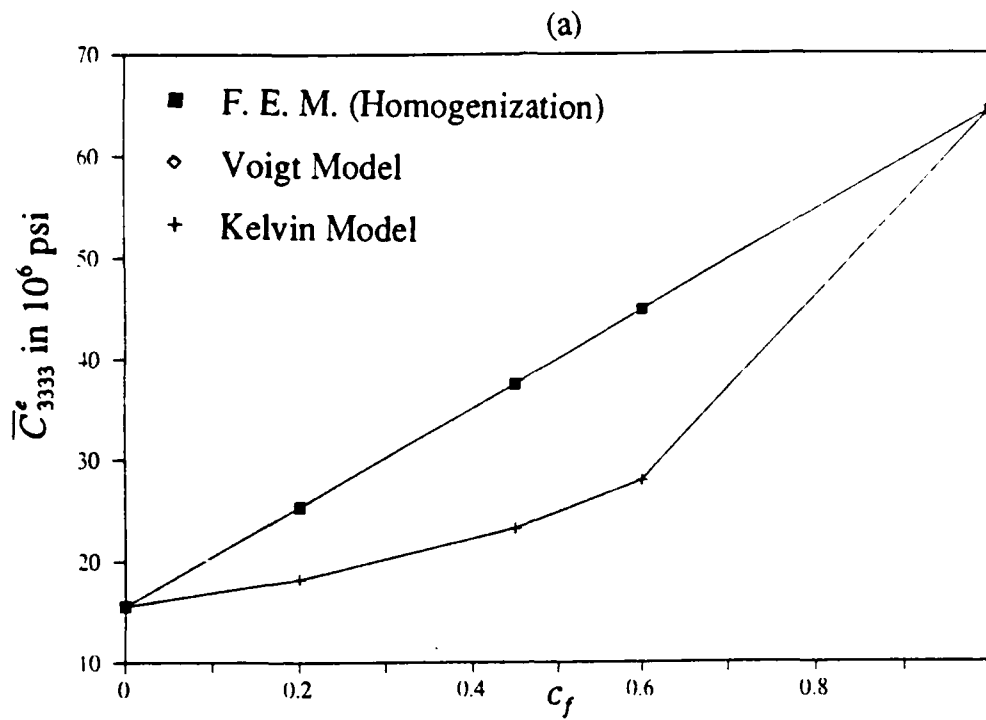
Fig. 7. Variation of the composite elastic moduli $\overline{C}^e_{3333}$ with fiber volume fraction c_f. (a) and (b), respectively, represent the results for the B/Al and Gr/Al.
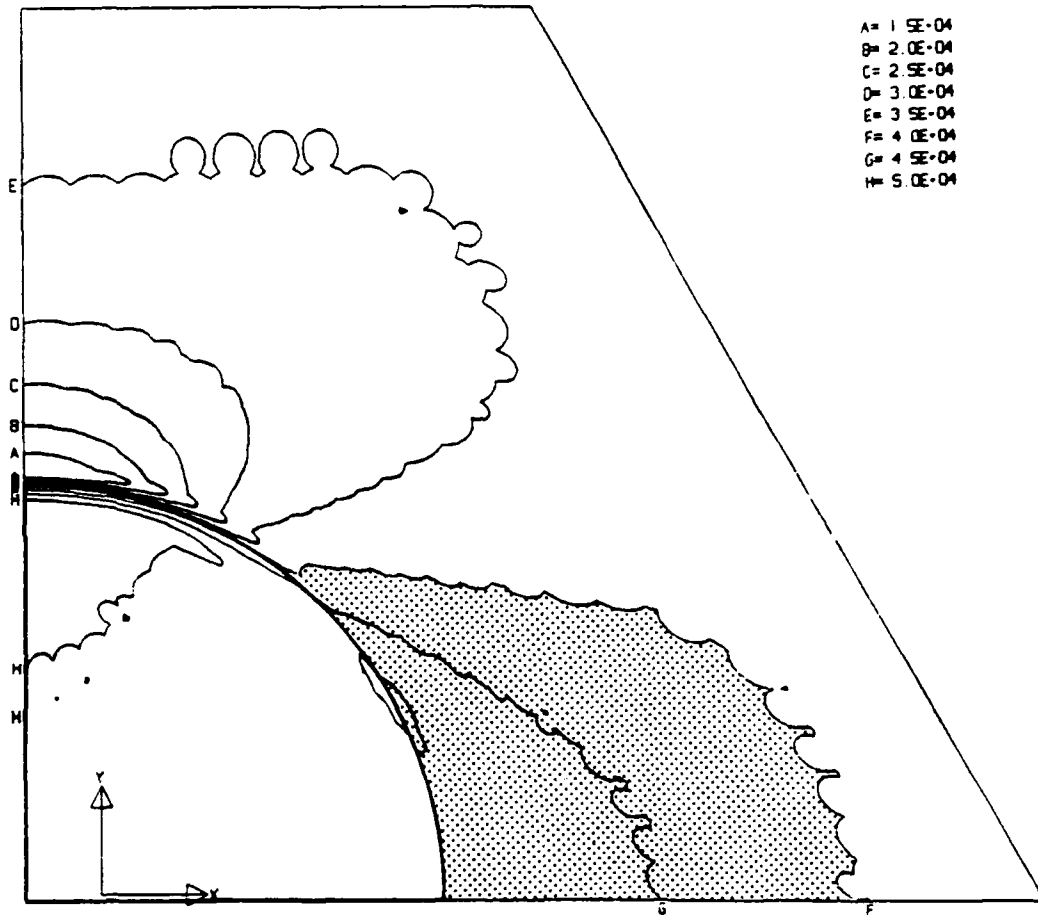
Fig.8. Contour of equivalent stress $\bar{\sigma}$ in B/Al at 4th step. $c_f = 20\%$, $n = 5$, $\beta = 0.5$, and $\chi = 0.0$. The dotted region represents the plastic zone.
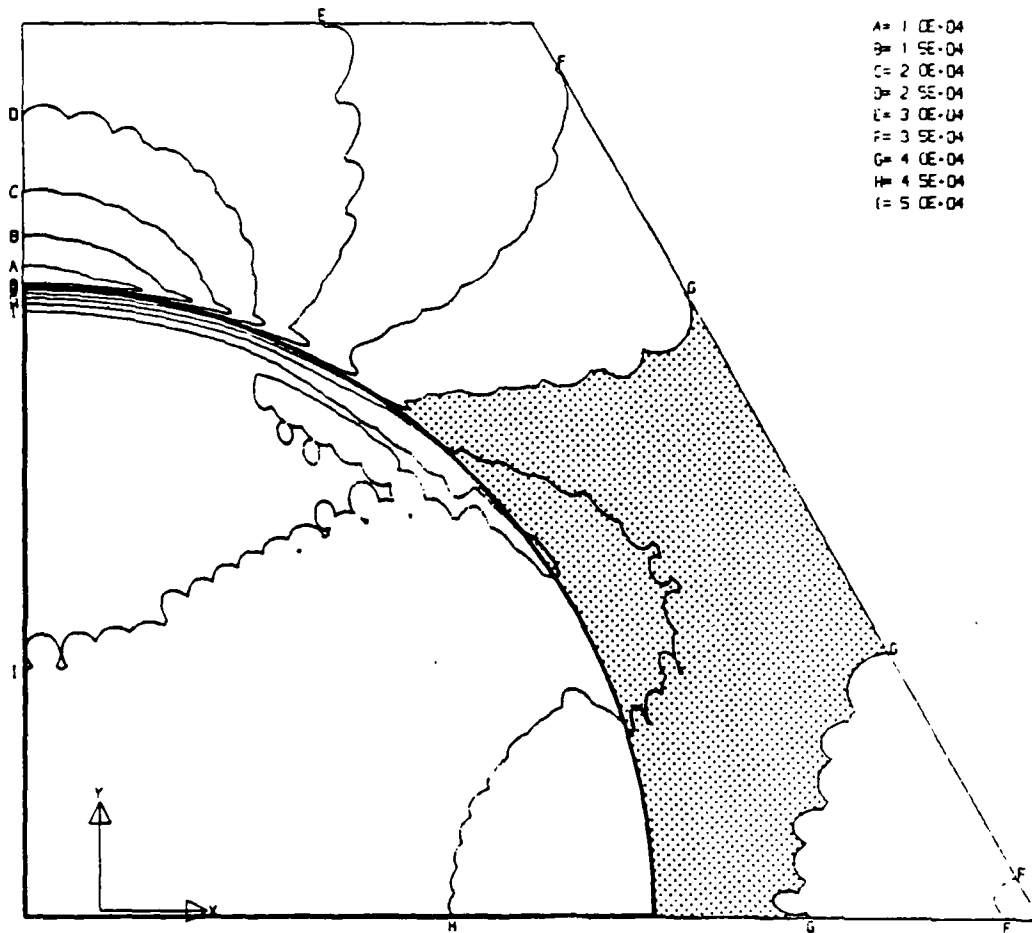
Fig.9. Contour of equivalent stress $\bar{\sigma}$ in B/Al at 3rd step. $c_f = 45\%$, $n = 5$, $\beta = 0.5$, and $\chi = 0.0$. The dotted region represents the plastic zone.
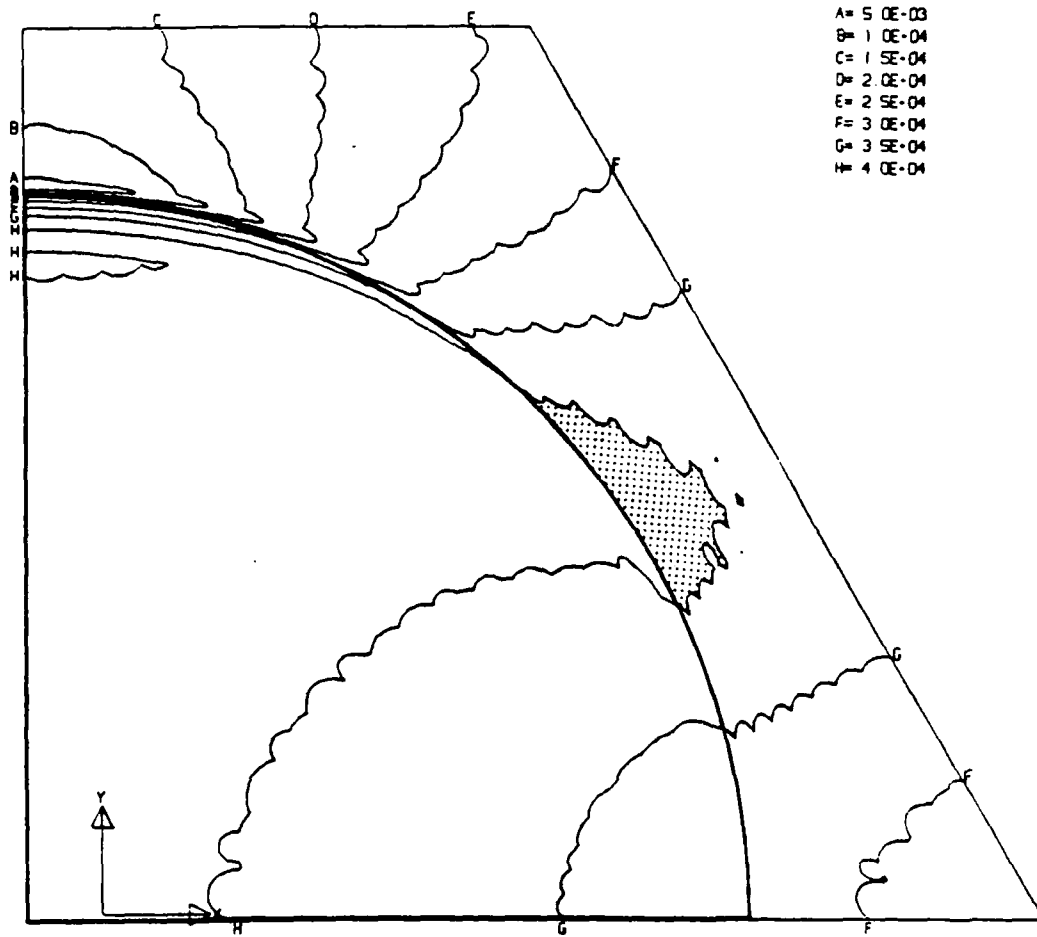
Fig.10. Contour of equivalent stress $\bar{\sigma}$ in B/Al at 2nd step. $c_f = 60\%$, $n = 5$, $\beta = 0.5$, and $\chi = 0.0$. The dotted region represents the plastic zone.
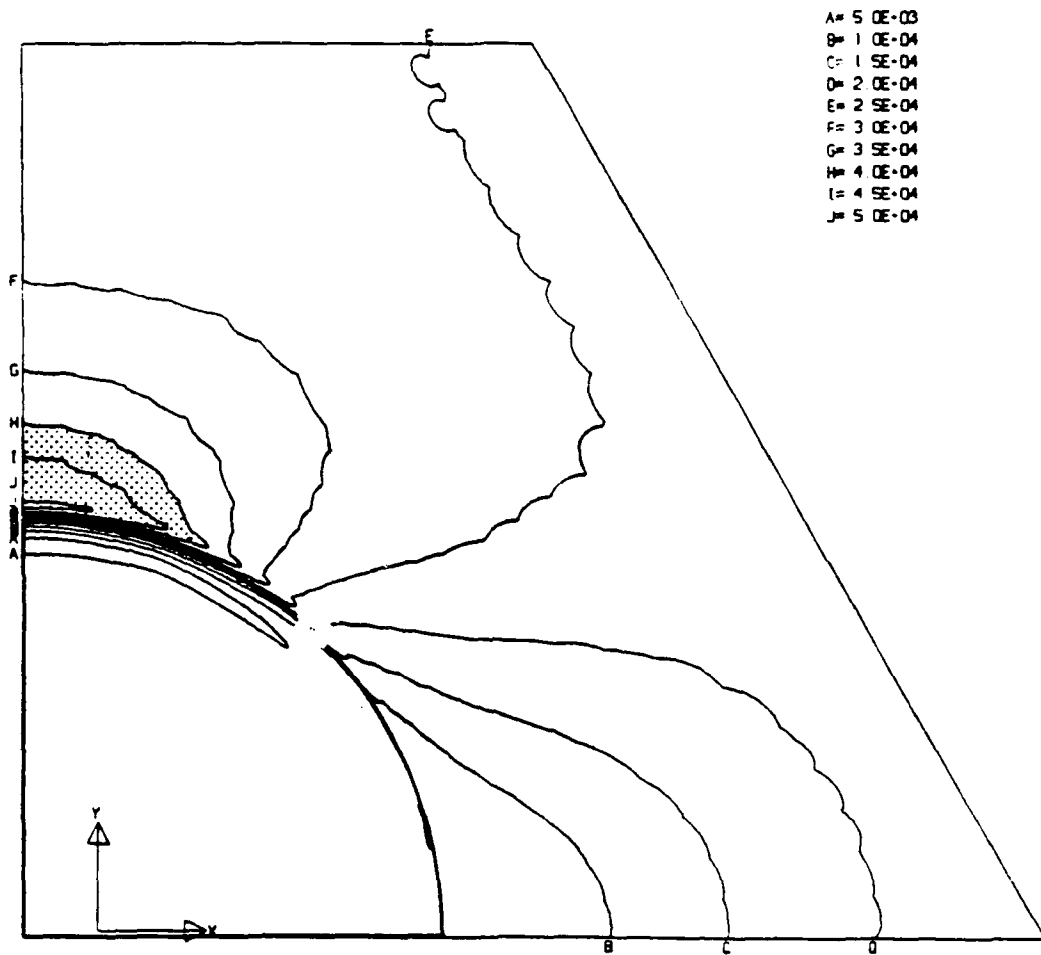
Fig.11. Contour of equivalent stress $\bar{\sigma}$ in Gr/Al at 4th step. $c_f = 20\%$, $n = 5$, $\beta = 0.5$, and $\chi = 0.0$. The dotted region represents the plastic zone.
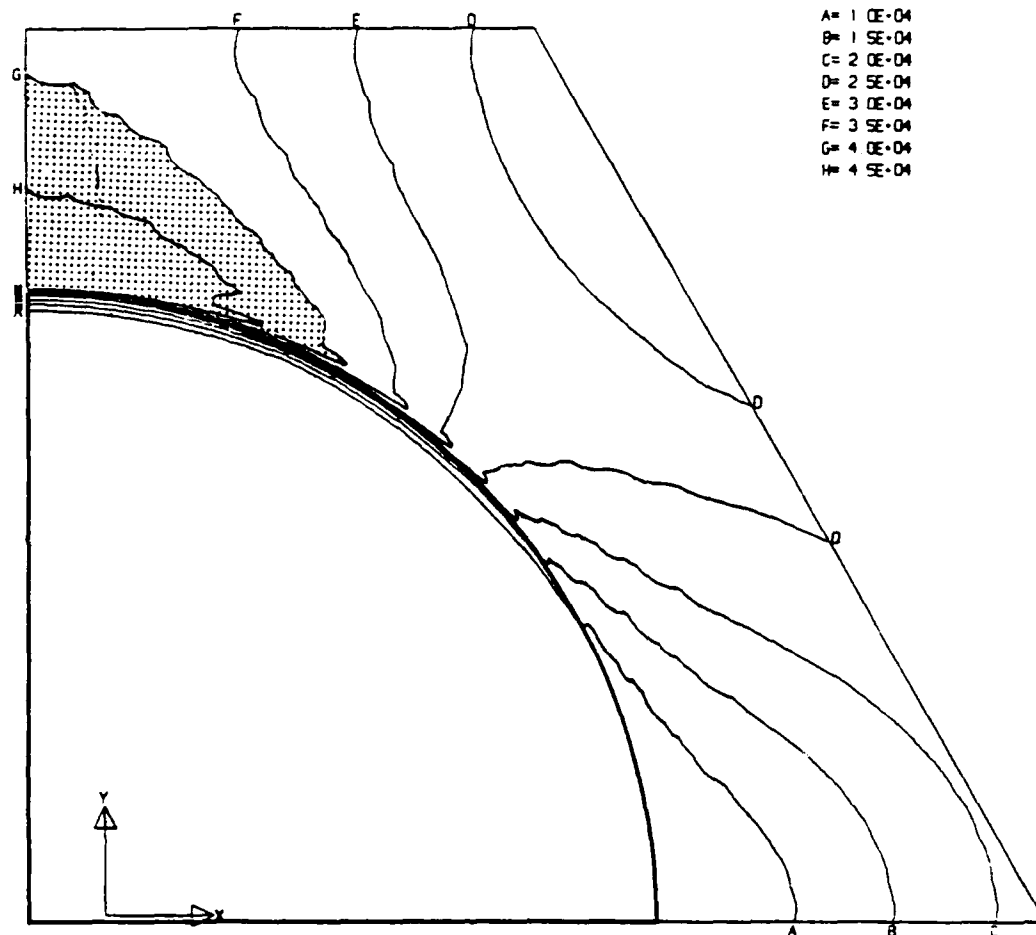
Fig.12. Contour of equivalent stress $\bar{\sigma}$ in Gr/Al at 6th step. $c_f = 45\%$, $n = 5$, $\beta = 0.5$, and $\chi = 0.0$. The dotted region represents the plastic zone.
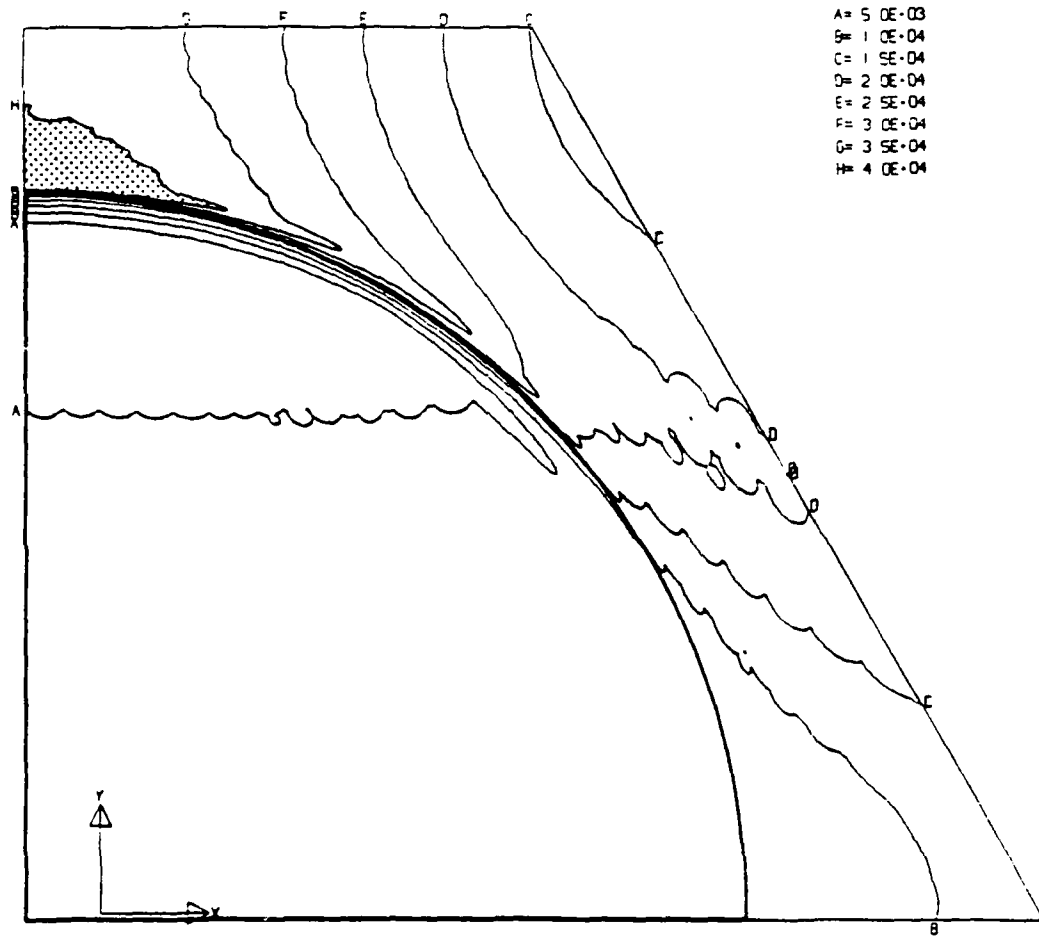
Fig.13. Contour of equivalent stress $\bar{\sigma}$ in Gr/Al at 6th step. $c_f = 60\%$, $n = 5$, $\beta = 0.5$, and $\chi = 0.0$. The dotted region represents the plastic zone.
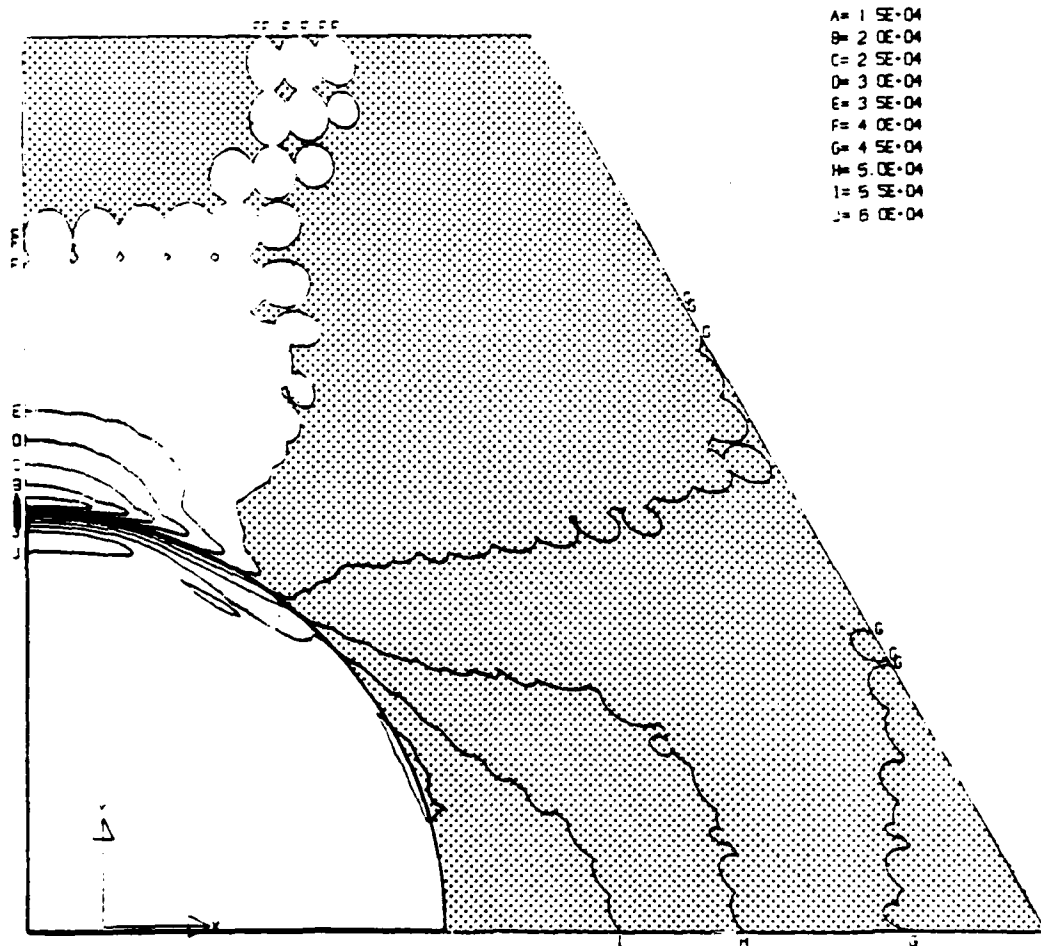
Fig.14. Contour of equivalent stress $\bar{\sigma}$ in B/Al at 5th step. $c_f = 20\%$, $n = 5$, $\beta = 0.5$, and $\chi = 0.0$. The dotted region represents the plastic zone.
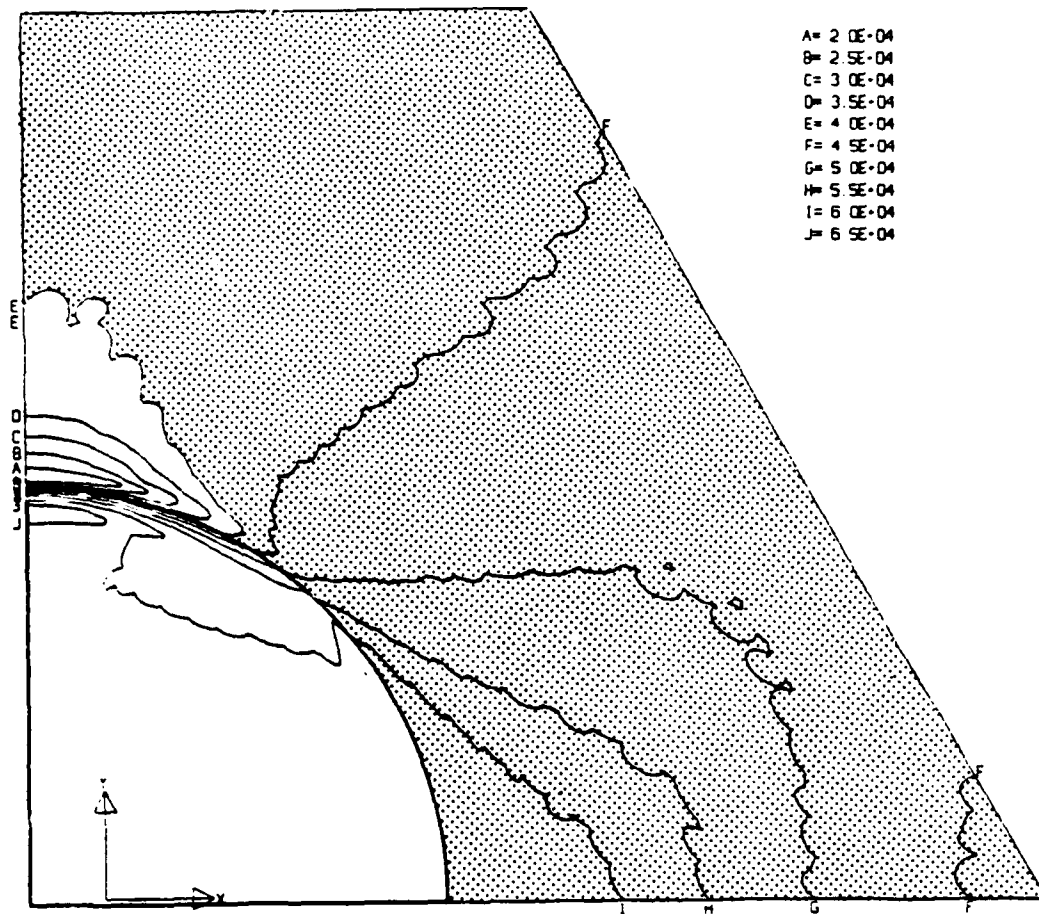
Fig.15. Contour of equivalent stress $\bar{\sigma}$ in B/Al at 6th step. $c_f = 20\%$, $n = 5$, $\beta = 0.5$, and $\chi = 0.0$. The dotted region represents the plastic zone.
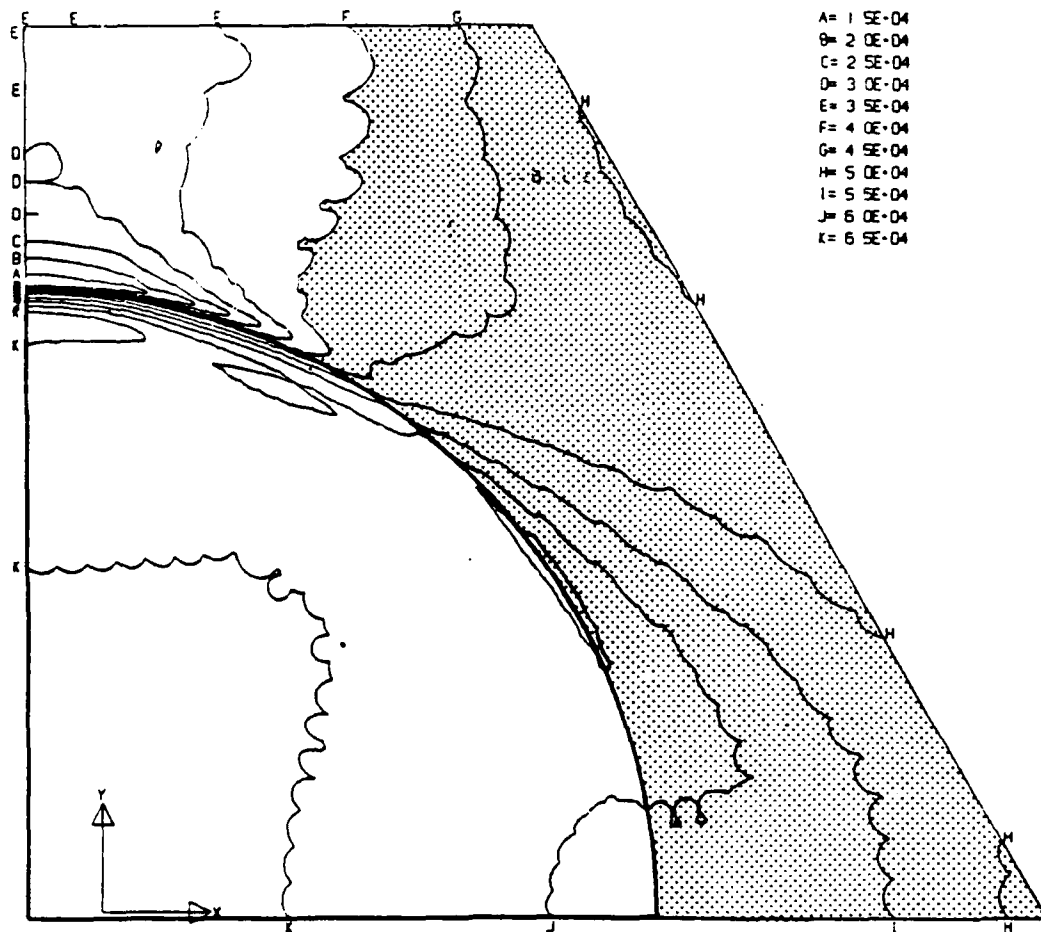
Fig.16. Contour of equivalent stress $\bar{\sigma}$ in B/Al at 5th step. $c_f = 45\%$, $n = 5$, $\beta = 0.5$, and $\chi = 0.0$. The dotted region represents the plastic zone.
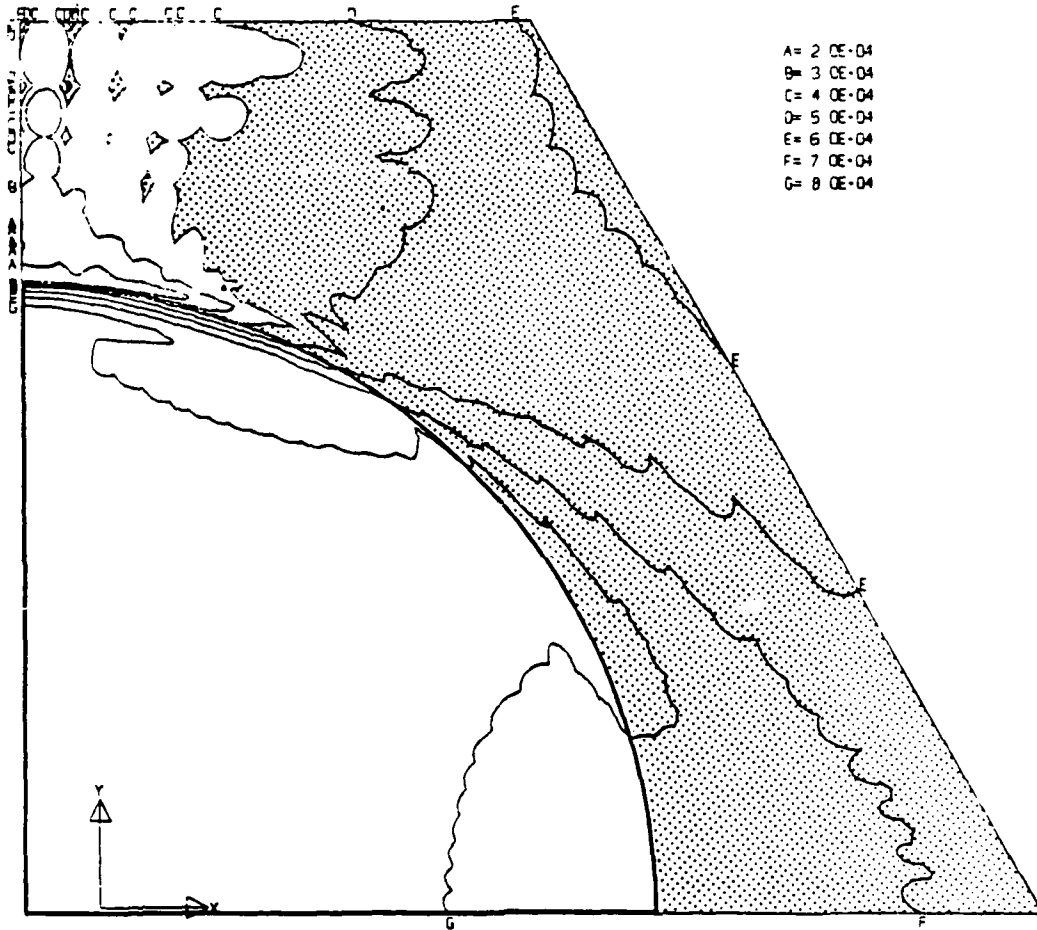
Fig.17. Contour of equivalent stress $\bar{\sigma}$ in B/Al at 15th step. $c_f = 45\%$, $n = 5$, $\beta = 0.5$, and $\chi = 0.0$. The dotted region represents the plastic zone.

A= 1 0E-04
B= 1 5E-04
C= 2 0E-04
D= 2.5E-04
E= 3 0E-04
F= 3 5E-04
G= 4 0E-04
H= 4 5E-04
I= 5 0E-04
J= 5 5E-04
K= 6 0E-04
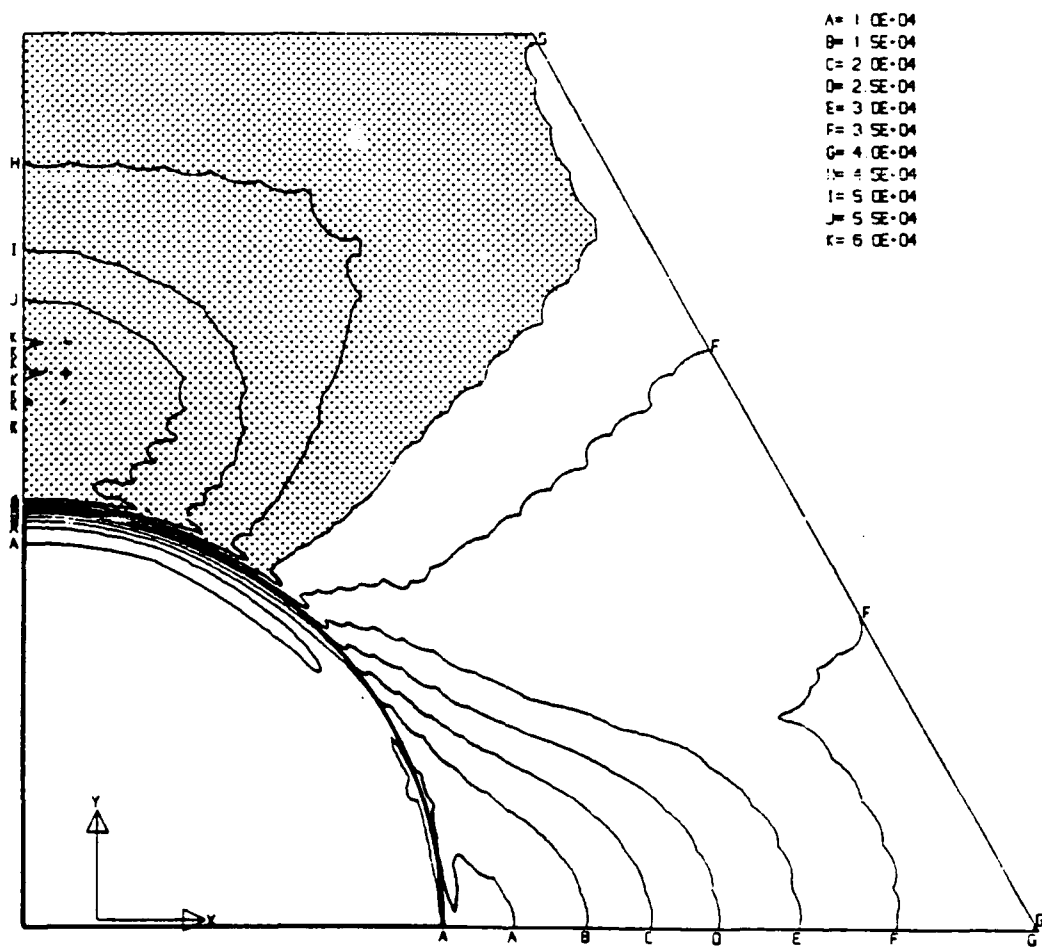
Fig.18. Contour of equivalent stress $\bar{\sigma}$ in Gr/Al at 7th step. $c_f = 20\%$, $n = 5$, $\beta = 0.5$, and $\chi = 0.0$. The dotted region represents the plastic zone.
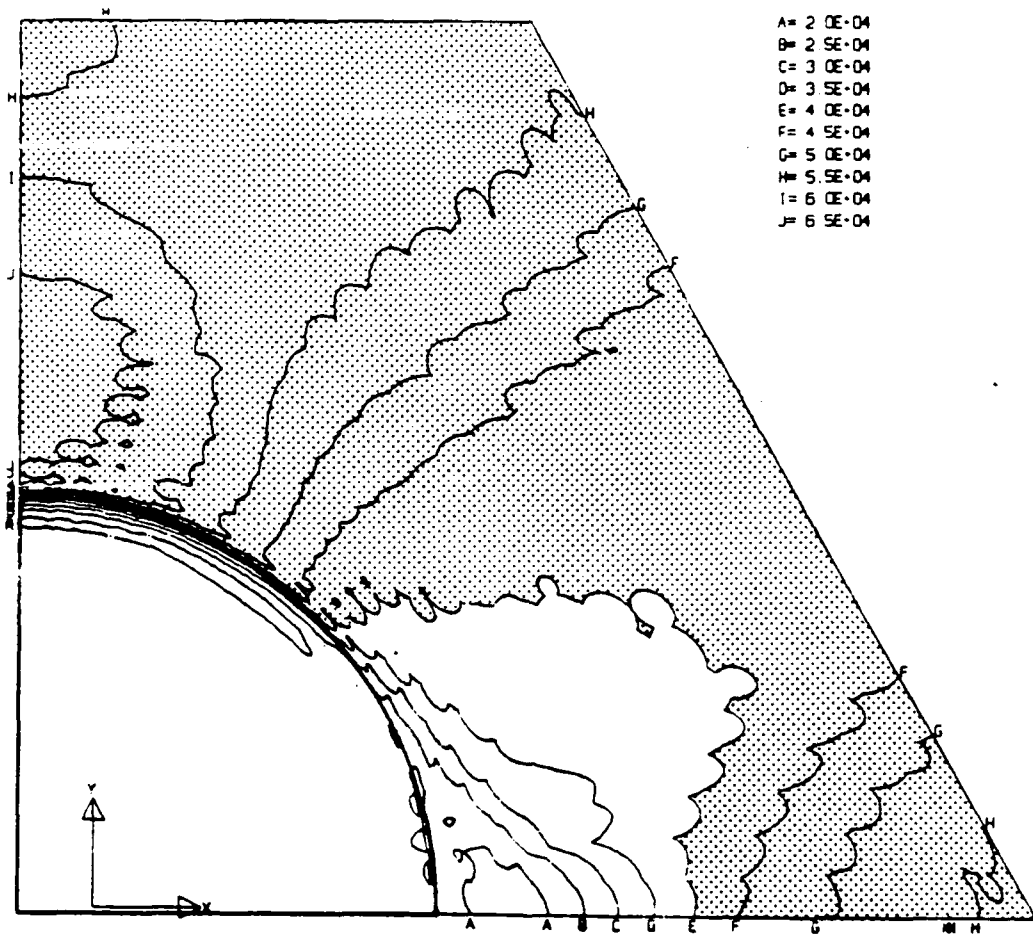
Fig.19. Contour of equivalent stress $\bar{\sigma}$ in Gr/Al at 15th step. $c_f = 20\%, n = 5$, $\beta = 0.5$, and $\chi = 0.0$. The dotted region represents the plastic zone.
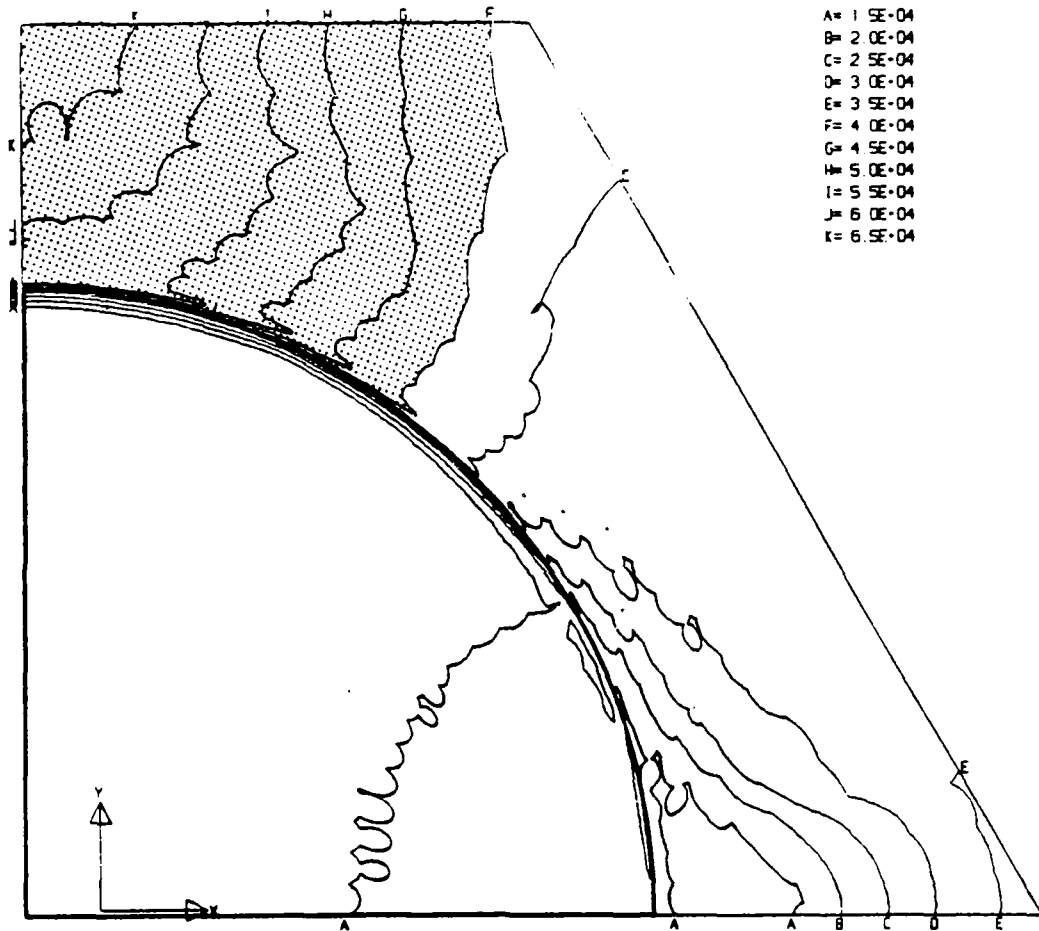
Fig.20. Contour of equivalent stress $\bar{\sigma}$ in Gr/Al at 12th step. $c_f = 45\%, n = 5$, $\beta = 0.5$, and $\chi = 0.0$. The dotted region represents the plastic zone.
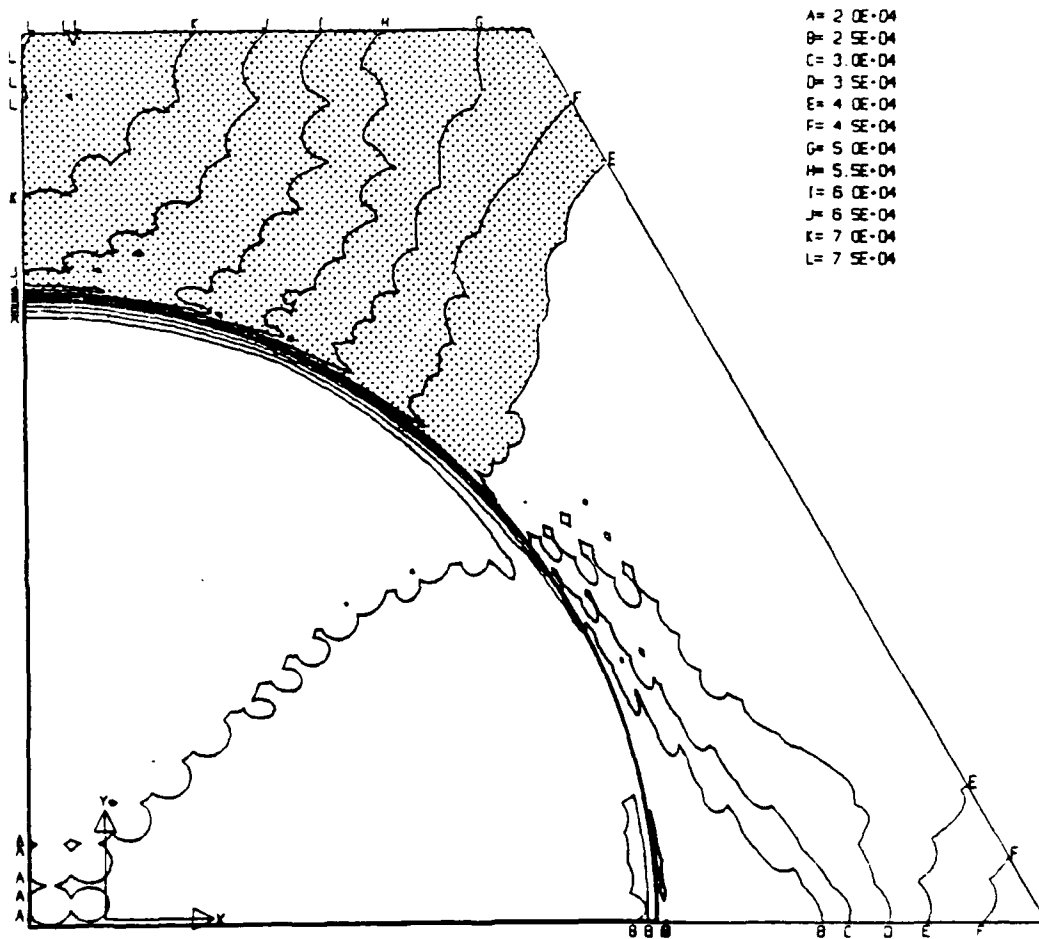
Fig.21. Contour of equivalent stress $\bar{\sigma}$ in Gr/Al at 18th step. $c_f = 45\%, n = 5$, $\beta = 0.5$, and $\chi = 0.0$. The dotted region represents the plastic zone.
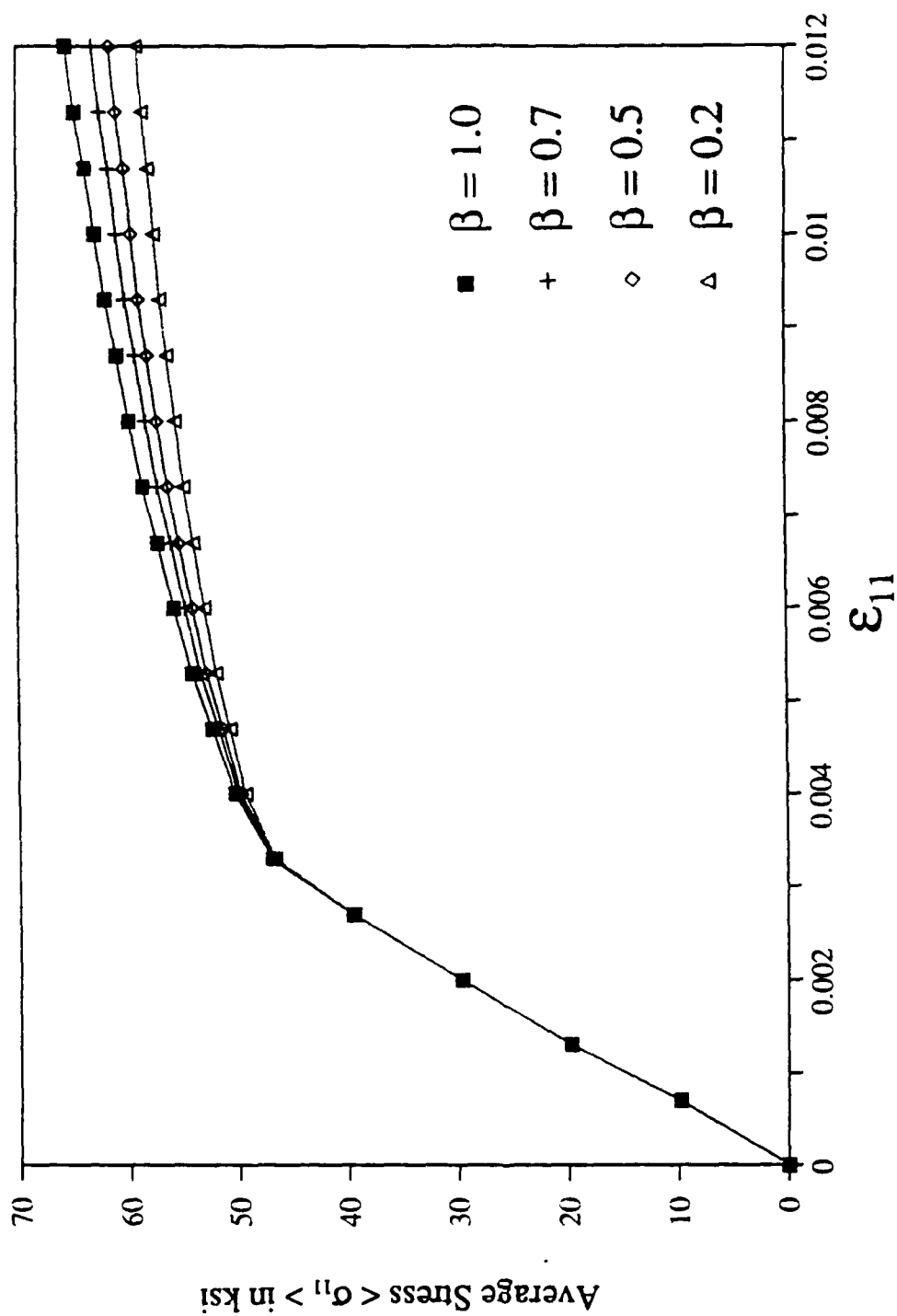
Fig. 22. Variation of the averaged transverse stress with prescribed strain in B/Al. $c_f = 20\%$ and $n = 5$.
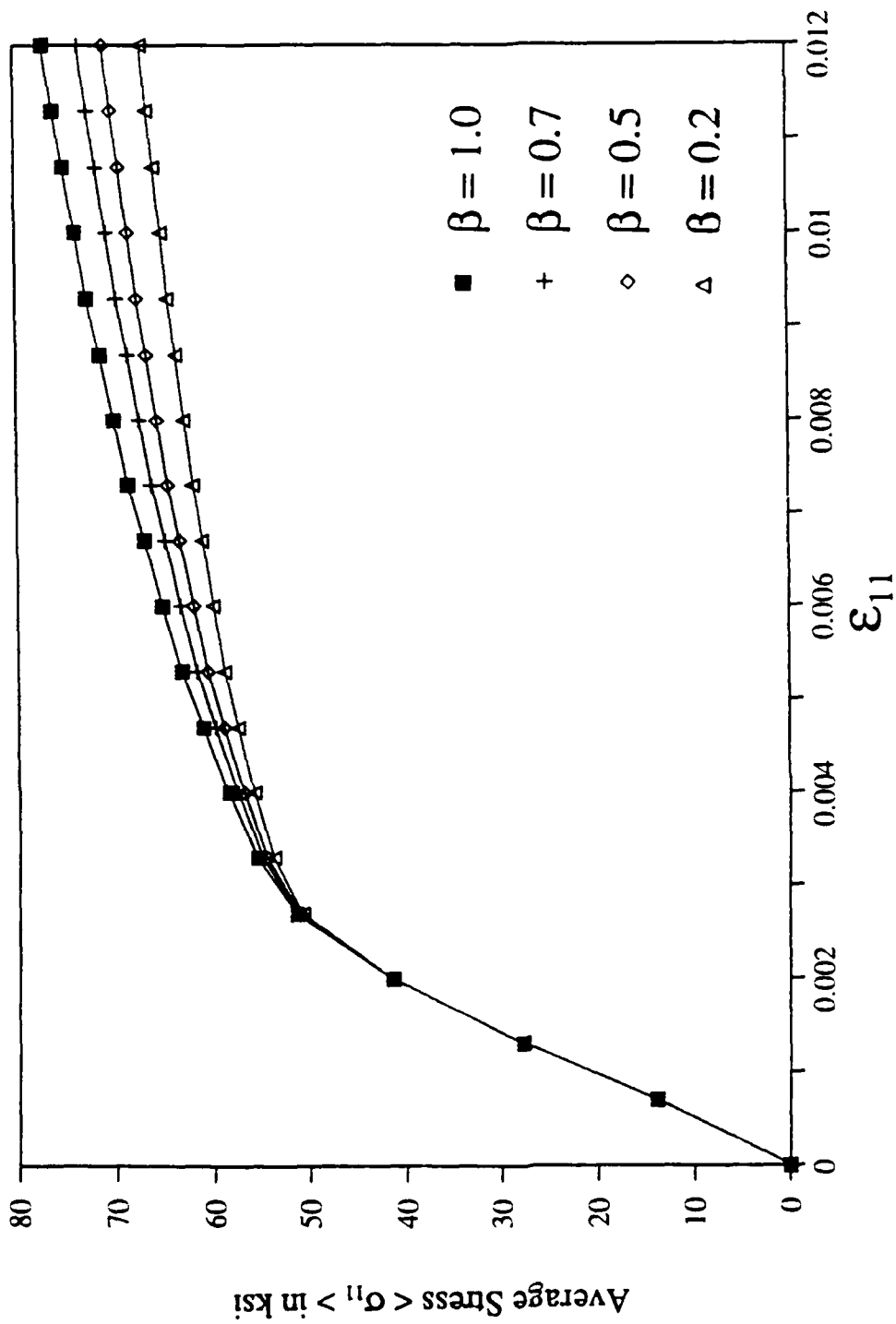
Fig. 23. Variation of the averaged transverse stress with prescribed strain in B/Al. $c_f = 45\%$ and $n = 5$.
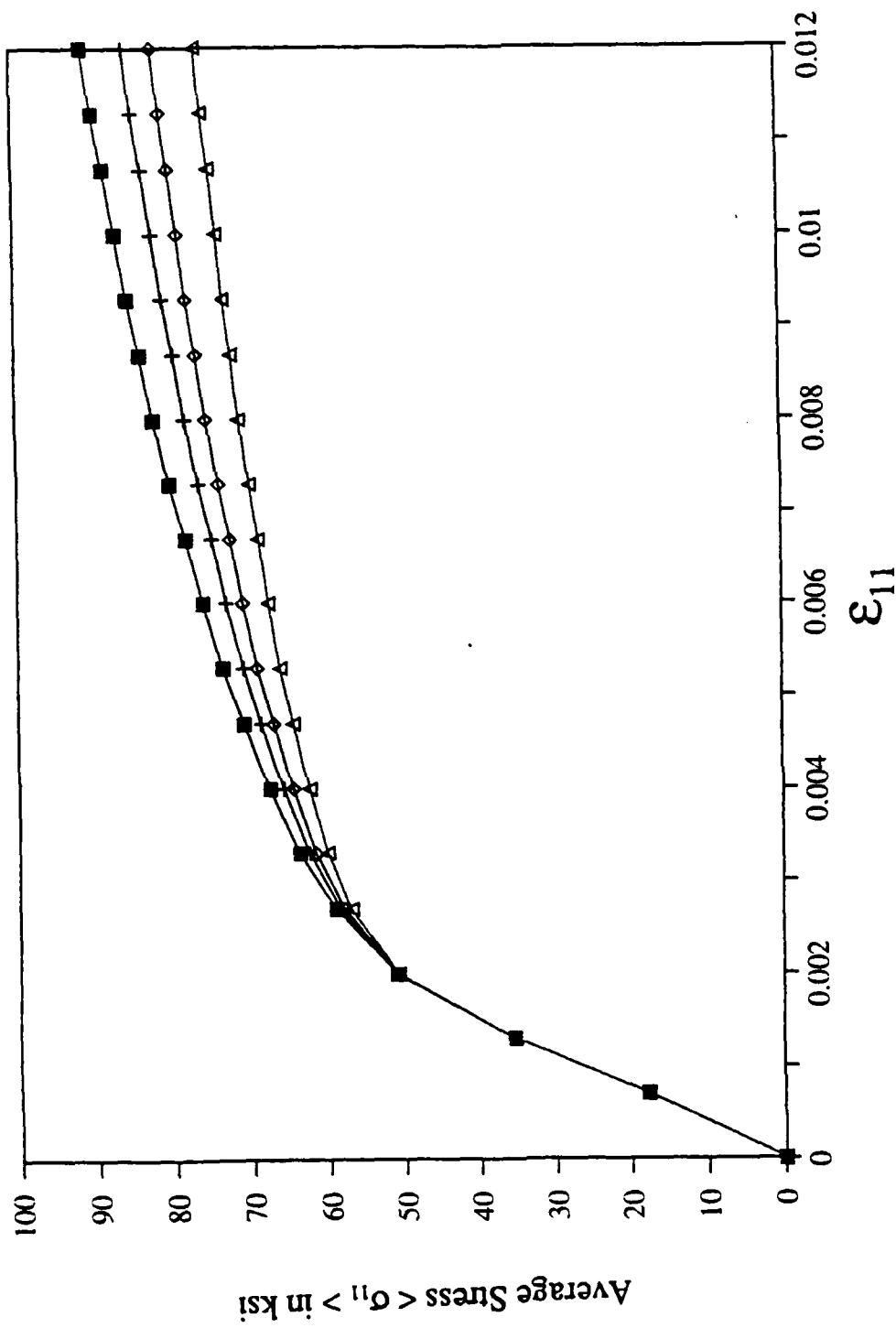
Fig. 24. Variation of the averaged transverse stress with prescribed strain in B/Al. $c_f = 60\%$ and $n = 5$.
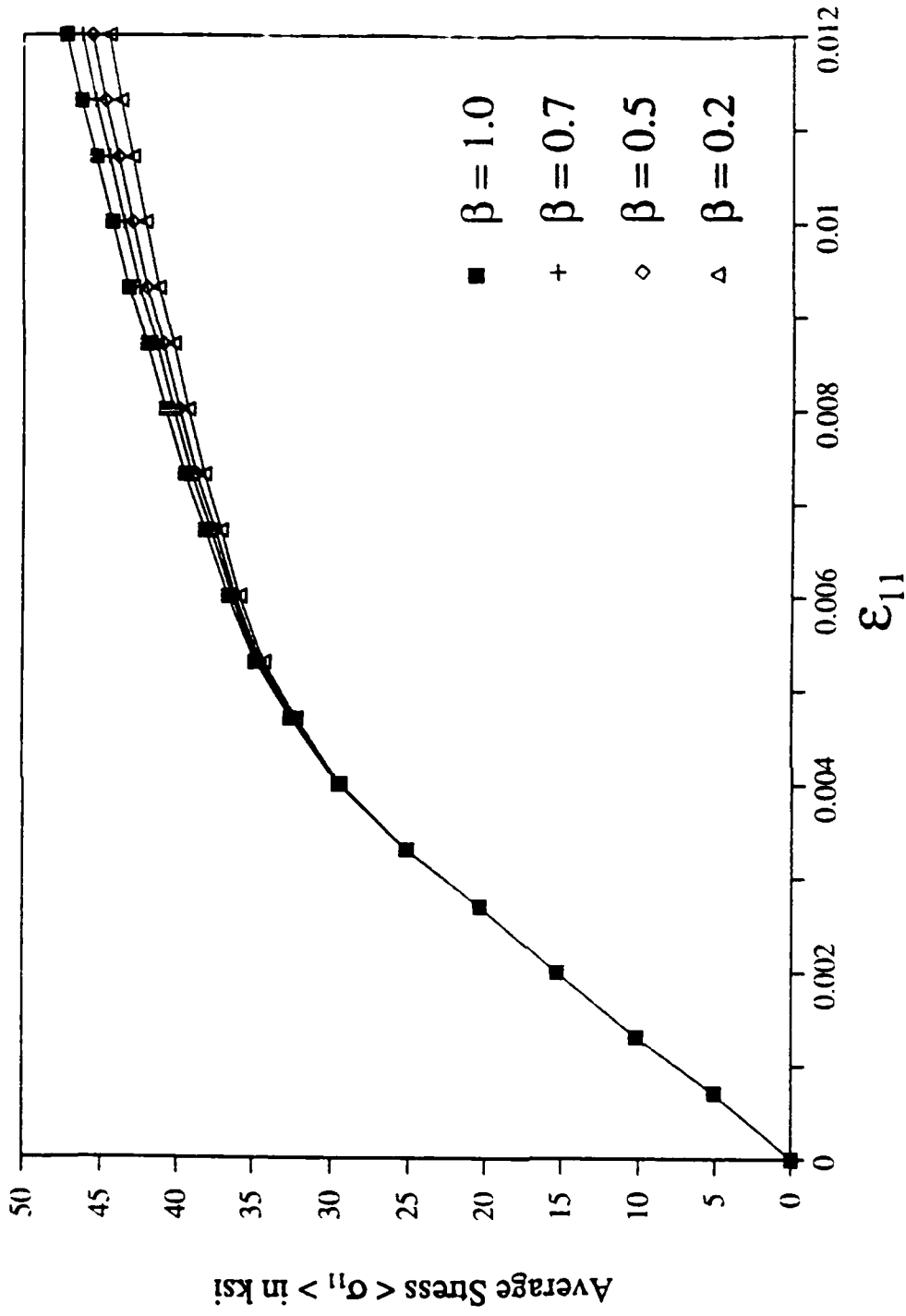
Fig. 25. Variation of the averaged transverse stress with prescribed strain in Gr/Al. $c_f = 20\%$ and $n = 5$.
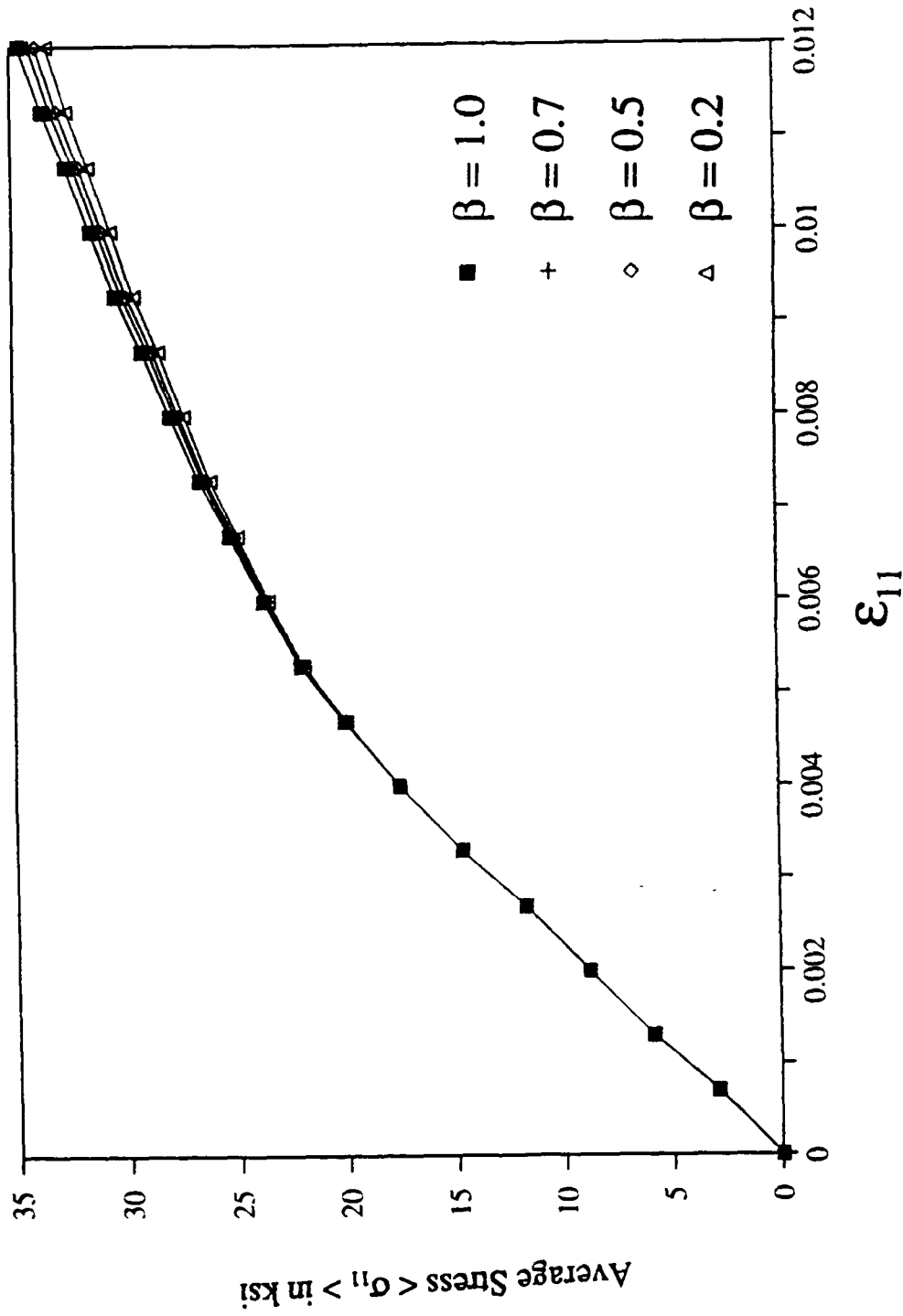
Fig. 26. Variation of the averaged transverse stress with prescribed strain
in Gr/Al. $c_f = 45\%$ and $n = 5$.
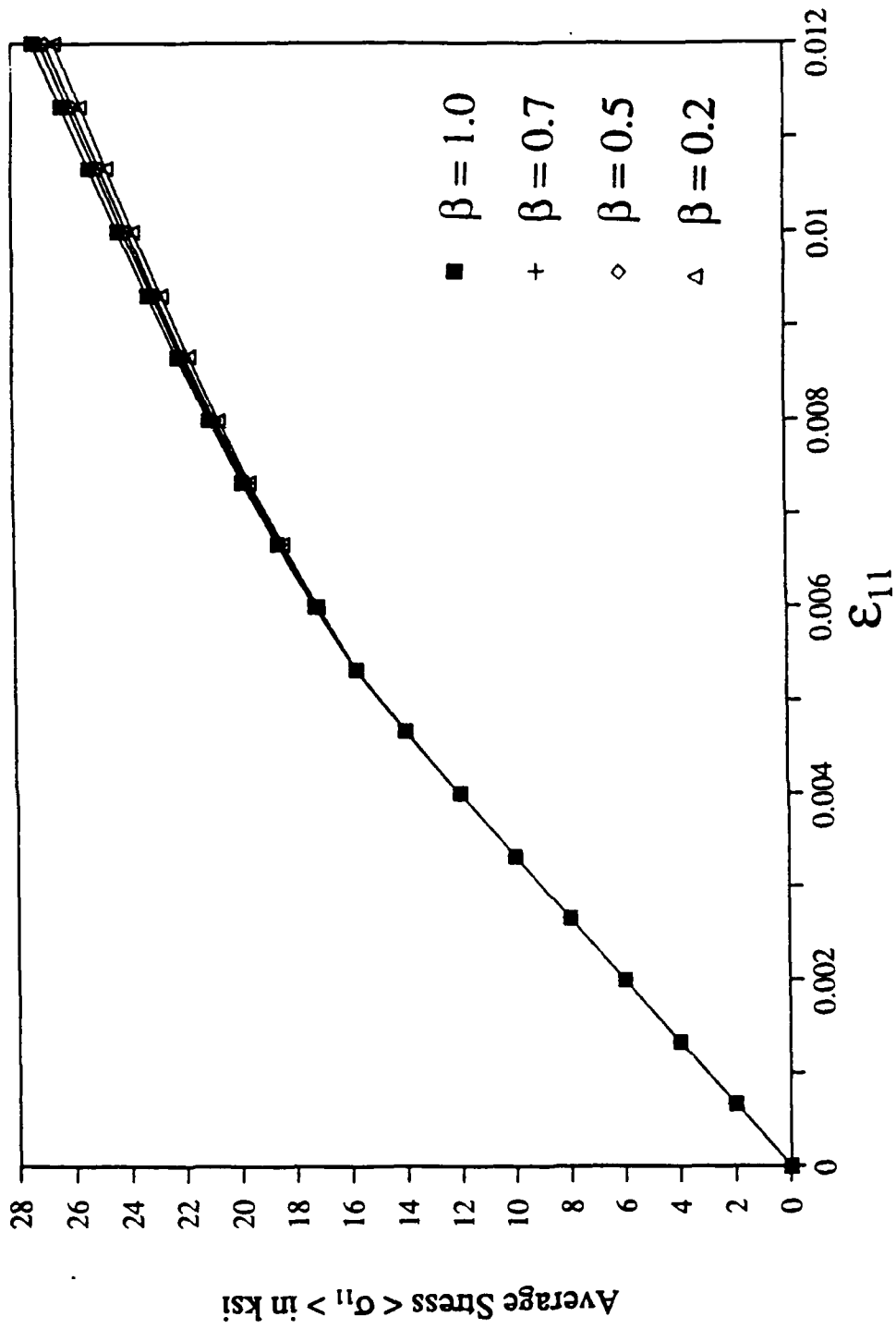
Fig. 27. Variation of the averaged transverse stress with prescribed strain in Gr/Al. $c_f = 60\%$ and $n = 5$.
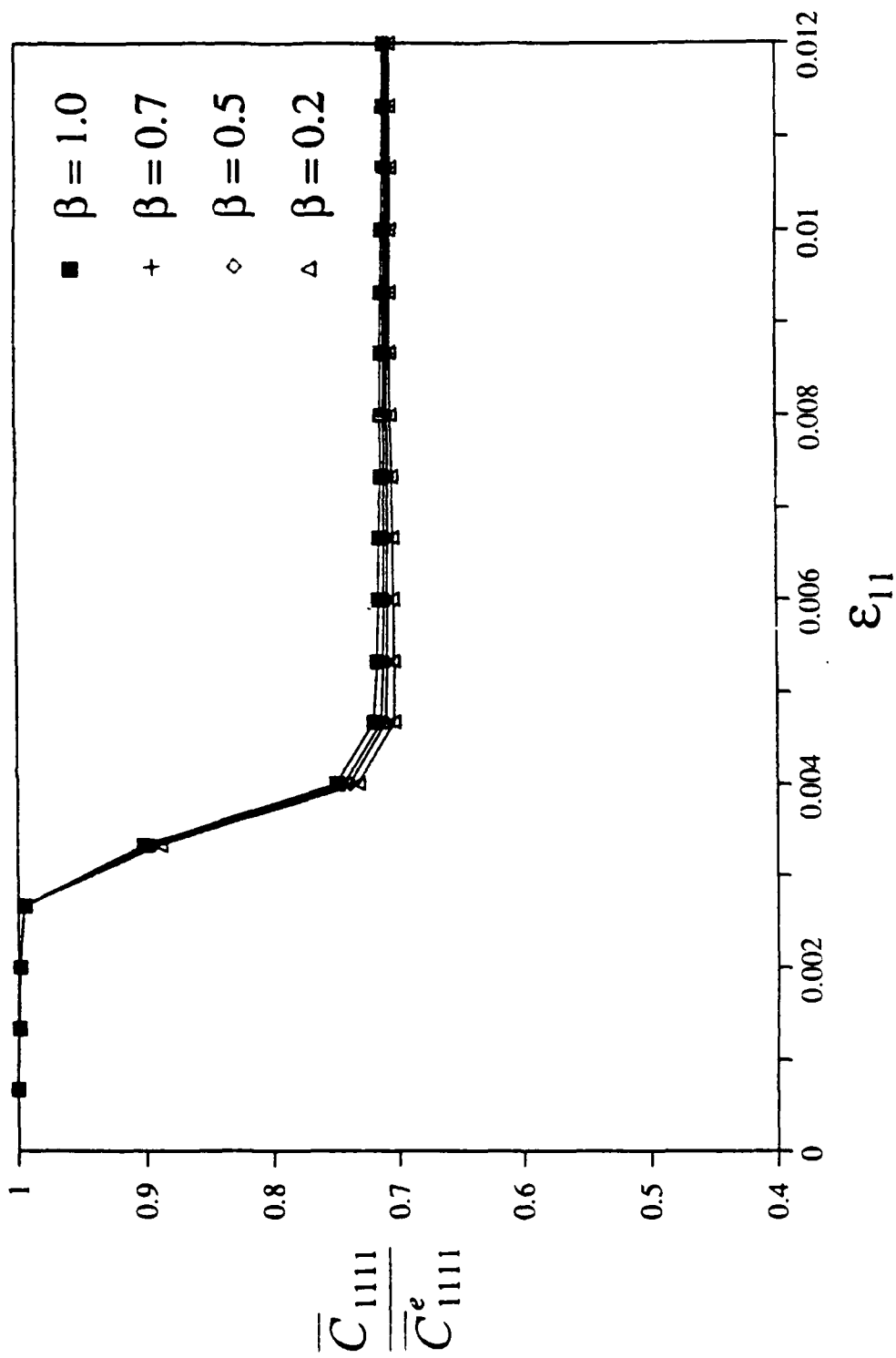
Fig. 28. Variation of the non-dimensionalized moduli $\overline{C}_{1111}/\overline{C}^e_{1111}$ with prescribed transverse strain in B/Al. $c_f = 20\%$ and $n = 5$.
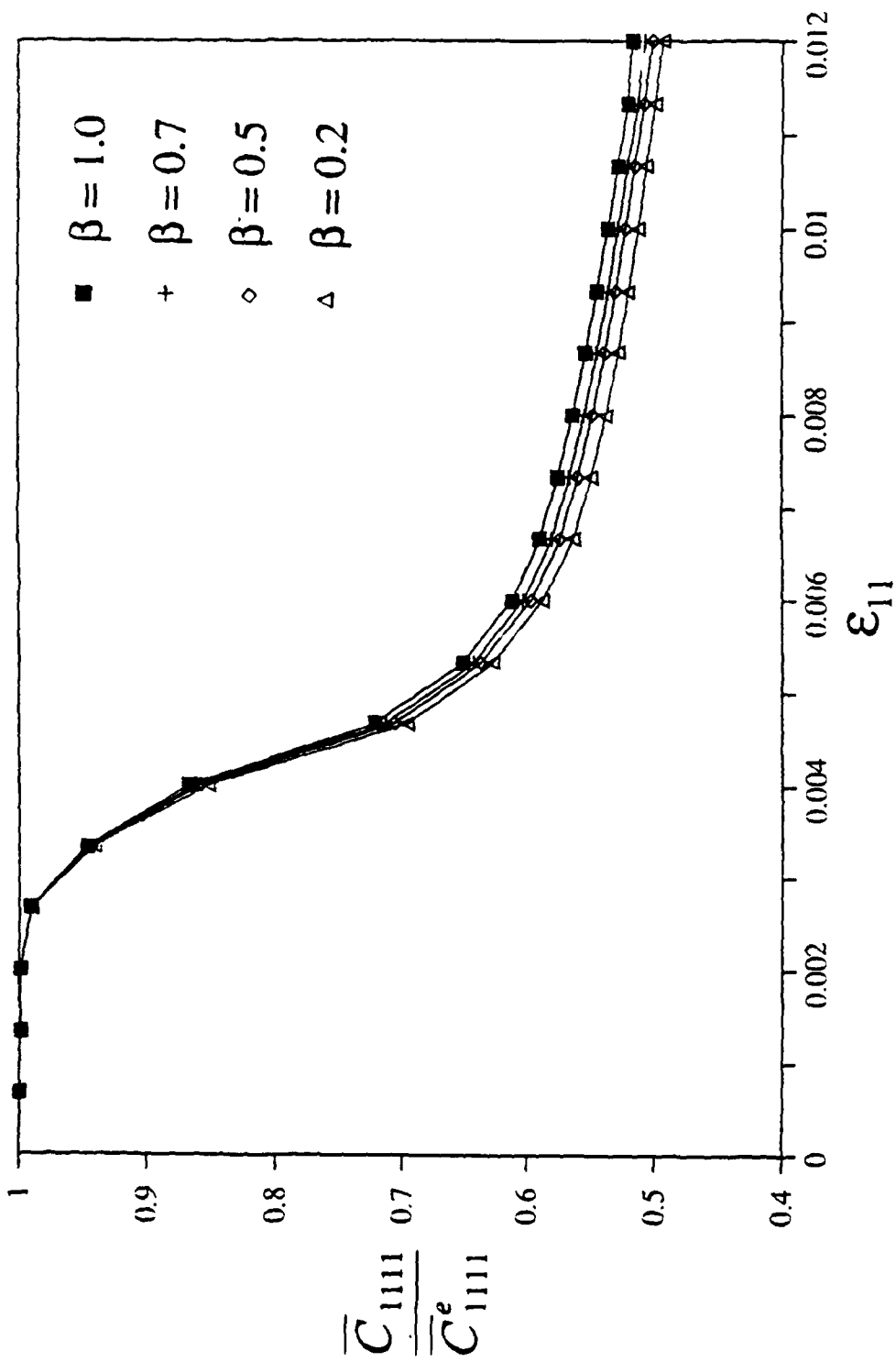
Fig. 29. Variation of the non-dimensionalized moduli $\overline{C}_{1111}/\overline{C}^e_{1111}$ with prescribed transverse strain in Gr/Al. $c_f = 20\%$ and $n = 5$.
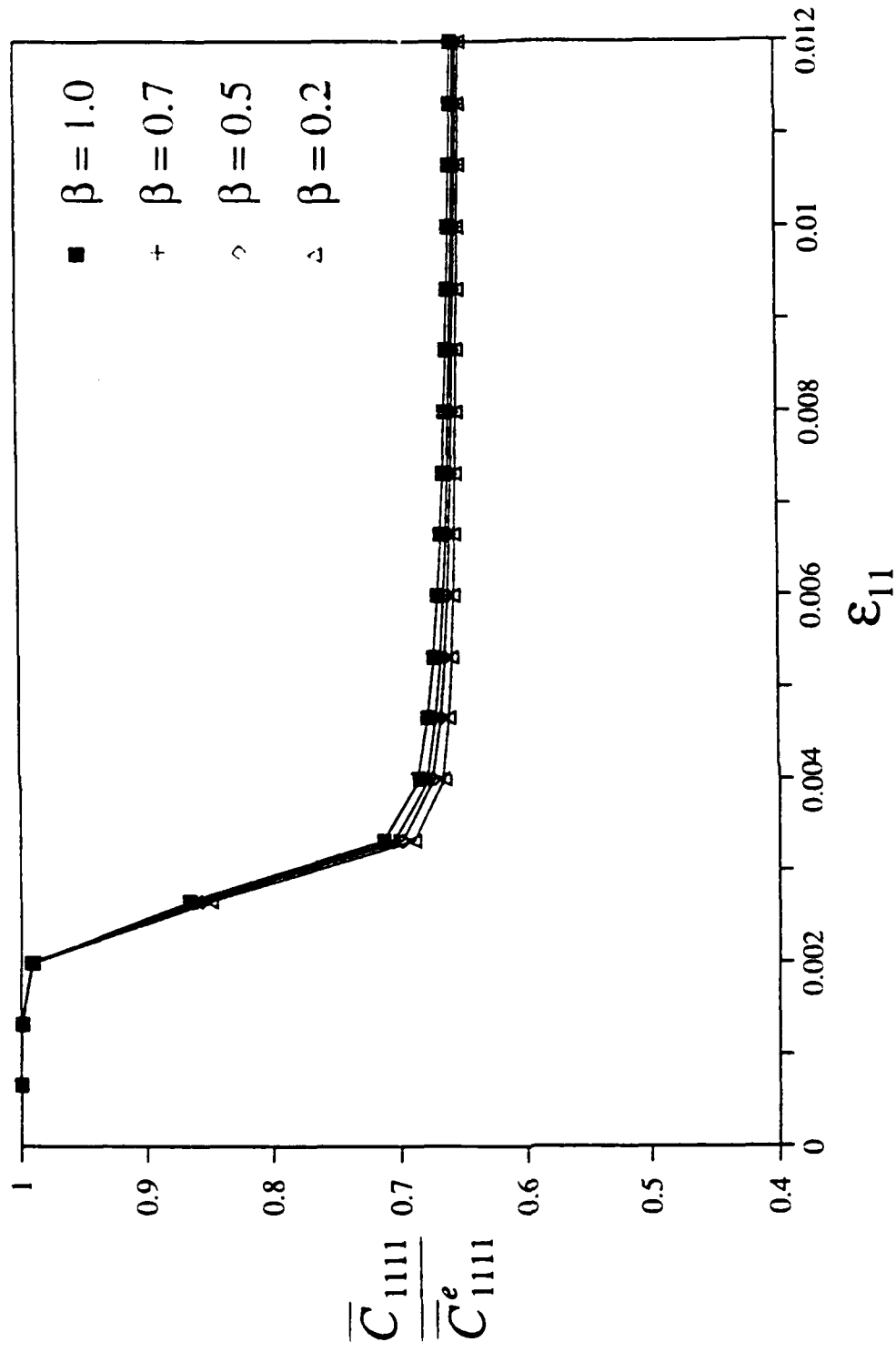
Fig. 30. Variation of the non-dimensionalized moduli $\overline{C}_{1111}/\overline{C}_{1111}^{e}$ with prescribed transverse strain in B/Al. $c_f = 45\%$ and $n = 5$.
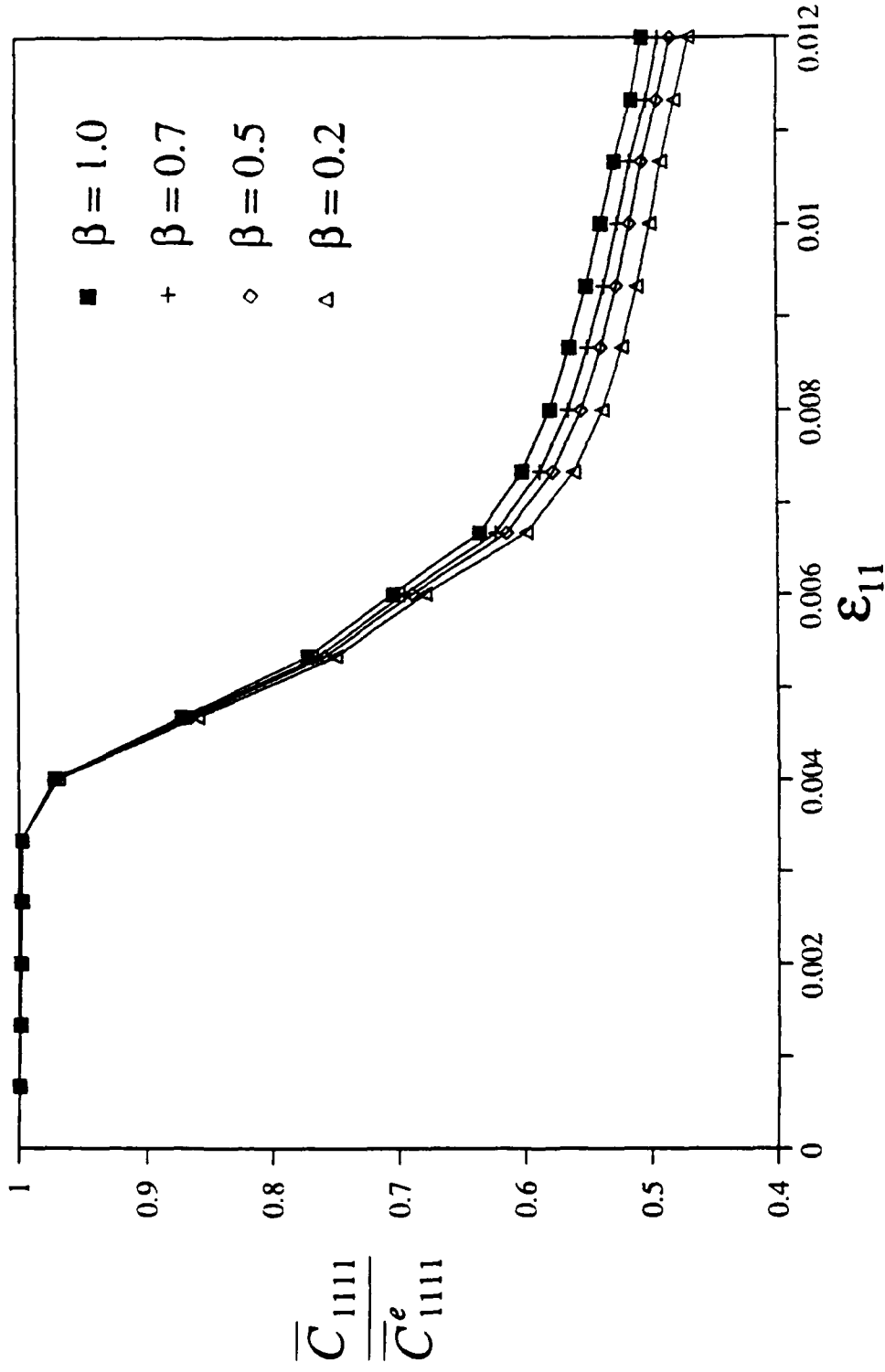
Fig. 31. Variation of the non-dimensionalized moduli $\overline{C}_{1111}/\overline{C}^e_{1111}$ with prescribed transverse strain in Gr/Al. $c_f = 45\%$ and $n = 5$.
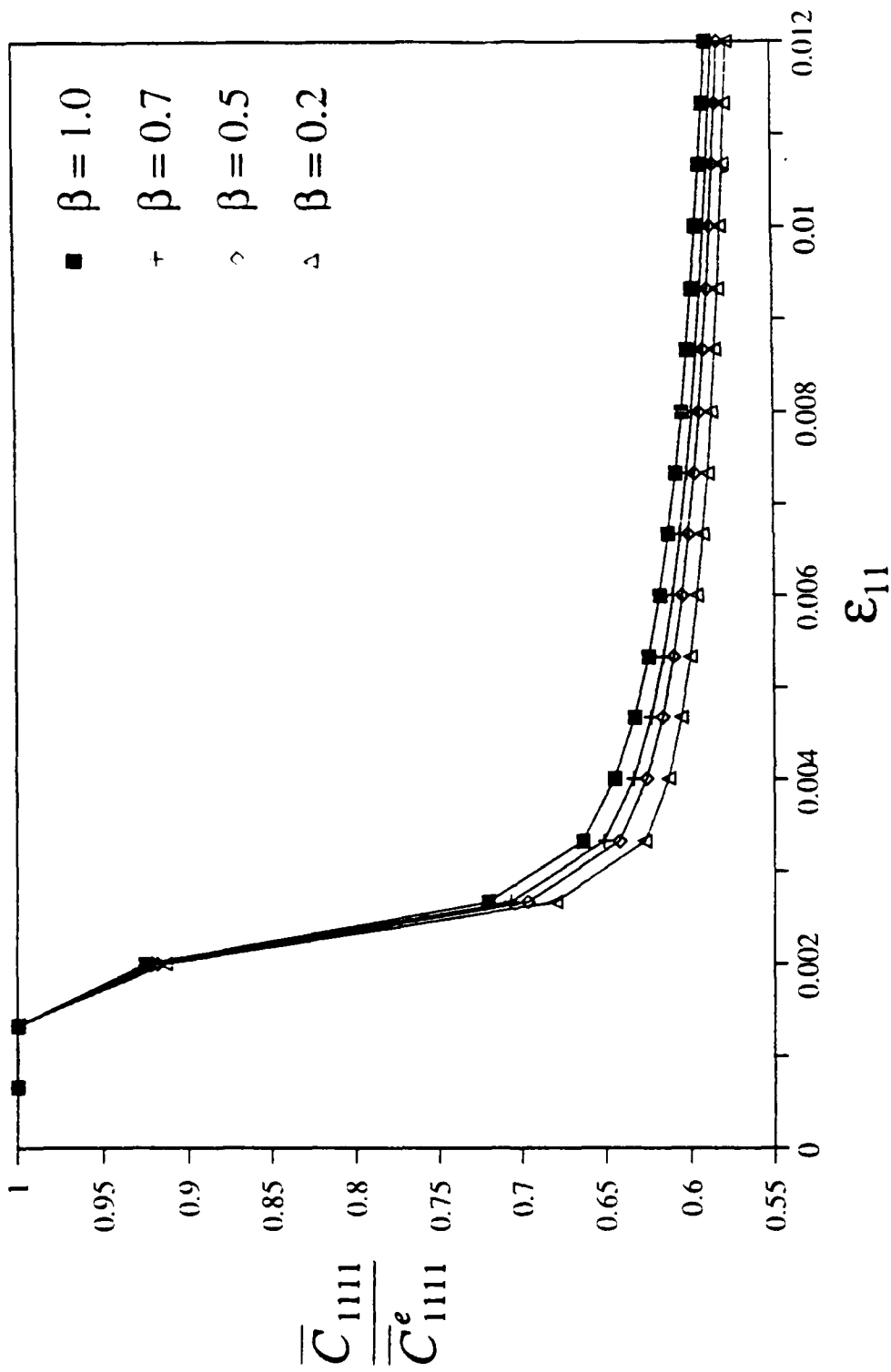
Fig. 32. Variation of the non-dimensionalized moduli $\overline{C}_{1111}/\overline{C}^e_{1111}$ with prescribed transverse strain in B/Al. $c_f = 60\%$ and $n = 5$.
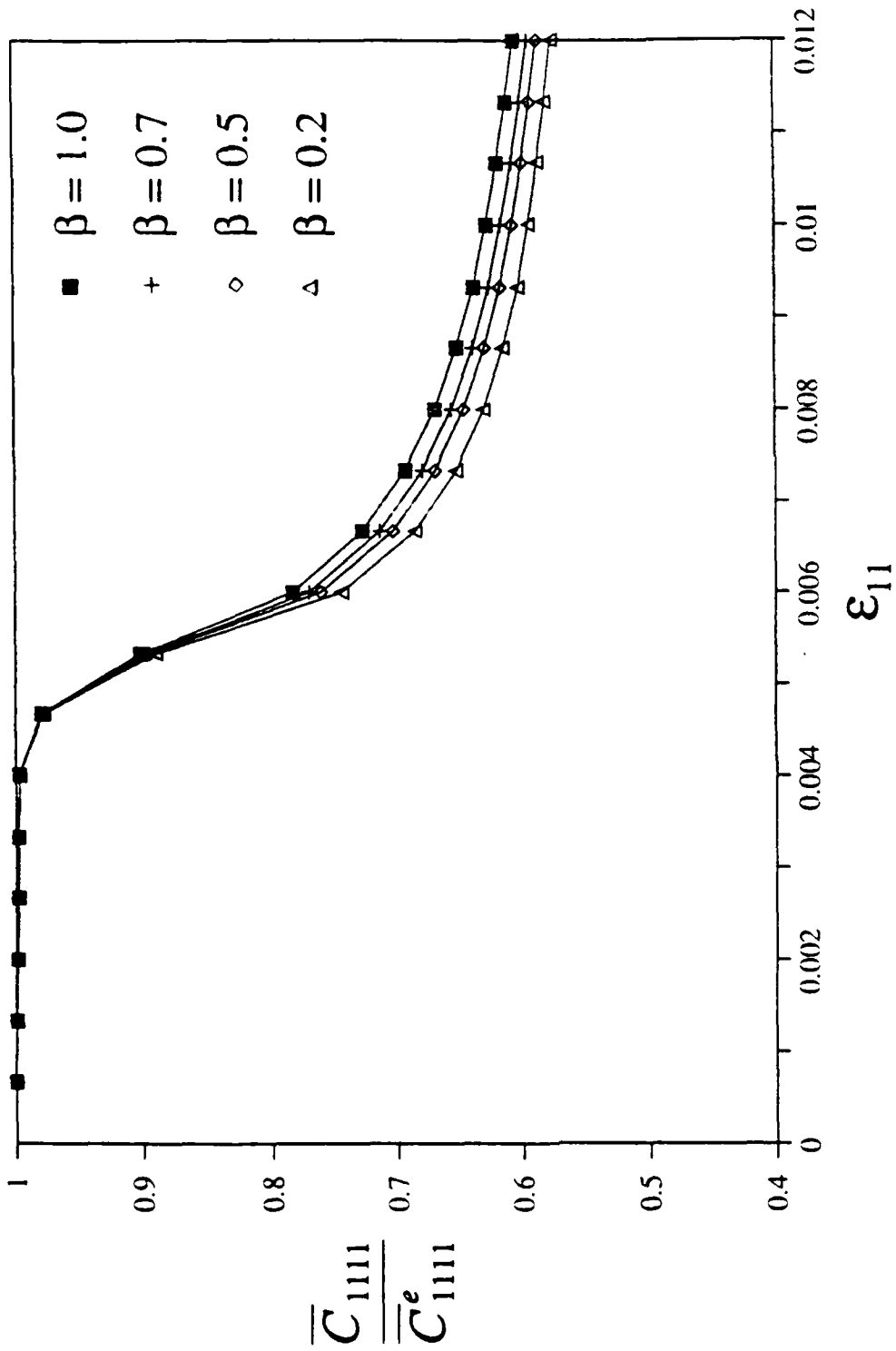
Fig. 33. Variation of the non-dimensionalized moduli $\overline{C}_{1111}/\overline{C}_{1111}^e$ with prescribed transverse strain in Gr/Al. $c_f = 60\%$ and $n = 5$.
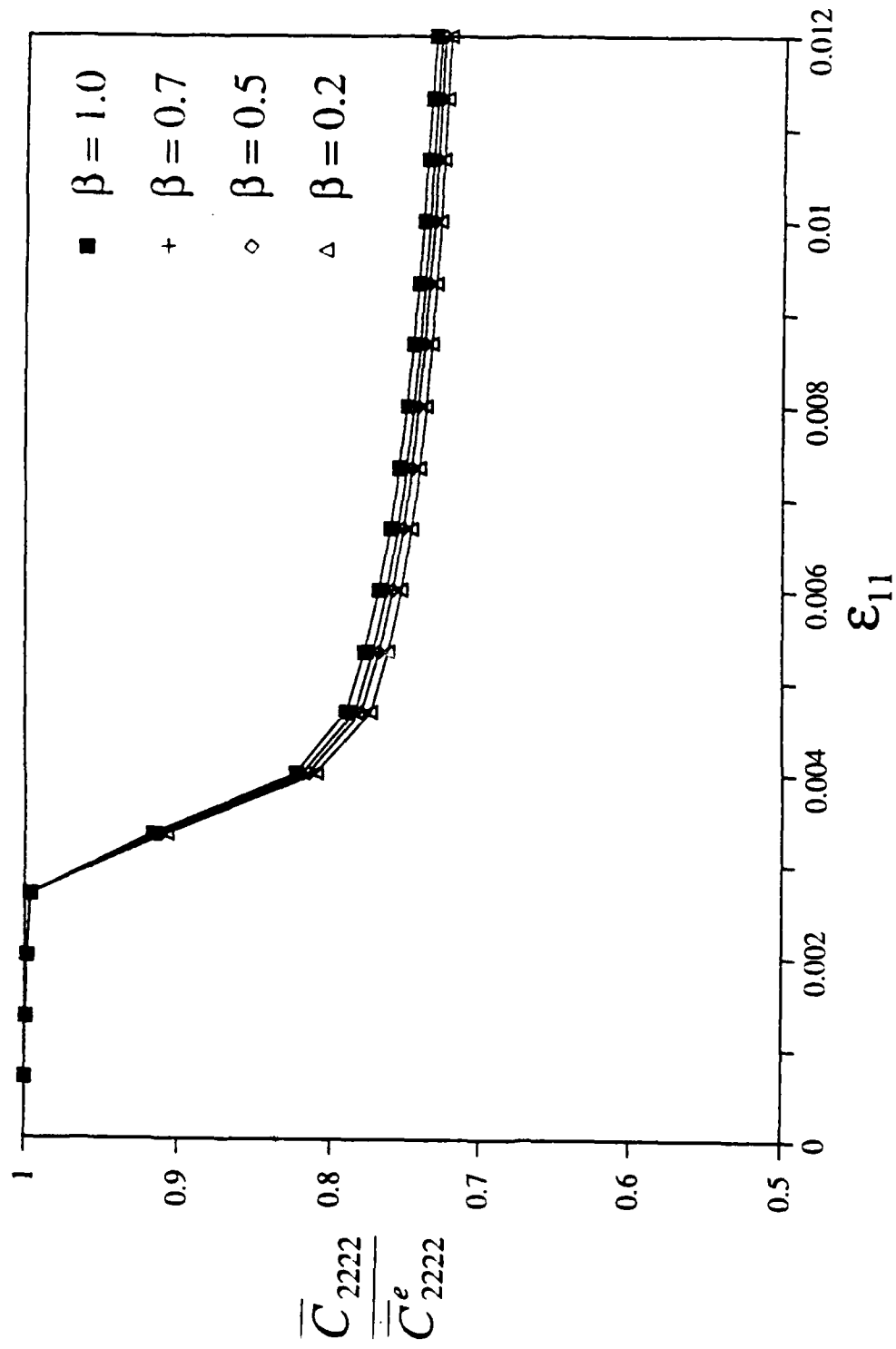
Fig. 34. Variation of the non-dimensionalized moduli $\overline{C}_{2222}/\overline{C}^e_{2222}$ with prescribed transverse strain in B/Al. $c_f = 20\%$ and $n = 5$.
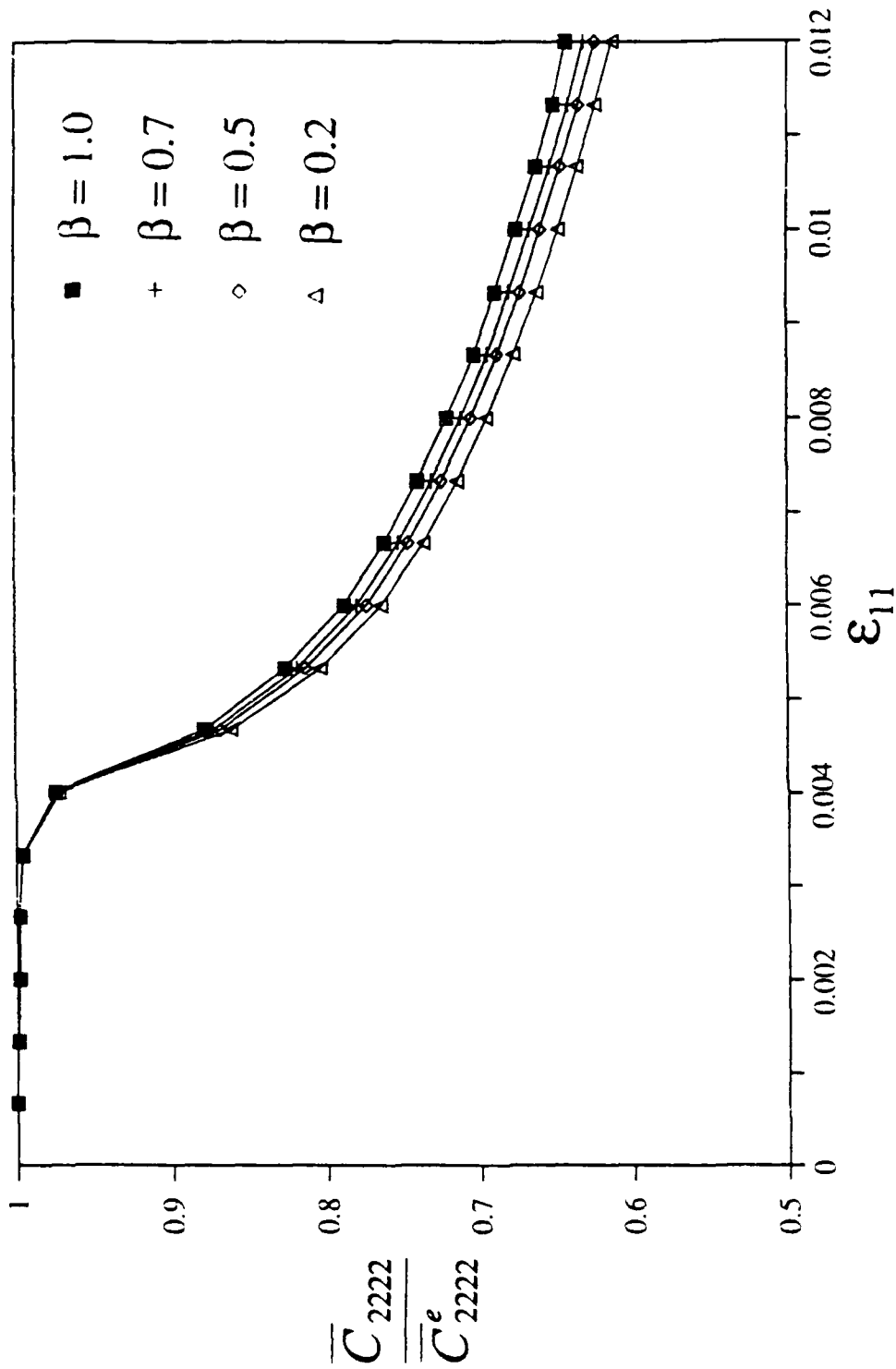
Fig. 35. Variation of the non-dimensionalized moduli $\overline{C}_{2222}/\overline{C}_{2222}^{e}$ with prescribed transverse strain in Gr/Al. $c_f = 20\%$ and $n = 5$.
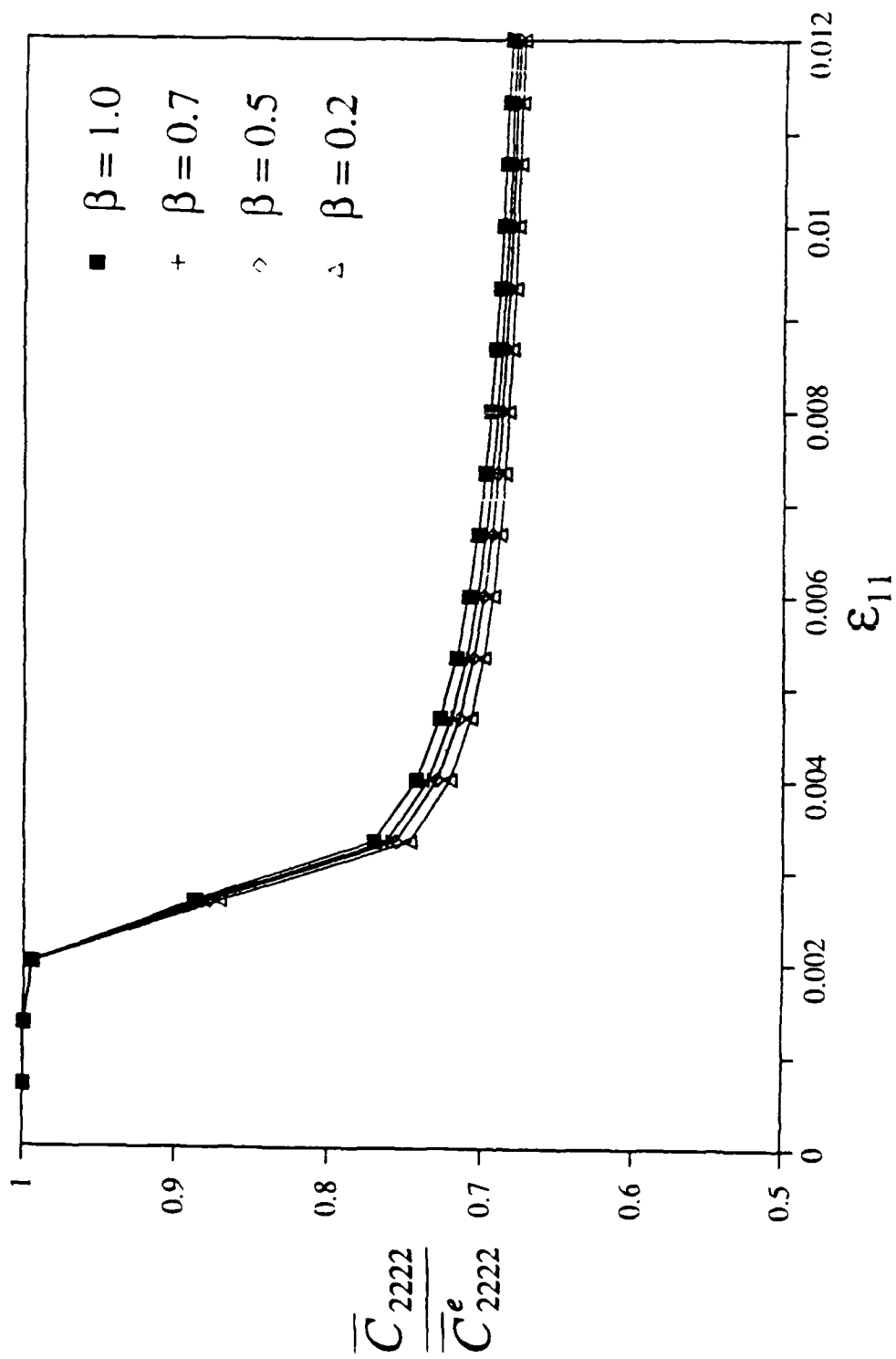
Fig. 36. Variation of the non-dimensionalized moduli $\overline{C}_{2222}/\overline{C}_{2222}^{e}$ with prescribed transverse strain in B/Al. $c_f = 45\%$ and $n = 5$.
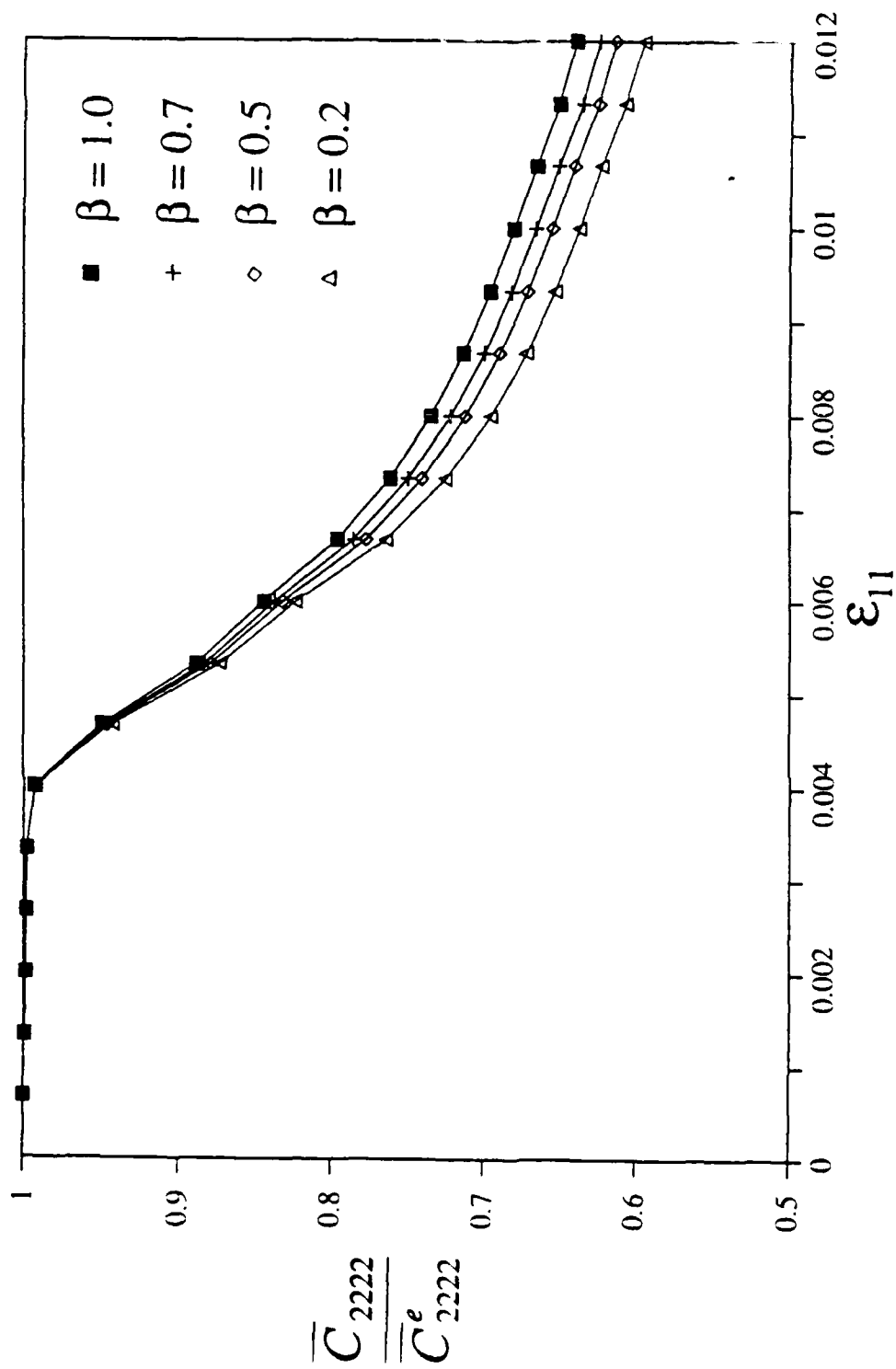
Fig. 37. Variation of the non-dimensionalized moduli $\overline{C}_{2222}/\overline{C}_{2222}^e$ with prescribed transverse strain in Gr/Al. $c_f = 45\%$ and $n = 5$.
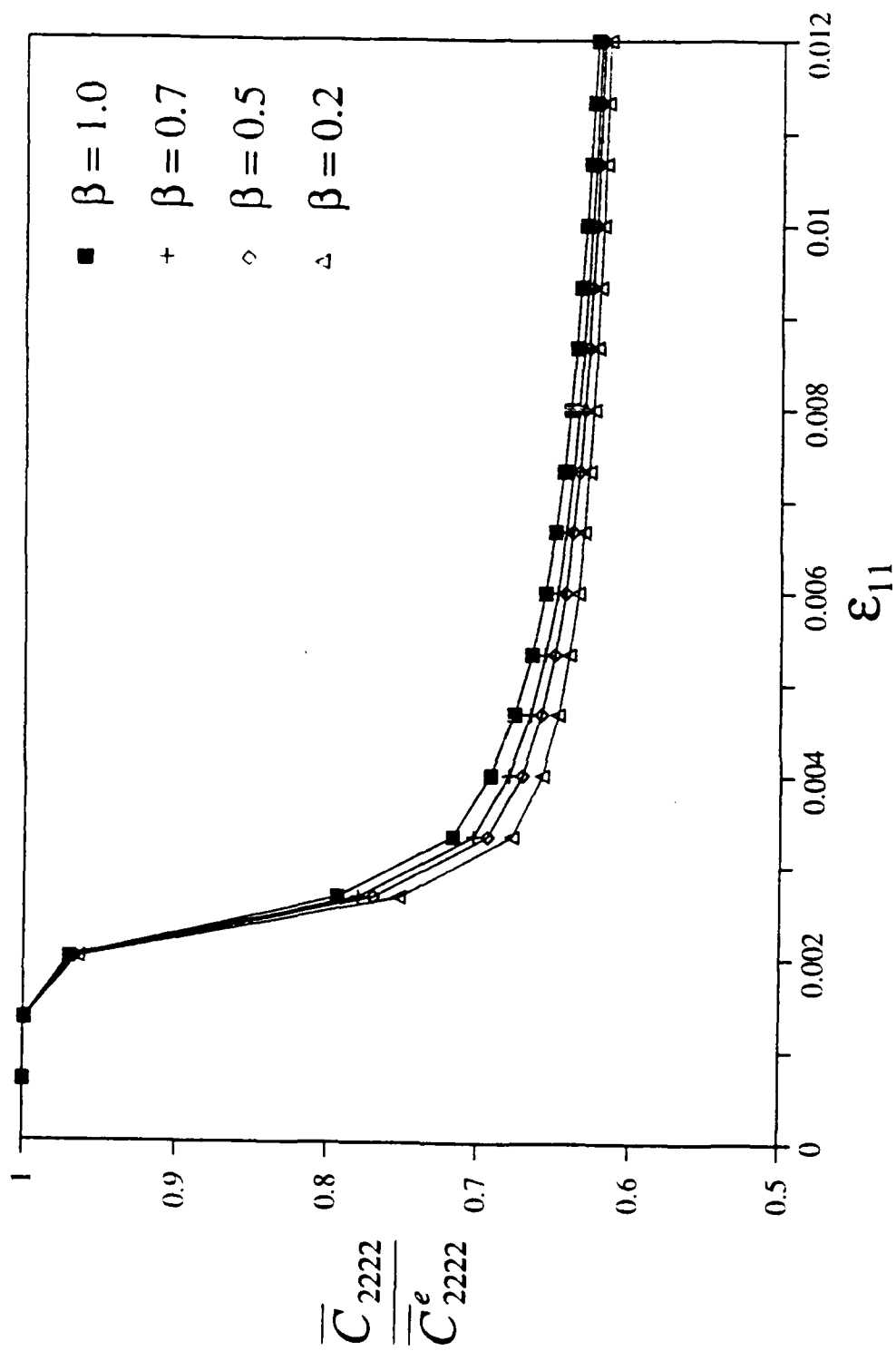
Fig. 38. Variation of the non-dimensionalized moduli $\overline{C}_{2222}/\overline{C}^e_{2222}$ with prescribed transverse strain in B/Al. $c_f = 60\%$ and $n = 5$.
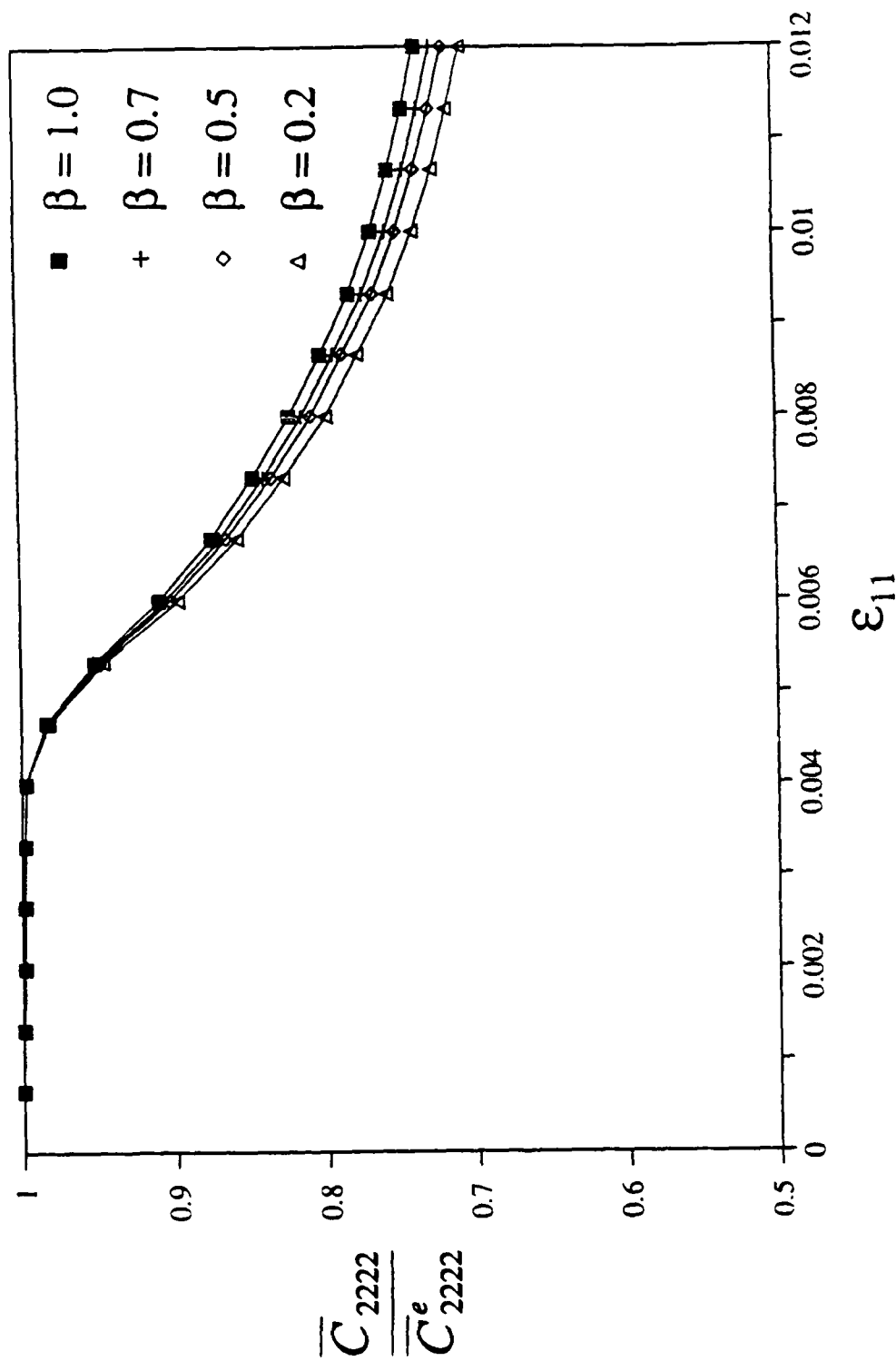
Fig. 39. Variation of the non-dimensionalized moduli $\overline{C}_{2222}/\overline{C}_{2222}^{e}$ with prescribed transverse strain in Gr/Al. $c_f = 60\%$ and $n = 5$.
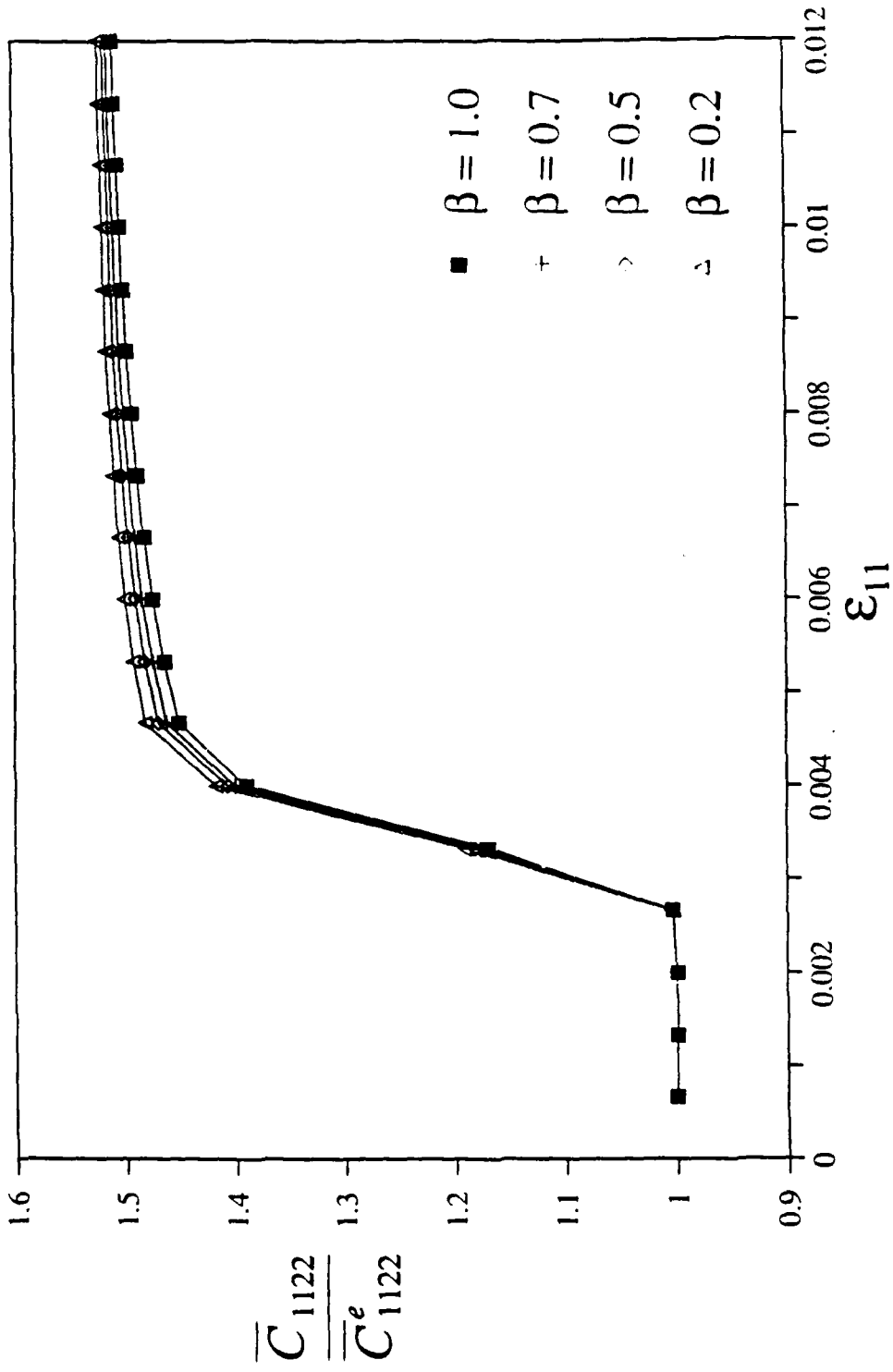
Fig. 40. Variation of the non-dimensionalized moduli $\overline{C}_{1122}/\overline{C}_{1122}^{e}$ with prescribed transverse strain in B/Al. $c_f = 20\%$ and $n = 5$.
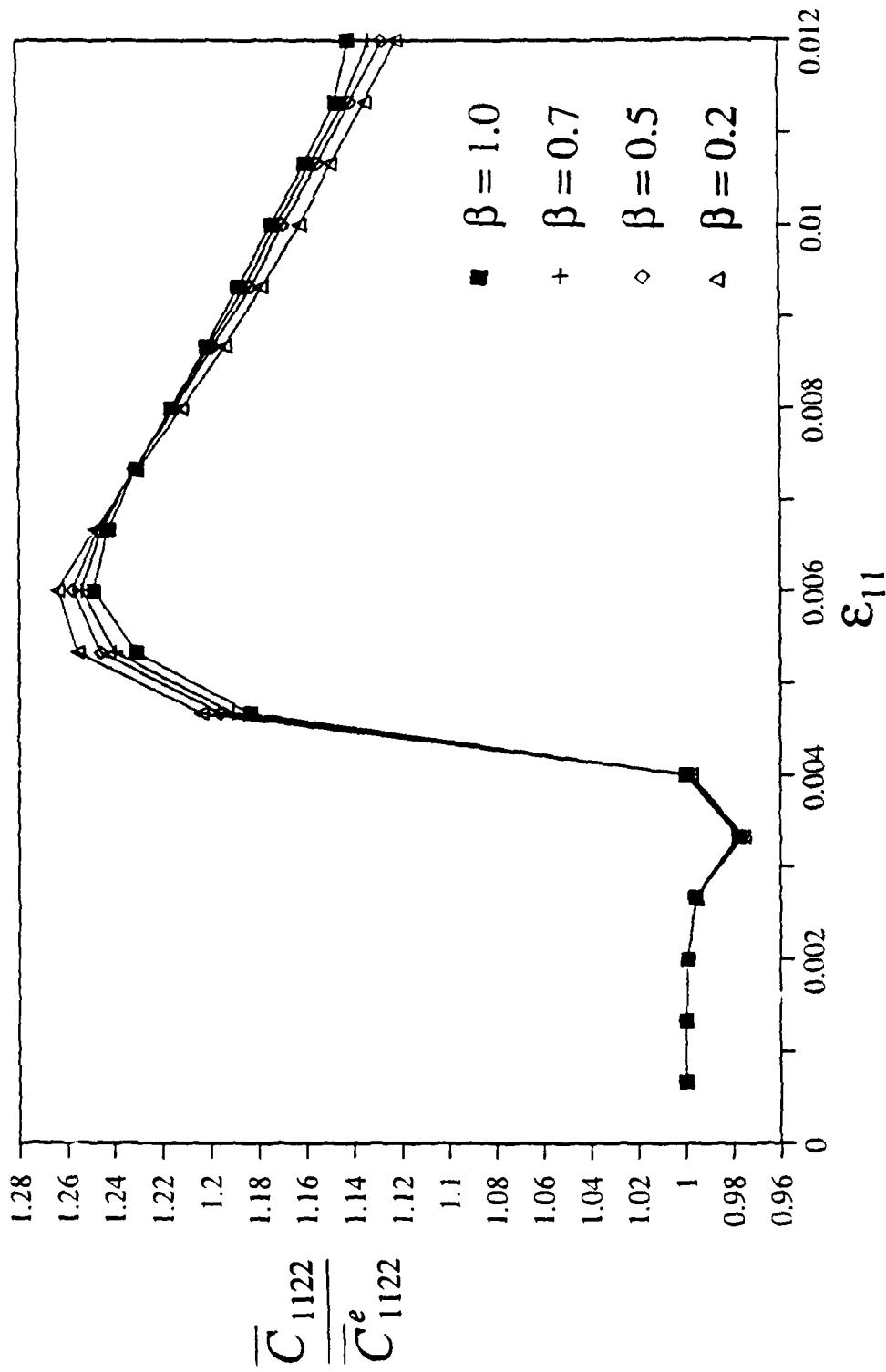
Fig. 41. Variation of the non-dimensionalized moduli $\overline{C}_{1122}/\overline{C}_{1122}^e$ with prescribed transverse strain in Gr/Al. $c_f = 20\%$ and $n = 5$.
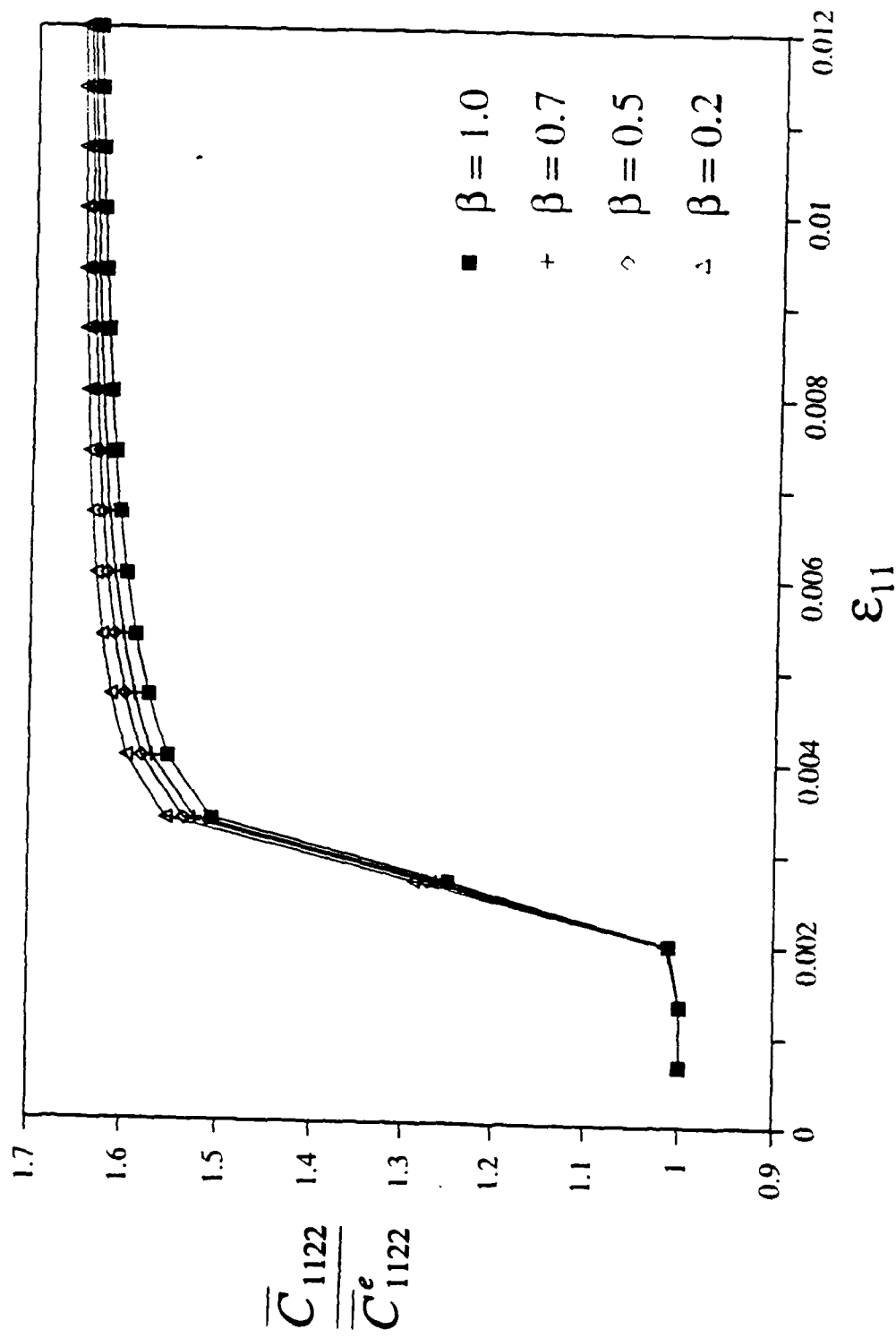
Fig. 42. Variation of the non-dimensionalized moduli $\overline{C}_{1122}/\overline{C}^e_{1122}$ with prescribed transverse strain in B/Al. $c_f = 45\%$ and $n = 5$.
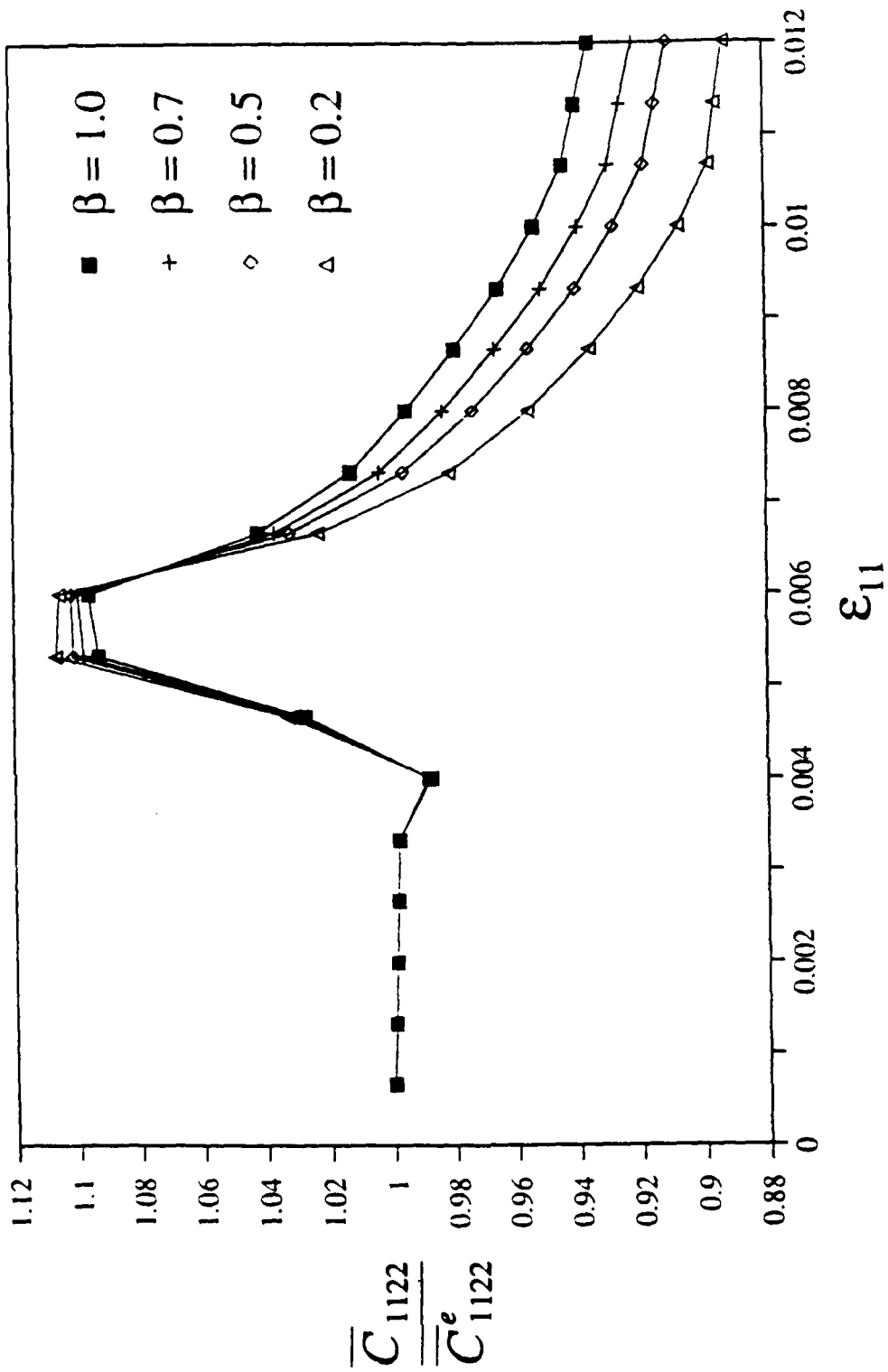
Fig. 43. Variation of the non-dimensionalized moduli $\overline{C}_{1122}/\overline{C}^e_{1122}$ with prescribed transverse strain in Gr/Al. $c_f = 45\%$ and $n = 5$.
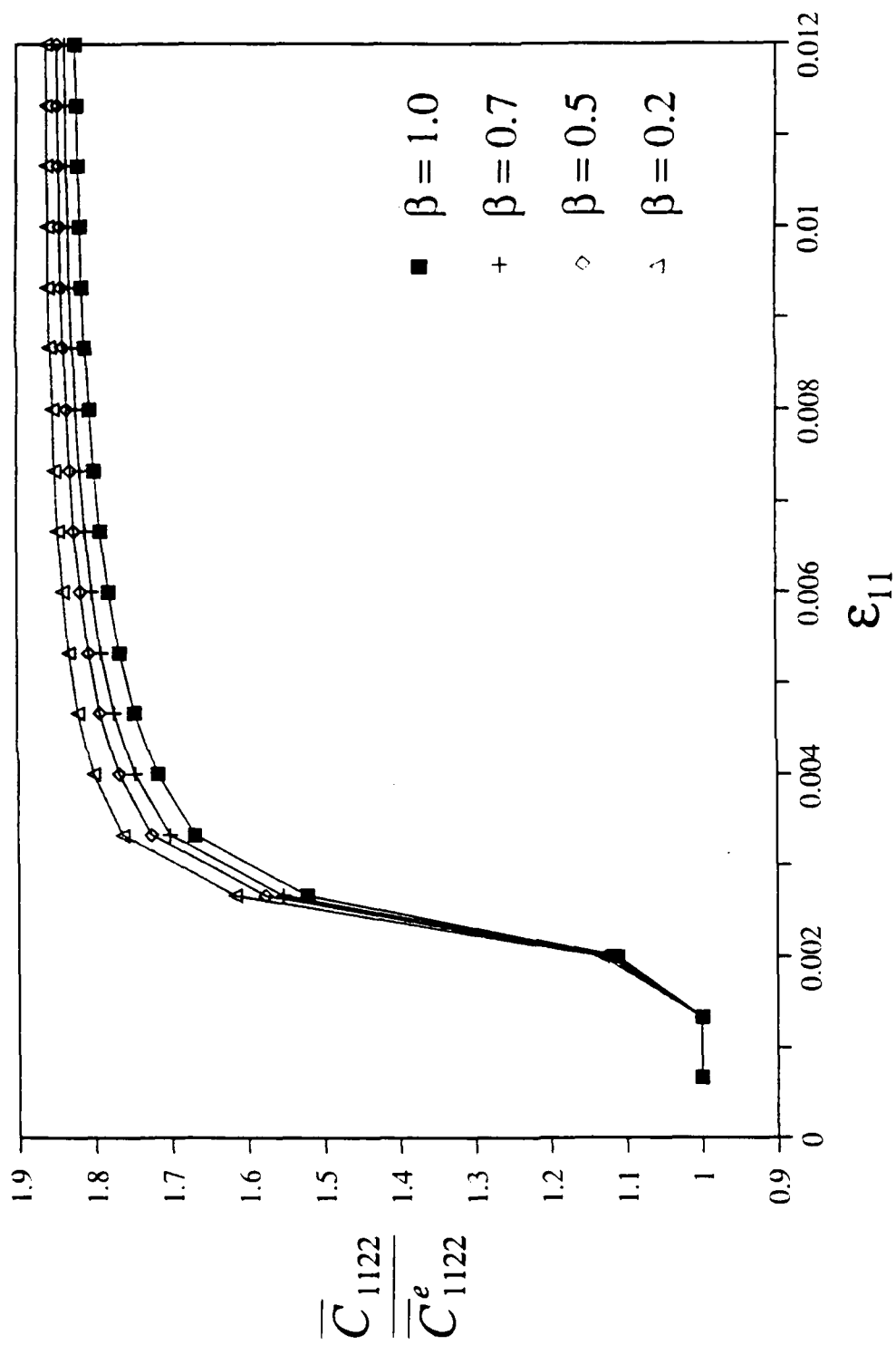
Fig. 44. Variation of the non-dimensionalized moduli $\overline{C}_{1122}/\overline{C}_{1122}^{e}$ with prescribed transverse strain in B/Al. $c_f = 60\%$, $\rho = 5$.
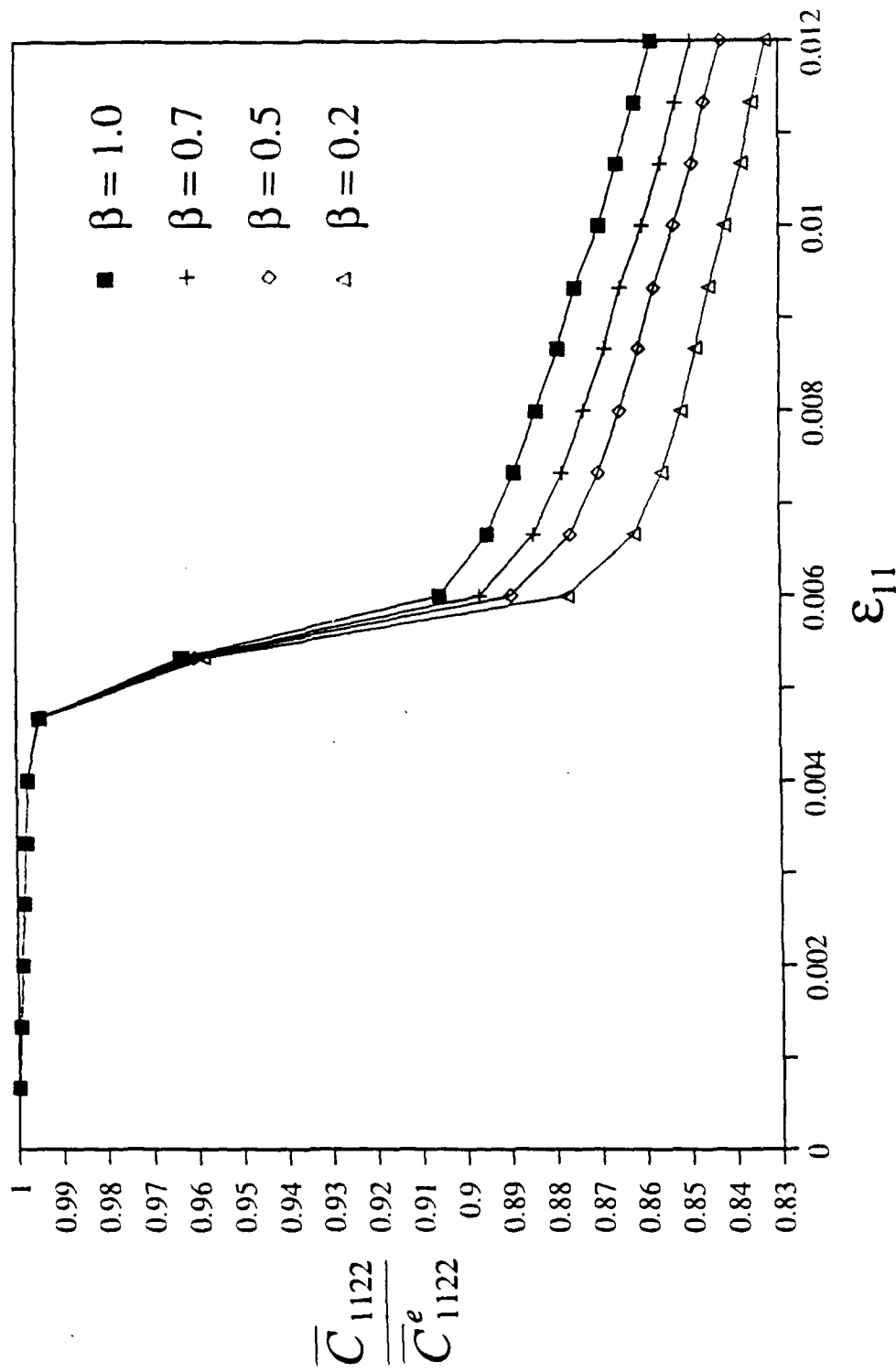
Fig. 45. Variation of the non-dimensionalized moduli $\overline{C}_{1122}/\overline{C}_{1122}^{e}$ with prescribed transverse strain in Gr/Al. $c_f = 60\%$ and $n = 5$.
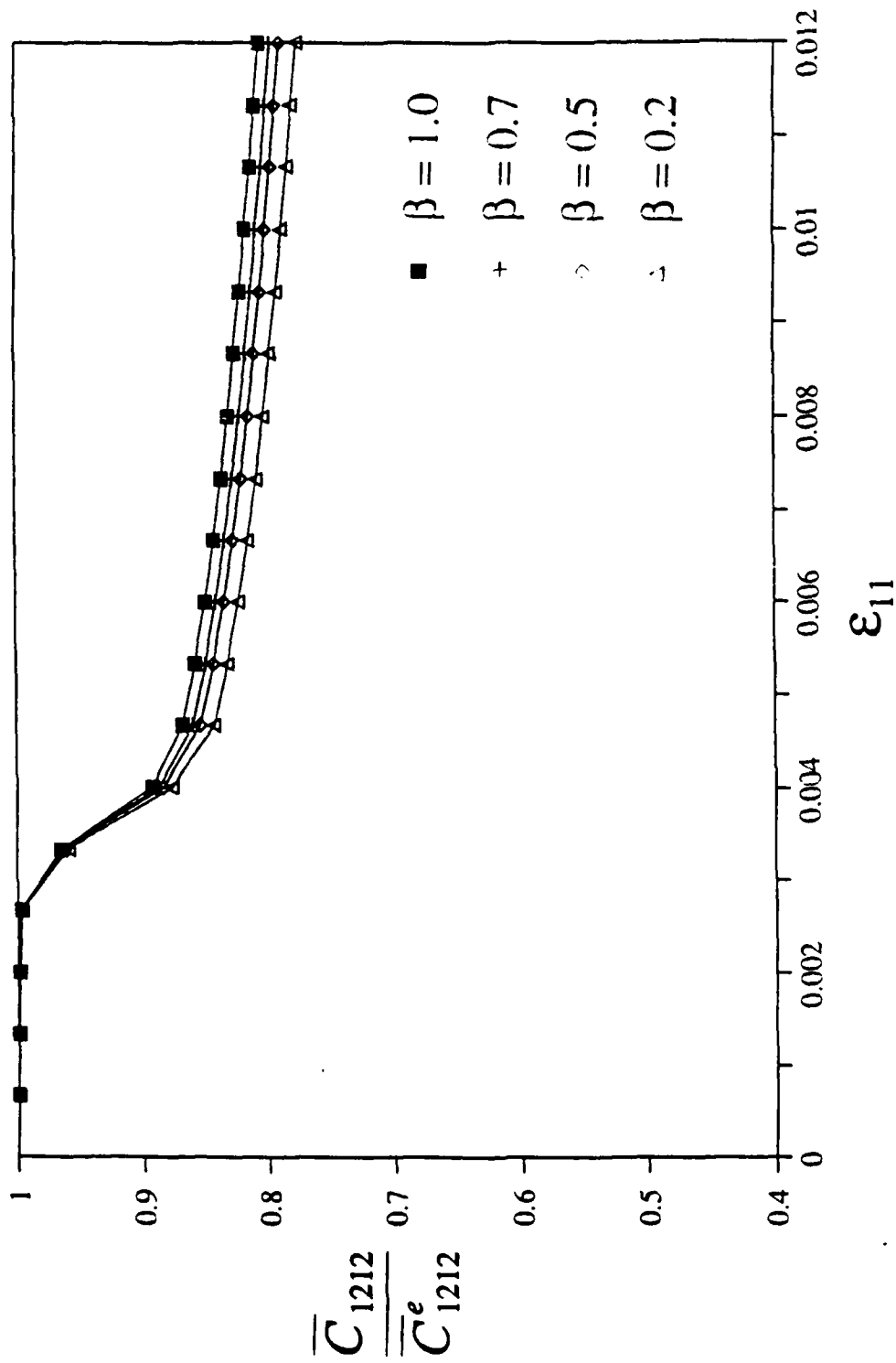
Fig. 46. Variation of the non-dimensionalized moduli $\overline{C}_{1212}/\overline{C}^e_{1212}$ with prescribed transverse strain in B/Al. $c_f = 20\%$ and $n = 5$.
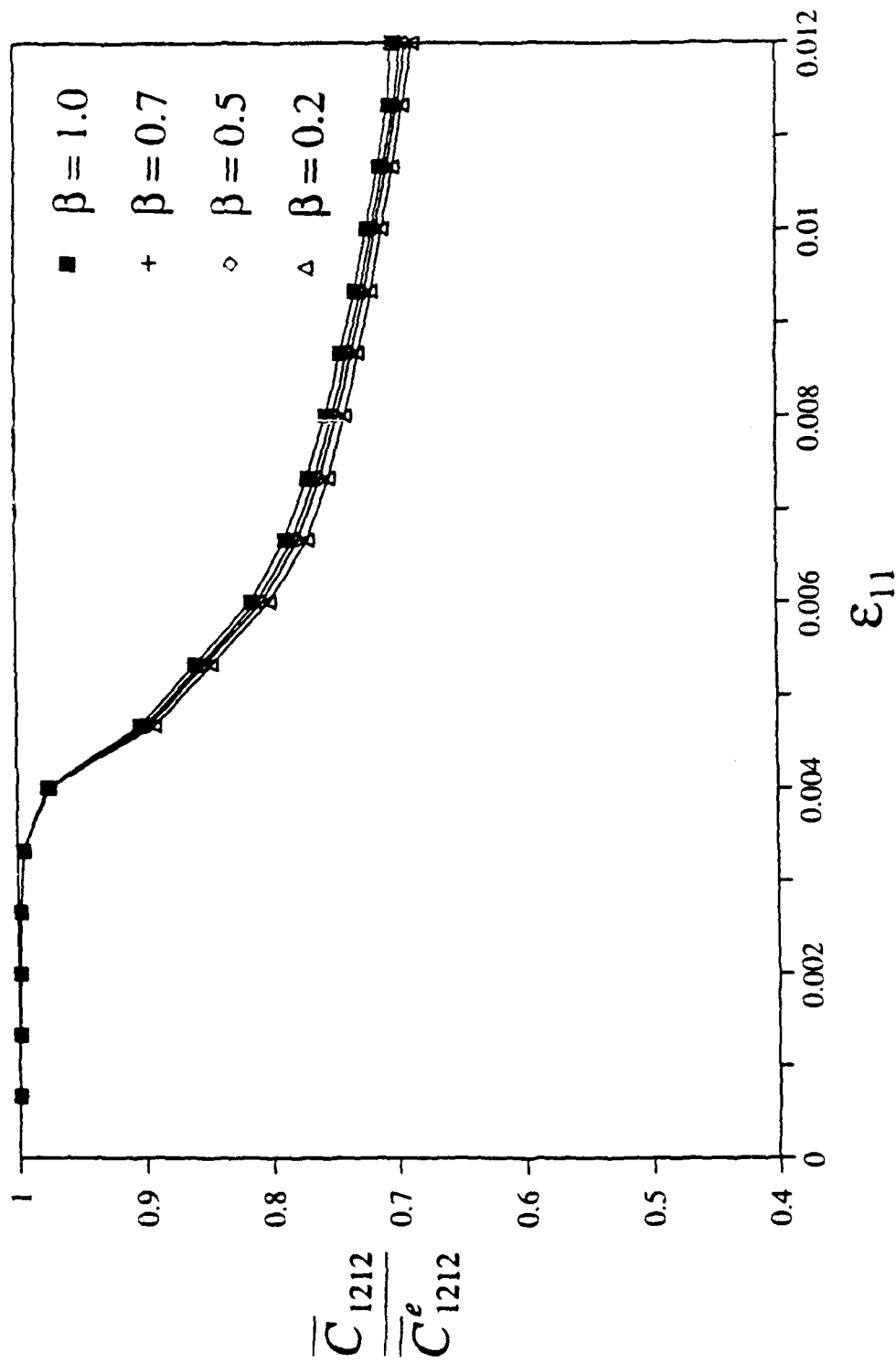
Fig. 47. Variation of the non-dimensionalized moduli $\overline{C}_{1212}/\overline{C}^e_{1212}$ with prescribed transverse strain in Gr/Al. $c_f = 20\%$ and $n = 5$.
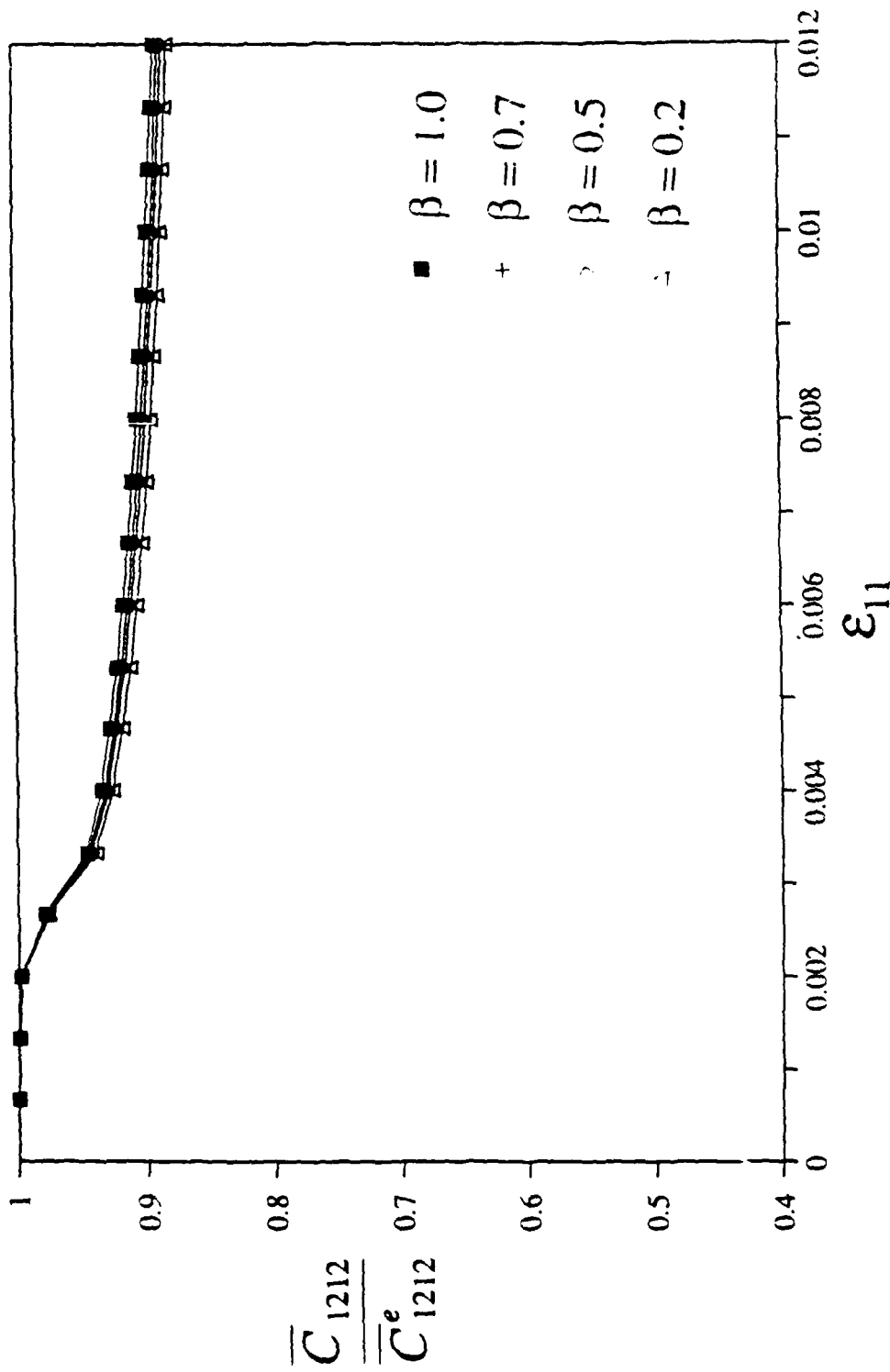
Fig. 48. Variation of the non-dimensionalized moduli $\overline{C}_{1212}/\overline{C}_{1212}^{e}$ with prescribed transverse strain in B/Al. $c_f = 45\%$ and $n = 5$.
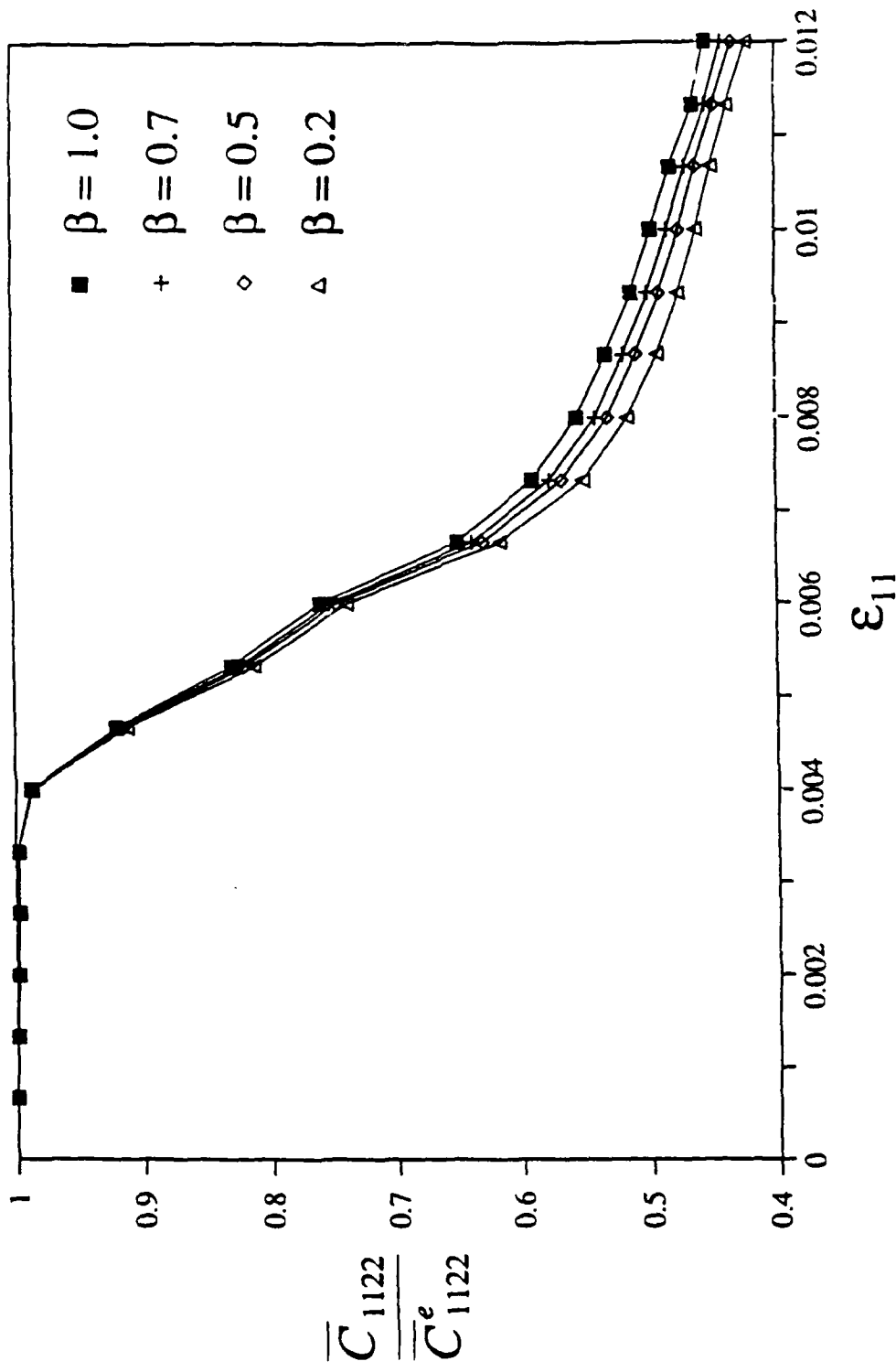
Fig. 49. Variation of the non-dimensionalized moduli $\overline{C}_{1212}/\overline{C}_{1212}^e$ with prescribed transverse strain in Gr/Al. $c_f = 45\%$ and $n = 5$.
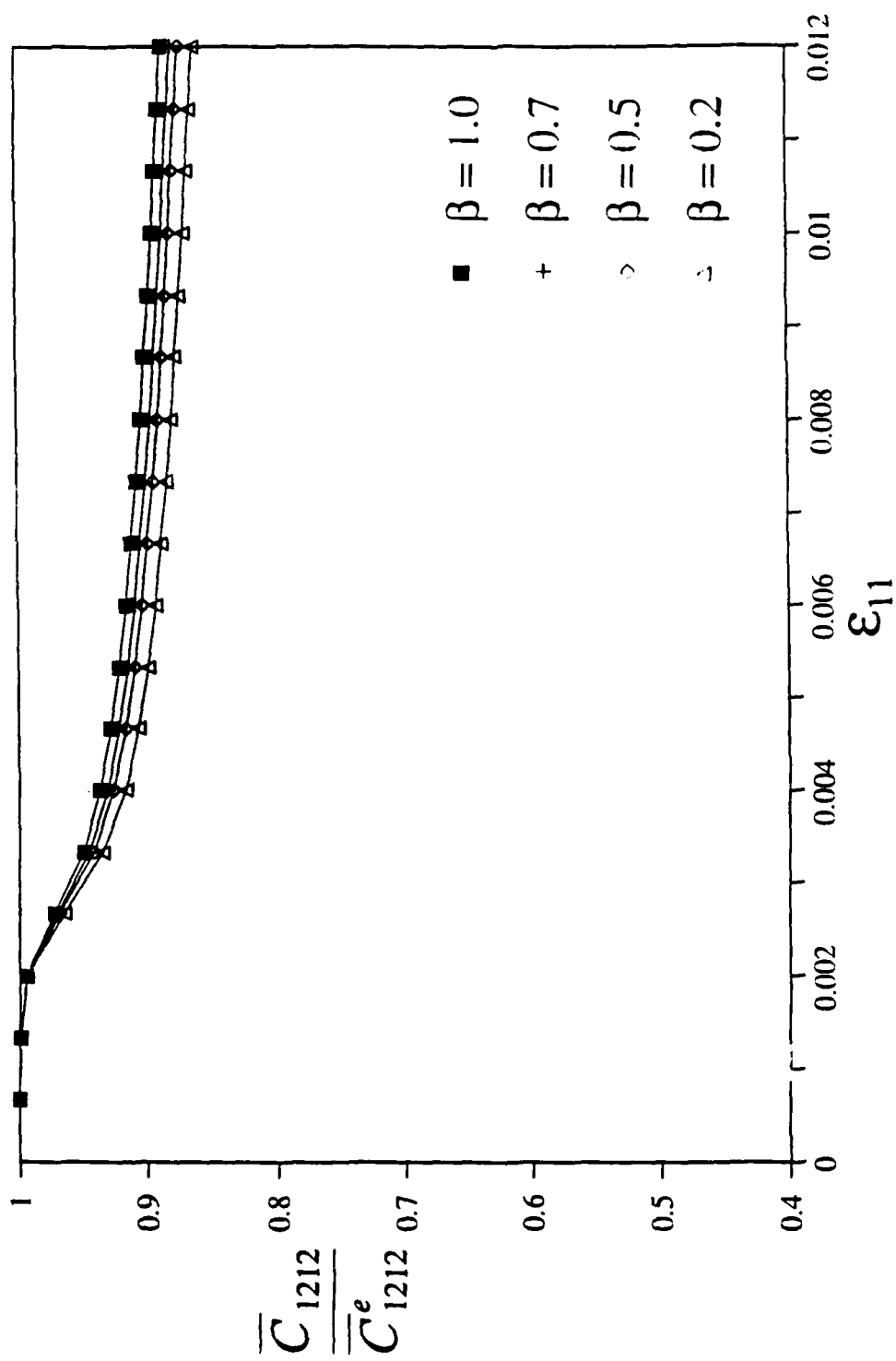
Fig. 50. Variation of the non-dimensionalized moduli $\overline{C}_{1212}/\overline{C}_{1212}^{e}$ with prescribed transverse strain in B/Al. $c_f = 60\%$ and $n = 5$.
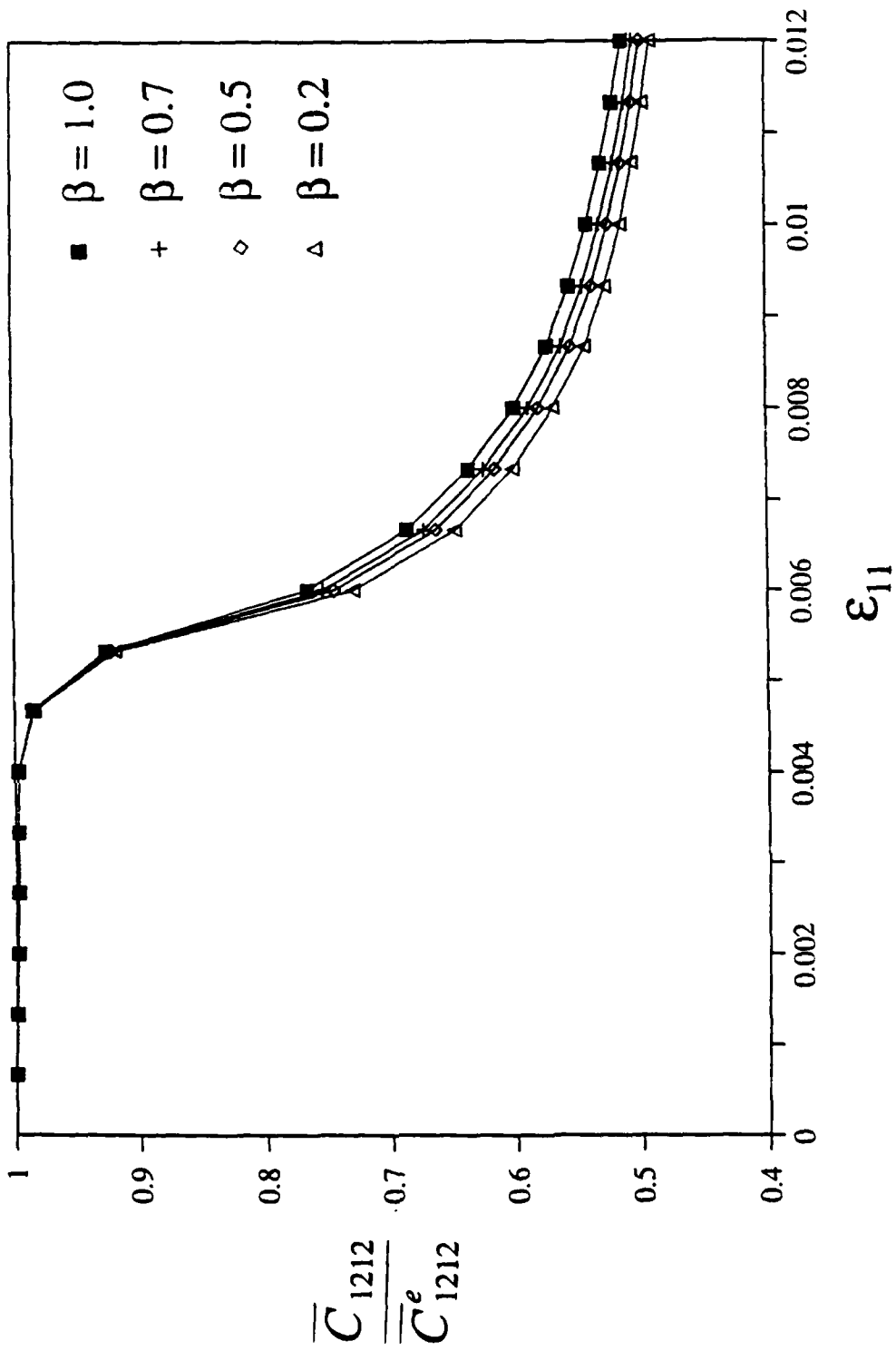
Fig. 51. Variation of the non-dimensionalized moduli $\overline{C}_{1212}/\overline{C}^e_{1212}$ with prescribed transverse strain in Gr/Al. $c_f = 60\%$ and $n = 5$.
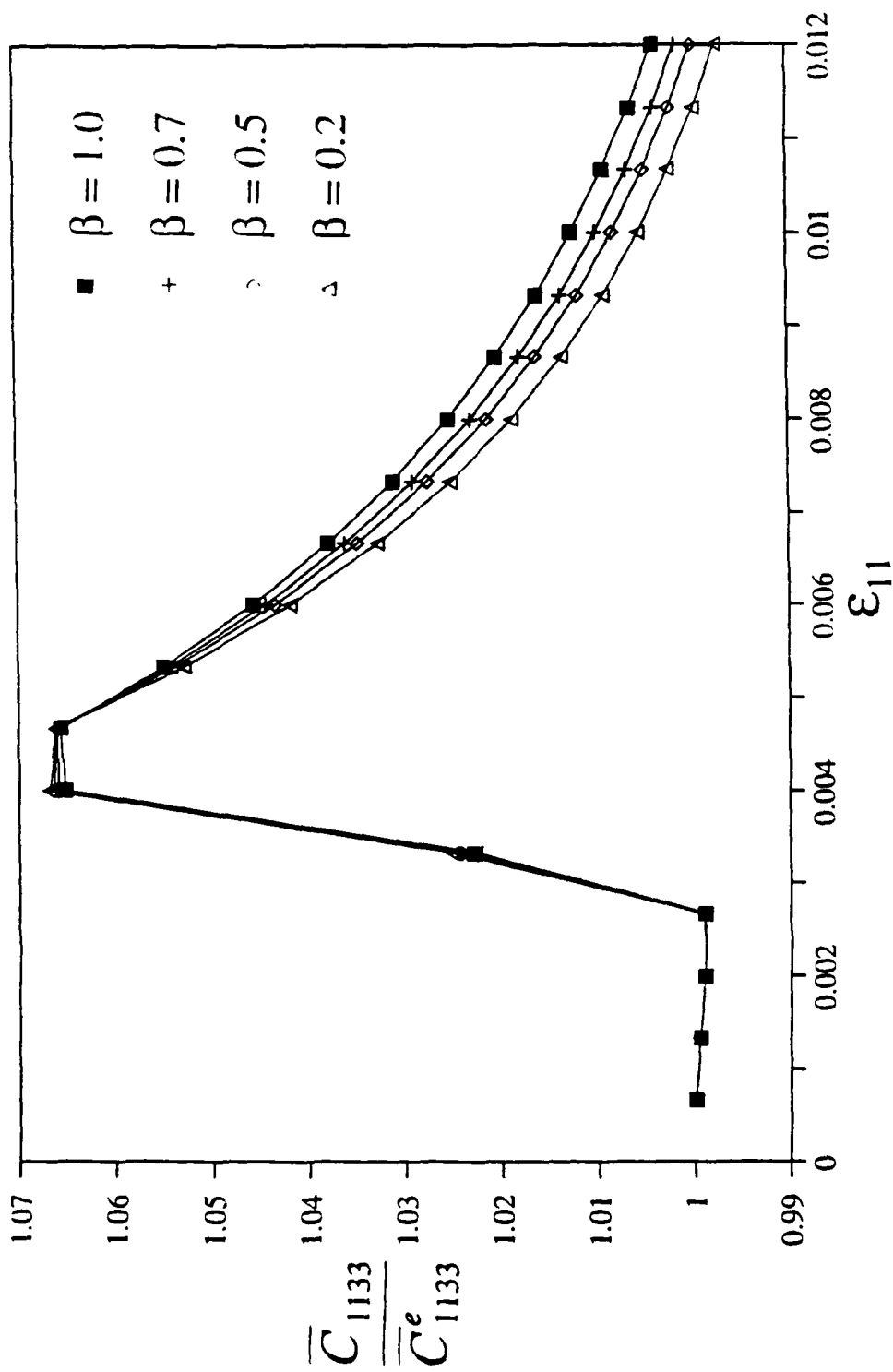
Fig. 52. Variation of the non-dimensionalized moduli $\overline{C}_{1133}/\overline{C}_{1133}^{e}$ with prescribed transverse strain in B/Al. $c_f = 20\%$ and $n = 5$.
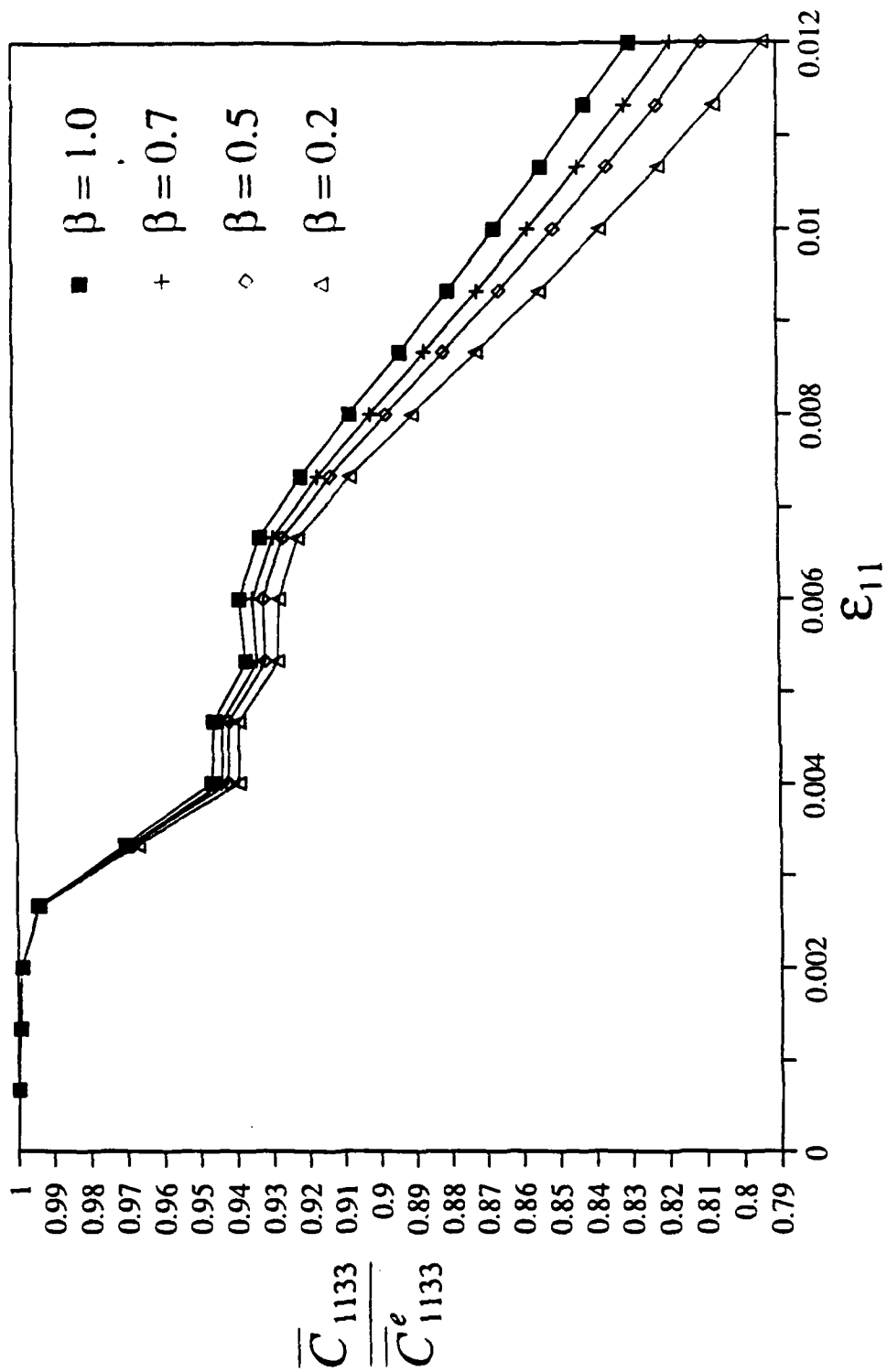
Fig. 53. Variation of the non-dimensionalized moduli $\overline{C}_{1133}/\overline{C}^e_{1133}$ with prescribed transverse strain in Gr/Al. $c_f = 20\%$ and $n = 5$.
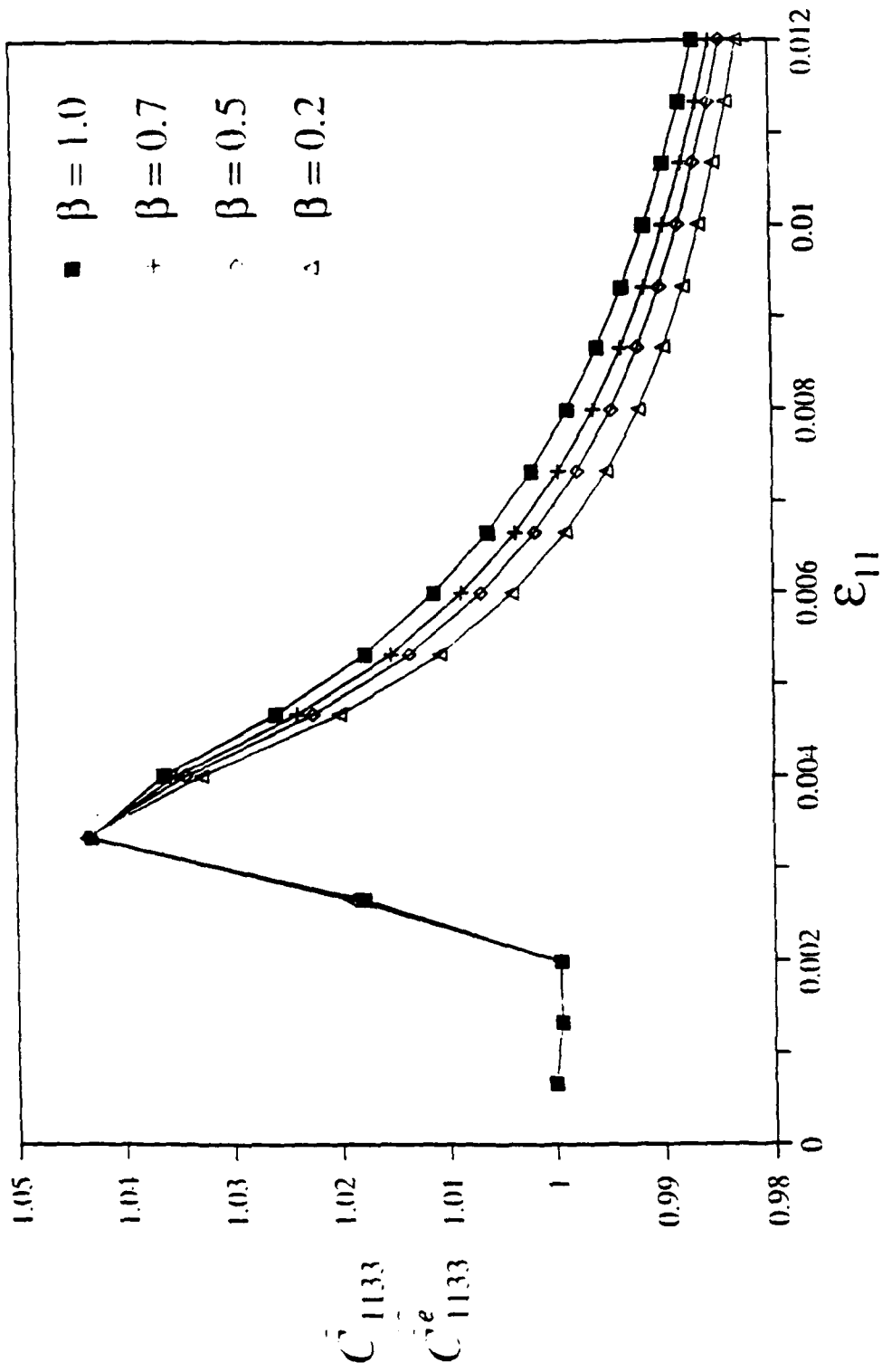
Fig. 54. Variation of the non-dimensionalized moduli $\overline{C}_{1133}/\overline{C}_{1133}^{e}$ with prescribed transverse strain in B/Al. $c_f = 45\%$ and $n = 5$.
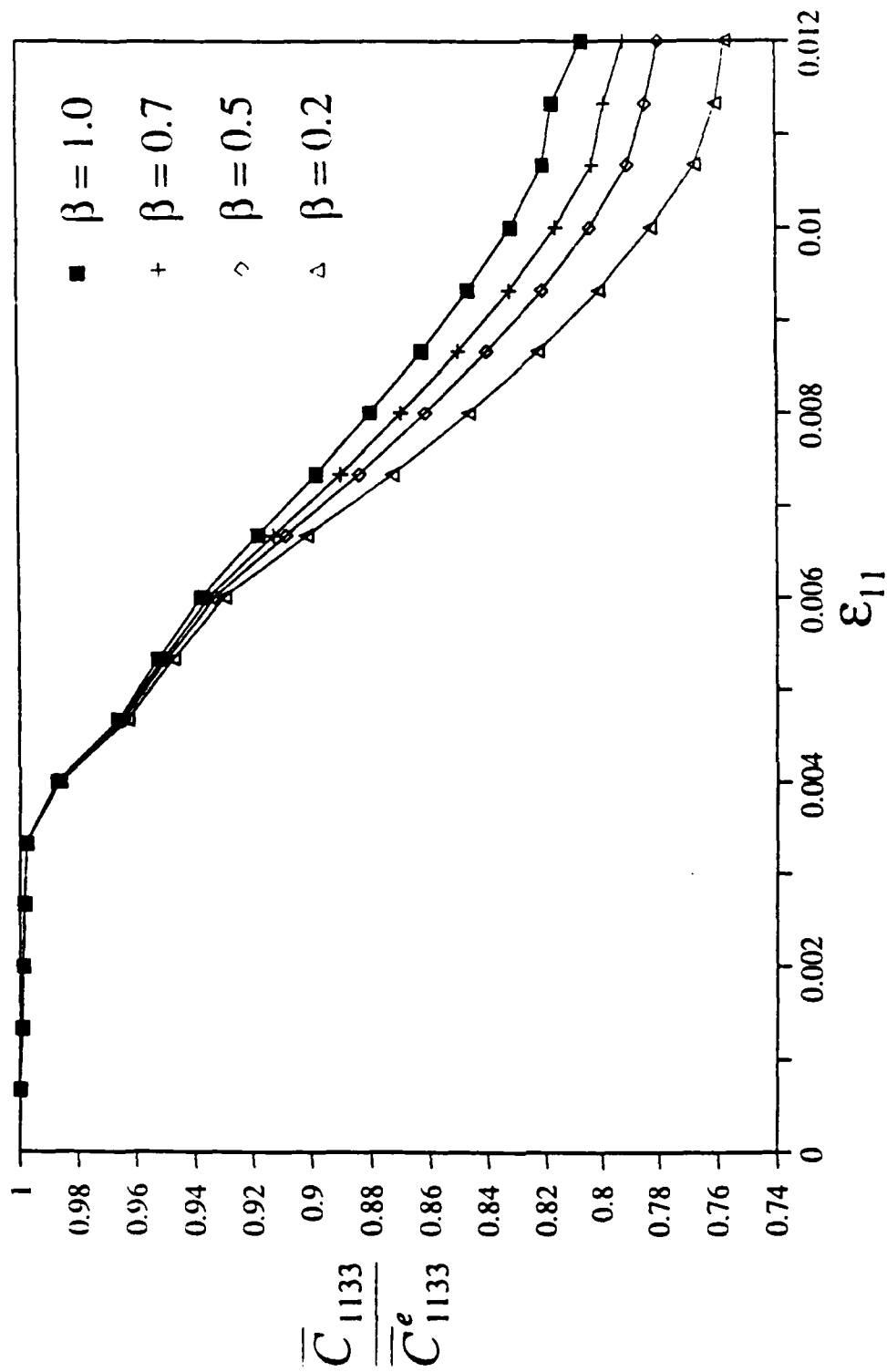
Fig. 55. Variation of the non-dimensionalized moduli $\overline{C}_{1133}/\overline{C}_{1133}^e$ with prescribed transverse strain in Gr/Al. $c_f = 45\%$ and $n = 5$.
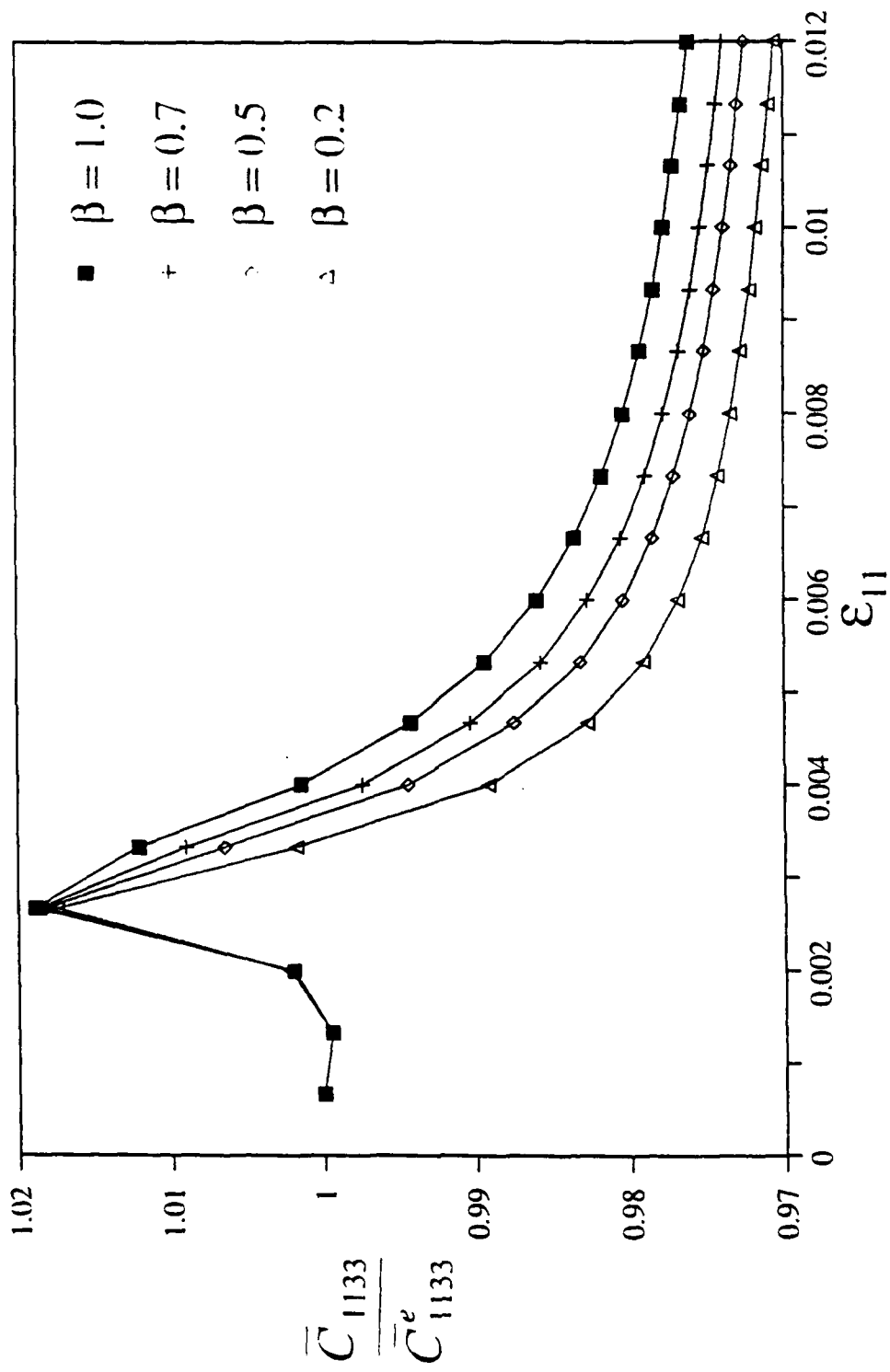
Fig. 56. Variation of the non-dimensionalized moduli $\overline{C}_{1133}/\overline{C}_{1133}^{e}$ with prescribed transverse strain in B/Al. $c_f = 60\%$ and $n = 5$.

Fig. 57. Variation of the non-dimensionalized moduli $\overline{C}_{1133}/\overline{C}_{1133}^{e}$ with prescribed transverse strain in Gr/Al. $c_f = 60\%$ and $n = 5$.